Table of Contents

Table of Contents i
List of Tables v
List of Figures vii

1. INTRODUCTION 1
1.1 Research Background 1
1.1.1 Passive Safety of Vehicles 2
1.1.2 Vehicle Structure under Frontal Collision (Concept of Safety Cage) 3
1.1.3 Numerical Simulation Method 5
1.1.4 Review of Load Path Analysis Methods 5
1.2 Research Objective 7
1.3 Thesis Structure 10

2. LOAD PATH ANALYSIS USING INDEXES U* AND U** 13
2.1 Review of the U* Index 13
2.1.1 Internal Stiffness 13
2.1.2 Definition of Index U* 14
2.2 Distribution of U* and Load Paths 18
2.3 Three Conditions for Structural Design 20
2.3.1 Uniformity of Load Path 20
2.3.2 Continuity of Load Path 20
2.3.3 Consistency of Load Path 21
2.4 Structural Optimization Using U* Index 21
2.4.1 Optimization model 21
2.4.2 Desirable structure 22
2.5 Review of Index U**: A Complementary Concept of Index U* 23
2.6 Comparison of U*, U**, and Stress Distributions 25
2.6.1 Stress and U* Distributions 25
2.6.2 Distributions of U* and U** 27
2.6.3 Definitions of Indexes U*sum and U**sum 29
2.6.4 Histograms of Indexes U*sum and U**sum 30

3. METHODOLOGY OF LOAD TRANSFER AND LOAD PATH ANALYSIS FOR VEHICLE STRUCTURES UNDER IMPACT 35
3.1 Background 35
3.2 Vehicle Structures 35
3.3 Calculation Method for Heavy Duty Vehicles (Trucks) 37
3.3.1 Dynamic-Static Method 38
3.3.2 Substitution Method 39
3.3.3 Calculation Procedure 42
3.4 Calculation Method for Passenger Vehicles (Passenger Cars) 42
3.4.1 Separation Structure Method 42
3.4.2 Relative Displacement Method 43
3.4.3 Calculation Procedure 44
3.5 Summary 44

4. CALCULATION MODEL AND BOUNDARY CONDITIONS 47
4.1 Heavy Duty Truck Model 47
4.2 Passenger Car Model 50
4.3 Calculation Environment 53
4.3.1 Dynamic Impact Calculation 53
4.3.2 Static U* and U** Calculation 54
4.4 Model Conversion 55

5. DYNAMIC CRASH RESULTS 57
5.1 Results of Truck 57
5.2 Results of Passenger Car 60
5.2.1 Original Boundary Condition 60
5.2.2 Simplified Boundary Condition 71

6. STATIC LOAD PATH ANALYSIS FOR TRUCK CAB STRUCTURES USING INDEX U** 73
6.1 Small Differences of U** Distribution with Regard to Sample Time *t* and Parameter *m* 73
6.1.1 U** Distribution in Floor Panels 73
6.1.2 Small Difference in Floor Cross-Sections 75
6.1.3 U** Variations along Load Paths 76
6.2 Load Transfer and Load Paths in Floor Structures 77
6.2.1 Load Paths along Floor Main Members 77
6.2.2 Load Transfer in Floor Structure 78
6.2.3 Load Transfer in Tunnel Structure 80
6.2.4 Load Transfer in Side Sills and Cross Members 81
6.3 Load Transfer in Front Panel 83
6.4 Load Transfer in Roof Panel 85
6.5 Summary 85

7. STATIC LOAD PATH ANALYSIS FOR TRUCK CAB STRUCTURES USING INDEX U* 87
7.1 Small Differences of U* Distribution 87
7.2 Load Transfer in Floor Structure 88
7.3 Comparison of Load Transfer and Load Path in Floor Structure (Comparison of U* and U**) 91
7.3.1 Load Path along Main Members 91
7.3.2 Load Path in Floor Panels 91
7.3.3 Load Transfer in Tunnel Structure 95
7.3.4 Load Transfer in Side Sills and Cross Members 95
7.4 Load Transfer in Front Panel 96
7.5 Load Transfer in Roof Panel 98
7.6 Load Transfer in Floor Structure and Comparison of U* and U** 99
7.7 Summary 100

8. STATIC LOAD PATH ANALYSIS USING INDEX U*SUM AND HISTOGRAM 101

8.1 Histogram of U*sum in Floor Structure 101
8.2 Load Paths and Histogram of Main Members 102
8.2.1 Load Paths along Main Members 102
8.2.2 Histogram of Maim Members 102
8.3 Distribution of U*sum in Tunnel Structure and Its Histogram 104
8.4 Load Transfer in Front Floor Panel 106
8.5 Distribution of U*sum along Load Paths 106
8.6 Summary 108

9. LOAD PATH ANALYSIS FOR PASSENGER CAR STRUCTURES USING SEPARATION STRUCTURE METHOD 111
9.1 Distribution of U** 111
9.1.1 Distribution of U** in Floor Panels from Dash Panels 111
9.1.2 Distribution of U** in Floor Panels from Rear Structure 114
9.1.3 Distribution of U**sum in Floor Panels and Its Histogram 114
9.2 Load Transfer and Load Paths in Floor Structures 115
9.2.1 Load Paths along Main Members 116
9.2.2 Load Transfer in Middle Floor Panels 117
9.2.3 Load Transfer in Side Sills 118
9.2.4 Load Transfer in Tunnel Structure 120
9.2.5 Load Transfer in Pillars 120
9.3 Summary 121

10. CONCLUSIONS 125
10.1 Novel Aspects of This Research 125
10.2 Research Achievements 126
10.3 Future Research 128

ACKNOWLEDGEMENTS 131

REFERENCES 133

Appendix A. Summary of LS-DYNA Calculation 139

List of Tables

Table 4. 1 Parameters of Truck Cab Model.....48

Table A. 1 Truck Compartment Model 139

Table A. 2 Passenger Car Model.....141

List of Figures

Fig. 1. 1 Parameter of General Advanced Body Engineering.....1

Fig. 1. 2 Concept of Crash Safety 3

Fig. 1. 3 Distribution of U* or U** and Load Path.....6

Fig. 1. 4 Diagrams of Load Transfer 7

Fig. 1. 5 Flow Chart of Load Transfer and Load Path Study.....9

Fig. 2. 1 Internal Stiffness.....13

Fig. 2. 2 Definition of Index U*.....14

Fig. 2. 3 Linearization of Index U* 16

Fig. 2. 4 Distribution of U* and Load Paths 18

Fig. 2. 5 Uniformity and Continuity of Load Path 19

Fig. 2. 6 Consistency of Load Path.....20

Fig. 2. 7 Structural Optimization.....22

Fig. 2. 8 Index U**.....24

Fig. 2. 9 Distribution of Principal Stress and U** (Frontal View) 26

Fig. 2. 10 Distribution of U* and U** in Simplified Airplane Main Wing.....27

Fig. 2. 11 Distribution of U* and U** in Plate with Circular Hole 28

Fig. 2. 12 Comparison of U* and U** Distributions 29

Fig. 2. 13 Definition of Summation of Index U*sum or U**sum 31

Fig. 2. 14 Uniformity of U* or U** and U*sum or U**sum.....33

Fig. 3. 1 Vehicle Structures.....36

Fig. 3. 2 Truck Cab under Frontal Collision 37

Fig. 3. 3 Passenger Car under Frontal Collision 39

Fig. 3. 4 Substitution Stress Method 40

Fig. 3. 5 Substitution Modulus 41

Fig. 3. 6 Calculation Procedure....41
Fig. 3. 7 Relative Deformation....43
Fig. 4. 1 Heavy Duty Truck....47
Fig. 4. 2 Boundary Conditions of Truck Cab....49
Fig. 4. 3 Stress Strain Curve....49
Fig. 4. 4 Passenger Car....50
Fig. 4. 5 Approaches of Passenger Car....51
Fig. 4. 6 Frontal Impact of Passenger Car....53
Fig. 4. 7 Model Conversion....54
Fig. 4. 8 Spot-Weld and Rigid Bar Convention....56
Fig. 5. 1 Deformation of Truck Cab under Frontal Impact....58
Fig. 5. 2 Distribution of Plastic Strain in Truck Cab....59
Fig. 5. 3 Variation of Distance between A-Pillars and B-Pillars....60
Fig. 5. 4 Comparisons of Simulation Results (0-40ms)....61
Fig. 5. 5 Comparisons of Simulation Results (40-45ms)....62
Fig. 5. 6 Comparisons of Simulation Results (100ms)....63
Fig. 5. 7 Comparisons of Numerical and Experimental Results (150ms)....63
Fig. 5. 8 Comparison of Displacement....65
Fig. 5. 9 Comparison of Velocity....65
Fig. 5. 10 Comparison of Acceleration....67
Fig. 5. 11 Comparison of Internal Energy....67
Fig. 5. 12 Distribution of Plastic Strain in Original Passenger Car....68
Fig. 5. 13 Variation of Distance between A-B Pillars and B-C Pillars....69
Fig. 5. 14 Comparison of Deformed Shapes....70
Fig. 6. 1 Small Differences of U** Distribution....73

Fig. 6. 2 Cross-Sectional Distribution of U** (*m*=2) 75
Fig. 6. 3 Decay of U** along Load Paths (*m*=2) 76
Fig. 6. 4 Distribution of "m2-4msU**" and Load Paths 77
Fig. 6. 5 Multi-Corner Cross-Sections 78
Fig. 6. 6 Load Transfer in Floor Structure 79
Fig. 6. 7 Distribution of "m2-4msU**" (Tunnel Wall) 80
Fig. 6. 8 Distribution of U** and Load Paths (*m*=2, Side Sills) 81
Fig. 6. 9 Distribution of U** (*m*=2, Frontal Panel) 82
Fig. 6. 10 Distribution of U** (*m*=2, Floor Panel) 83
Fig. 6. 11 Distribution of U** (*m*=2, Roof) 84
Fig. 7. 1 Small Variation of U* Distribution from Frontal Barrier (*m*=2) 87
Fig. 7. 2 Decay of U* along Load Paths (*m*=2) 89
Fig. 7. 3 Distribution of "m2-4msU*" and Load Paths 90
Fig. 7. 4 Cross-Sectional Distribution of U* and U** (*m*=2) 91
Fig. 7. 5 Load Transfer in Floor Structure (m2-4msU* and m2-4msU**) 93
Fig. 7. 6 Load Transfer in Tunnel Wall 94
Fig. 7. 7 Load Transfer in Side Sills 96
Fig. 7. 8 Distribution of U* and U** (Frontal Panel) 97
Fig. 7. 9 Distribution of U** in Floor Panels 98
Fig. 8. 1 Small Variation of U*sum Distribution 101
Fig. 8. 2 Small Variation of U* Distribution 101
Fig. 8. 3 Histogram of Floor Structure 102
Fig. 8. 4 Load Paths (m2-4msU*) 103
Fig. 8. 5 Histogram of Main Member and Tunnel (m2-4msU*sum) 104
Fig. 8. 6 Distribution of U*sum and Histogram in Tunnel Wall (m2-4msU*sum) 105

Fig. 8. 7 Distribution of U*sum and Histograms in Floor Panels (m2-4msU*sum).....107
Fig. 8. 8 Distribution of U*sum along A Load Path 108
Fig. 9. 1 Distribution of U** in Floor Panels (Frontal) 112
Fig. 9. 2 Distribution of U** in Floor Panels (Rear).....113
Fig. 9. 3 Distribution of U**sum in Floor Panels 115
Fig. 9. 4 Enlarged Histogram of Floor Panels (0-1.5×10^{-6}) 116
Fig. 9. 5 Histogram of Floor Panels 116
Fig. 9. 6 Distribution of U** in Floor Panels.....118
Fig. 9. 7 Distribution of U** in Side Sills 119
Fig. 9. 8 Distribution of U** in Pillars and Roof Panels 120
Fig. 9. 9 Distribution of U** in Pillars and Roof Cross Members.....122

1. Introduction

1.1 Research Background

In the twenty-first century, automotives should be in harmony with people and compatible with nature. For body engineers, the design of a vehicle should meet parameters shown in Fig. 1.1, especially the requirements of the safety of structures. Recently, automakers introduce novel clean energy automotives to reduce CO_2 emissions and improve fuel economy, such as Hybrid Electric Vehicles (HEV) and Electric

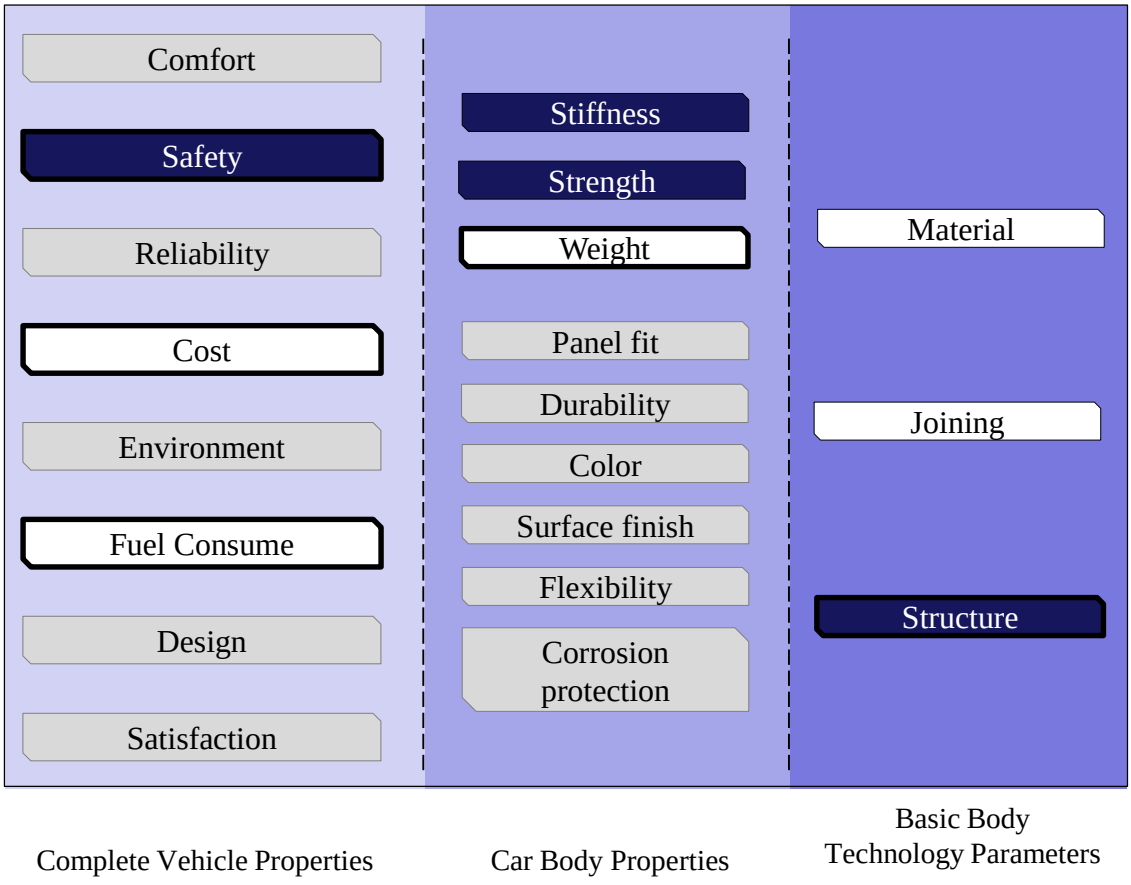

Fig. 1. 1 Parameter of General Advanced Body Engineering

Vehicles (EV) [1, 2]. Except considering the environmental compatibility of the design, the safety of occupants is another major concern. The crashworthiness of vehicle structures is still a crucial aspect in the structural design for both conventional gasoline vehicles and future clean energy vehicles.

1.1.1 Passive Safety of Vehicles

Safety of occupants is regarded as a complete vehicle characteristic which depicts active safety which is the ability of vehicles to reduce the risk of being involved in an accident, and passive safety which is the ability to avoid or mitigate injuries or damage to occupants and car. In contrast to almost all other characteristics of vehicle structures, passive safety cannot be evaluated by the customer prior to purchase or after purchasing it. Thus, automakers and governments provide two ways which are listing the safety features equipped with and the results of standardized crash tests. The standardized crash test allow to make an evaluation and to rate the passive safety performance of a vehicle. Based on the actual road accidents, several types of crash tests are derived [3, 4] shown as follows.

- Frontal impact: rigid/deformable barrier, full width/offset, straight/oblique;
- Side impact: plain barrier/pole;
- Rear impact: rigid/deformable barrier, full width/offset, straight/oblique;
- Rollover;

In the automotive markets, mandatory evaluation (U.S. FMVSS, and Europe ECE) and non-mandatory evaluation (US-NCAP, Euro-NCAP, Japan-NCAP, China-NCAP etc.) of

crash tests [3-7] are introduced to evaluate the safety for new cars. According to the requirements of customers, the quantitative rating of the safety performance for a vehicle (New Car Assessment Program - NCAP) has been founded by manufacturers, governments, and insurance companies all over the world, which has become an important factor to affect customers' purchase decision of new vehicles. In the present crash analysis, parameters of the numerical simulation are determined based on the Japan-NCAP standard.

1.1.2 Vehicle Structure under Frontal Collision (Concept of Safety Cage)

Crashworthiness was considered by the automotive engineers in structural design for many years, which must meet different kinds of assessment standards (such as NCAP) to lead to a decrease in the injury and accident rate. Nevertheless, road accidents are the most frequent cause of death in car crashes each year in spite of the improvements of crashworthiness. According to the accident review [6, 8], the most frequent fatal and

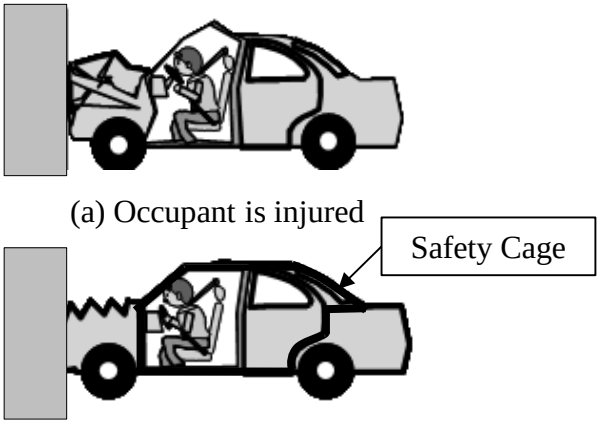

(a) Occupant is injured

(b) Occupant is safe

Fig. 1. 2 Concept of Crash Safety

serious injury is caused by the frontal collision. Thus, from the point view of safety issues, together with the energy absorption characteristics of front-end structures, increasing the stiffness of compartment structures is the major concern in the present study of vehicle structures under frontal collision.

Two schematic figures are presented in Fig. 1.2 to reveal the two typical deformations of vehicle structures. In Fig. 1.2(a), a cabin deforms significantly because front-end structures are too weak to function well as collision energy absorbers and the stiffness of the cabin is not large to protect the safety of occupants. In contrast, the collision energy is well absorbed by front-end structures without any cabin deformation after a proper structural design, schematically shown in Fig. 1.2(b).

From the viewpoint of occupant's safety issues, the structural design of passenger compartment in Fig. 1.2(b) is preferable. Consequently, a general concept of *Safety Cage* (the central section of the car body acting as the passenger compartment) shown in Fig. 1.2(b) is proposed by many automakers [3, 4, 8-12]. Aiming to achieve a safe vehicle body in the event of a collision, the deformation of 'Safety Cage' is required to be minimized to protect occupants, and the collision energy should be absorbed by a limited deformation of front-end structures which are 'Crumple Zones' designed to help decelerate the car by absorbing the crash energy and reduce the risk of injuries. To ensure the safety of passengers, reinforced box-type structures are applied to all body apertures around the passenger area. However, how loads transfer in these reinforced structures cannot be examined.

Moreover, aiming to obtain a high rigidity of the passenger compartment, the ultra high strength steel [3, 11, 13-17] or high strength composite materials [18-24] should be used to make critical parts for load transfer in the passenger compartment.

1.1.3 Numerical Simulation Method

Since all of the actual crash tests are extremely expensive, automakers must afford over millions of dollars costs for a prototype [1, 2, 4, 5, 9, 10, 25-29]. This is why the technique of using high performance computers to make visual vehicle structural analyses [30-66] has become the key link between structural design and computer aided drafting today. In contrast to the conventional objective of experimental hardware crash tests, now it has been expected to prove the validation of numerical simulations because of the high accuracy of simulation results. Virtual and real crash tests are compared [3, 13, 40, 67-69], based on Euro-NCAP frontal impact crash standard. Based on literatures [3, 5, 8, 28, 40], there is no significant difference of the geometric deformation between experimental and numerical results, which proves the validation of using the numerical simulation to assess vehicle structures. Thus, the real crash test is excluded in the present study, and the study of load transfer and load paths is based on numerical simulation.

1.1.4 Review of Load Path Analysis Methods

(1) Load Path Analysis Based on Load Transfer

The distribution of the principal stresses is used to express the load transfer or load paths by Kelly and Tosh [70-76]. In this method, the load path is defined as the trajectory along which a force is being transferred, which is derived from fluid flow analogy. However,

when using this conventional method with a stress distribution, it is rather difficult to observe the load transfer because of the effect of stress concentrations around holes or notches. Since it is unreasonable to conclude that a hole is effective for load transfer, the stress distribution is likely to be misleading with respect to the determination of load paths.

(2) Transferred and Potential Transferred Force Method

Apart from the stress distribution, load transfer in a structure has been studied by Harasaki and Arora [77-81] by introducing the concept of transferred forces and potential transferred forces. This method of transferred forces is based on the portion of the load transferred through a region of the structure. The concept of potential transferred forces is introduced as a complementary method to give an indication of how well stiffening the

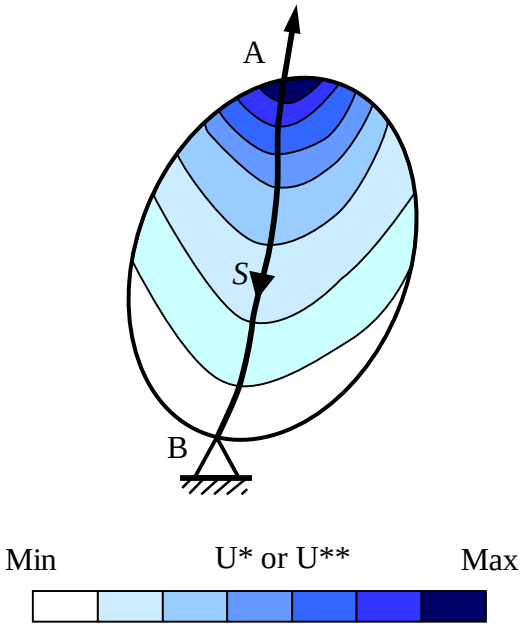

Fig. 1. 3 Distribution of U* or U and Load Path**

region will improve the stiffness of the structure. However, this method is hardly to visualize the load trajectories.

(3) Load Path Analysis Based on Indexes U* and U**

The parameters U* and U** [82-101] have been used to express the load transfer and load paths in vehicle bodies. A schematic illustration of U* and U** distributions and a load path is shown in Fig. 1.3.

Three typical indexes for load paths mentioned above have been investigated and compared [102].

1.2 Research Objective

Generally, in the study of impact problems, engineers are using schematic diagrams shown in Fig. 1.4 to illustrate the load transfer in body structures which are frequently seen in technical reports on structural design policies [4, 7, 11, 64, 103-120]. Examining

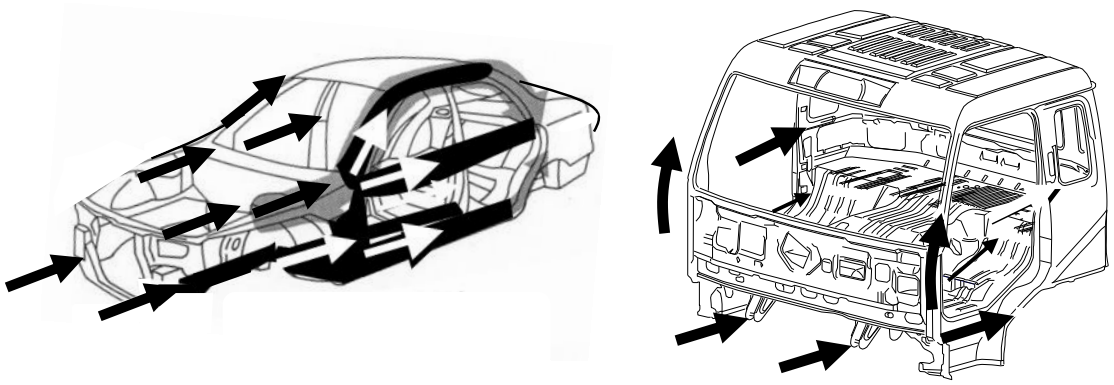

Fig. 1. 4 Diagrams of Load Transfer

the load transfers from a loading point to a supporting point in a structure is crucial in evaluating the efficiency of that structure. However, no actual data exist to support such schematic figures. To produce images like Fig. 1.3 based on a rigorous theoretical foundation for the load transfer during collisions has long been the dream of structural engineers.

This study aims to develop a general method to examine the load transfer and load paths and improve the stiffness of the passenger cabin under the frontal collision for automotive industries. The big picture of this study is that this methodology could provide a useful design aid for automotive engineers by highlighting the variation of the compartment stiffness during the stages of a frontal impact. The flow chart of the research objective and research procedures is shown in Fig. 1.5. The original output of this study bridges the gaps between the conventional load path analysis and nonlinear crash problems by introducing proper approaches.

The deformation of a vehicle structure is calculated using the crash simulation code LS-DYNA [121]. After conversion of numerical outputs, a deformed model is extracted for each sample time to calculate statically the U* and U** distributions. Indexes U* and U** are used to express the load transfer and load paths in vehicle structures in the early stages. The index U**, as a complementary quantity of index U*, is used to express load paths for distributed forces such as the inertial force caused by the crash impact. Both U* and U** analyses are extended to the summation expression: U*sum and U**sum, which

are important to show the effectiveness of the structure. The definitions of U*, U**, U*sum, and U**sum will be explained in the following chapter.

For the truck cab, applying the substitution-modulus method to represent the decreased

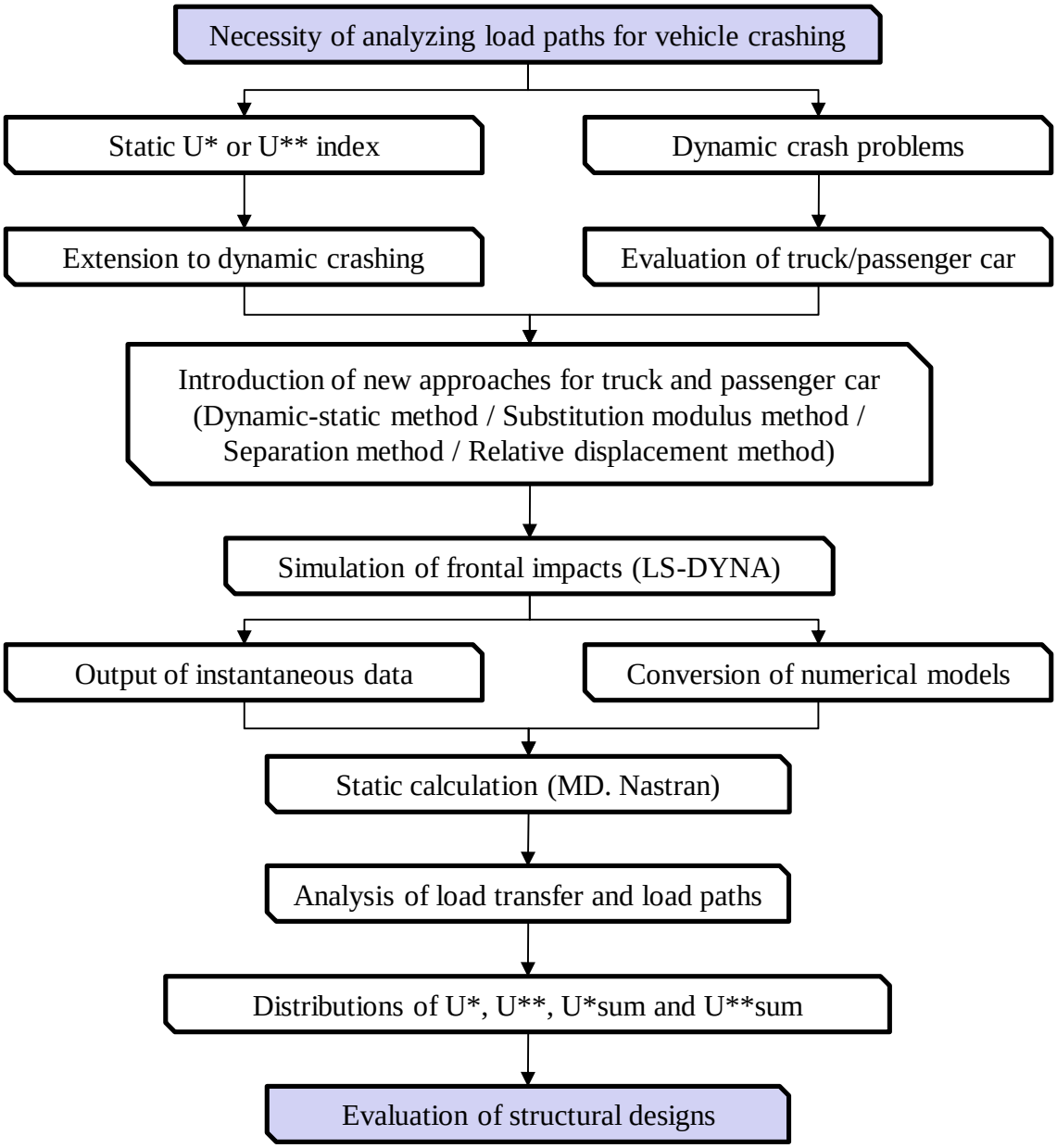

Fig. 1. 5 Flow Chart of Load Transfer and Load Path Study

performance of the load transfer in areas of panels affected by nonlinear phenomena such as plastic and large deformations, we use both U** and U* analyses to express the load transfer in the extremely early stages of a crash. For the passenger car, based on the explanation of 'Safety Cage' in Section 1.1.2, an elastic approach of the passenger compartment in the early stages of a crash is introduced. Index U** analysis is performed to present the load transfer and load paths.

1.3 Thesis Structure

The thesis starts with an overview of relevant literatures, then steps through each of the major aspects of the research shown in the flow chart (Fig. 1.5), and finally concludes with results, conclusions and recommendations for future research on this topic.

In **Chapter 1** the research background and the objective of present study is introduced. A review of literatures about load transfer analysis methods is covered. The procedure of this study using indexes U* and U**to analyze dynamic impact problems is shown.

Chapter 2 of this thesis, contains a review of conventional load path theories covering internal stiffness, index U* and its distribution, load path, three conditions for structural designs, verification of U* analysis using the structural optimization, internal compliance, index U**, comparison of U*, U** and stress distribution, index U*sum, index U**sum, and histograms of U*sum and U**sum.

In **Chapter 3** the methodology of the load transfer and load path analyses for vehicle structures under frontal impact is proposed and discussed, which is the innovation of this research. Dynamic-static method and substitution method are introduced for the analysis of truck cabs. The calculation procedure is plotted. Approaches of the elastic passenger compartment 'Safety Cage' are introduced for the analysis of passenger car models.

The sophisticated calculation models of the truck and the passenger car are described in **Chapter 4**. Here regarding to the characteristics of trucks and cars under frontal collisions, different boundary conditions are discussed from the realization of the load transfer and load paths. Based on the different boundary conditions, approaches for load path analyses are introduced. Related parameters of each model are listed as well.

The focus of **Chapter 5** is on the dynamic calculation results of both the truck model (UD. Truck) and the passenger car model (Dodge Neon). The effectiveness of the elastic assumption for the compartment of the passenger car model in the early crash stage is investigated, and the validation of the assumption is examined based on the comparison of the simulation results between simplified and original passenger car models.

In **Chapter 6**, the results of static load transfer and load path analyses for truck cab structures are shown. The effect of sample time t and parameter m in U** distribution is discussed. Load paths along the main members and the load transfer in both floor panels and tunnel structure are represented.

From the same manner, the index U* is used to obtain the results of static load transfer and load path analyses for truck cab structures. A comparison of index U* and index U** for investigating the load transfer and load paths for truck cab structures is discussed in **Chapter 7**.

The results using the index U*sum and histogram to examine the load transfer and load paths are described in **Chapter 8**. The study of histograms reveals the contributions of different substructures obviously. The load paths are also assessed by studying the uniformity of index U*sum.

The static load path analysis for passenger car using index U** is described in **Chapter 9**. The results of U** and U**sum distributions in the passenger car compartment are shown. Floor panels are the most important structure to resist impact loadings and transferring loadings based on the observation of U** and U**sum distributions. Pillars and side sills also demonstrate effects in the load transfer. The histogram of U**sum are discussed to examine the passenger car compartment.

Finally, in **Chapter 10**, the research findings are summarized, conclusions drawn and the scope for future research in this area is discussed.

2. Load Path Analysis Using Indexes U* and U**

2.1 Review of the U* Index [82, 88, 89]

2.1.1 Internal Stiffness

A linear elastic structure with a loading point A and a supporting point B is shown in Fig. 2.1(a). In Fig. 2.1(a), the simple spring is referred as the internal stiffness between point A and point B schematically. As shown in Fig. 2.1(b), point C is an arbitrary point on the body, and two springs which are connected with point A and point B are the internal stiffness to loading point and supporting point, respectively. The internal stiffness is proposed to represent the elastic constant between any two points. It should be noted that the terminology "Internal Stiffness" mentioned in this section is different from the stiffness terms using in Finite Element Method (FEM) in which by assembling the local

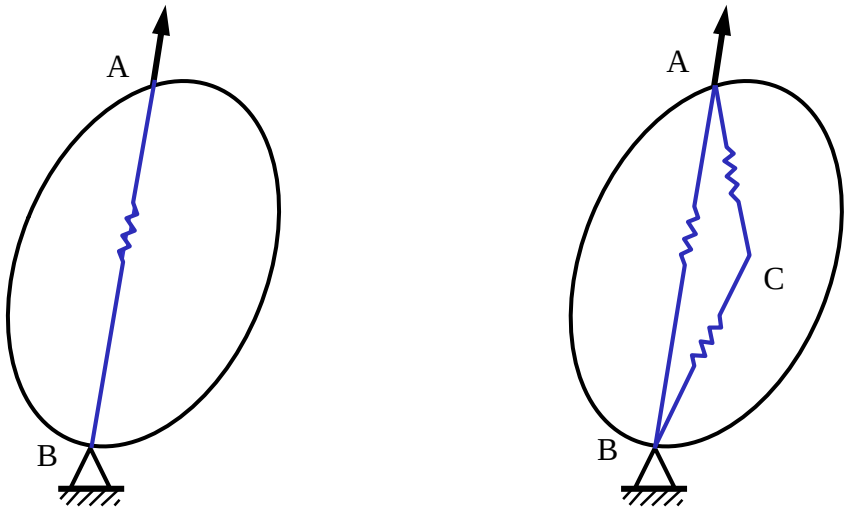

(a) (b)

Fig. 2. 1 Internal Stiffness

stiffness of each element the global stiffness matrix is obtained.

*2.1.2 Definition of Index U**

When the linear elastic body is subjected to the forced displacement as shown in Fig. 2.2(a), the relationship between forces and displacements is represented as follows:

$$\begin{Bmatrix} \boldsymbol{p}_A \\ \boldsymbol{p}_B \\ \boldsymbol{p}_C \end{Bmatrix} = \begin{bmatrix} \boldsymbol{K}_{AA} & \boldsymbol{K}_{AB} & \boldsymbol{K}_{AC} \\ \boldsymbol{K}_{BA} & \boldsymbol{K}_{BB} & \boldsymbol{K}_{BC} \\ \boldsymbol{K}_{CA} & \boldsymbol{K}_{CB} & \boldsymbol{K}_{CC} \end{bmatrix} \begin{Bmatrix} \boldsymbol{d}_A \\ \boldsymbol{d}_B \\ \boldsymbol{d}_C \end{Bmatrix} \tag{2.1}$$

where $\boldsymbol{K}$, $\boldsymbol{p}$, and $\boldsymbol{d}$ with suffixes are the internal stiffness tensor, force vector, and displacement vector, respectively. The expression of Eq. 2.1 is to indicate the overall behaviour of an entire structure with respect to a loading point, a constraint point and an arbitrary point. Equation 2.1 is not the elementary formulation of FEM. It indicates the overall behaviour of a whole structure.

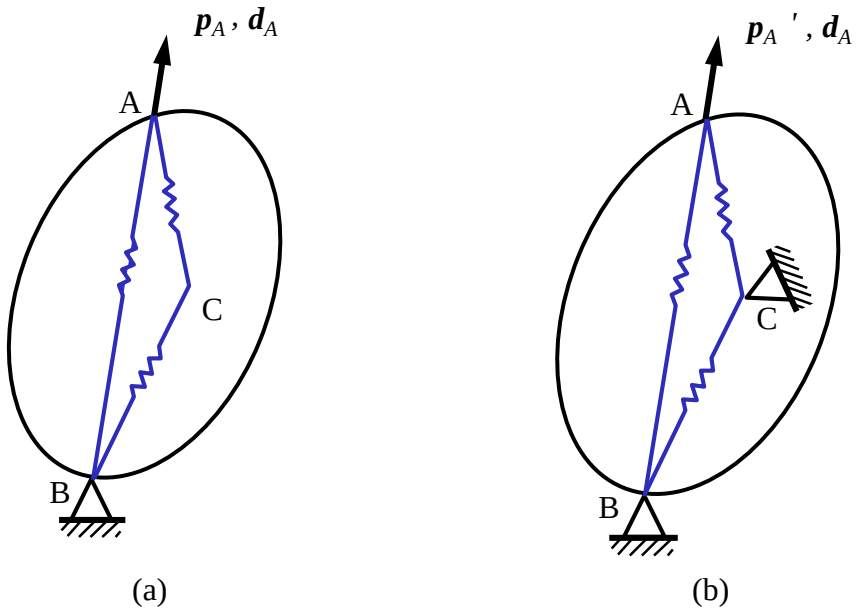

Fig. 2. 2 Definition of Index U*

As shown in Fig. 2.2(a), when a forced displacement is applied to Point A, and Point C is free, the strain energy stored in the entire elastic body is denoted as *U* shown in Eq. 2.2.

$$U = \frac{1}{2}\boldsymbol{p}_{\mathrm{A}} \cdot \boldsymbol{d}_{\mathrm{A}} \tag{2.2}$$

where $\boldsymbol{p}_{\mathrm{A}}$ can be obtained based on Eq. 2.1

$$\boldsymbol{p}_{\mathrm{A}} = \boldsymbol{K}_{\mathrm{AA}}\boldsymbol{d}_{\mathrm{A}} + \boldsymbol{K}_{\mathrm{AB}}\boldsymbol{d}_{\mathrm{B}} + \boldsymbol{K}_{\mathrm{AC}}\boldsymbol{d}_{\mathrm{C}} \tag{2.3}$$

When Point B is fixed ($\boldsymbol{d}_{\mathrm{B}}$=0), $\boldsymbol{p}_{\mathrm{A}}$ is simplified as shown in Eq. 2.4.

$$\boldsymbol{p}_{\mathrm{A}} = \boldsymbol{K}_{\mathrm{AA}}\boldsymbol{d}_{\mathrm{A}} + \boldsymbol{K}_{\mathrm{AC}}\boldsymbol{d}_{\mathrm{C}} \tag{2.4}$$

Substituting Eq. 2.4 into Eq. 2.2, we obtain the next relation.

$$U = \frac{1}{2}\left(\boldsymbol{K}_{\mathrm{AA}}\boldsymbol{d}_{\mathrm{A}} + \boldsymbol{K}_{\mathrm{AC}}\boldsymbol{d}_{\mathrm{C}}\right) \cdot \boldsymbol{d}_{\mathrm{A}} \tag{2.5}$$

Figure 2.2(b) shows the same elastic body under the condition that the point C is constrained. The external force at point A for the same forced displacement $\boldsymbol{d}_{\mathrm{A}}$ is denoted as $\boldsymbol{p}'_{\mathrm{A}}$ in this case. The Eq. 2.1 is still valid, but the displacements $\boldsymbol{d}_{\mathrm{B}}$ and $\boldsymbol{d}_{\mathrm{C}}$ are reduced to zero. Referring Eq. 2.4, we have

$$\boldsymbol{p}'_{\mathrm{A}} = \boldsymbol{K}_{\mathrm{AA}}\boldsymbol{d}_{\mathrm{A}} \tag{2.6}$$

and the strain energy stored in the entire elastic body is denoted as *U'* shown in Eq. 2.7.

$$\begin{aligned} U' &= \frac{1}{2}\boldsymbol{p}'_{\mathrm{A}} \cdot \boldsymbol{d}_{\mathrm{A}} \\ &= \frac{1}{2}\left(\boldsymbol{K}_{\mathrm{AA}}\boldsymbol{d}_{\mathrm{A}}\right) \cdot \boldsymbol{d}_{\mathrm{A}} \end{aligned} \tag{2.7}$$

Since the matrix $\boldsymbol{K}_{\mathrm{AA}}$ show the degree of connection between point A and point C as mentioned above, *U'* also expresses the degree of connection between point A and point

C for the displacement $\boldsymbol{d}_A$. A non-dimensional value of *U'* is expressed by dividing Eq. 2.7 by Eq. 2.5, shown in Eq. 2.8.

$$\frac{U'}{U} = \frac{\left(\boldsymbol{K}_{AA}\boldsymbol{d}_A\right)\cdot\boldsymbol{d}_A}{\left(\boldsymbol{K}_{AA}\boldsymbol{d}_A + \boldsymbol{K}_{AC}\boldsymbol{d}_C\right)\cdot\boldsymbol{d}_A} \tag{2.8}$$

The value of *U'*/*U* also expresses the degree of connection between point A and point C. For a structure modeled as a single spring as shown in Fig. 2.3(a) where *s* is the coordinate along the load path and *l* is the length of the load path, the value of *U'*/*U* decays hyperbolically plotted in Fig. 2.3(b). In Fig. 2.3(c), the non-dimensional value of

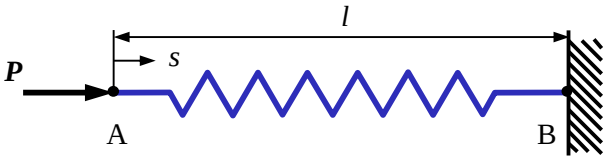

(a) Spring model

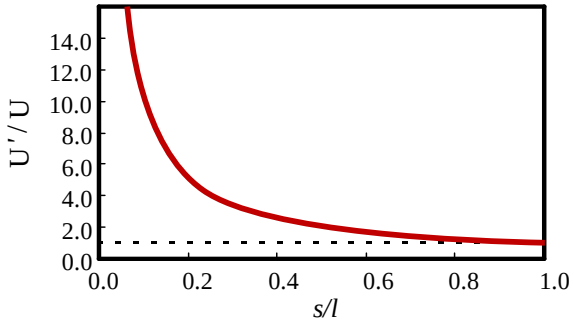

(b) U'/U distribution

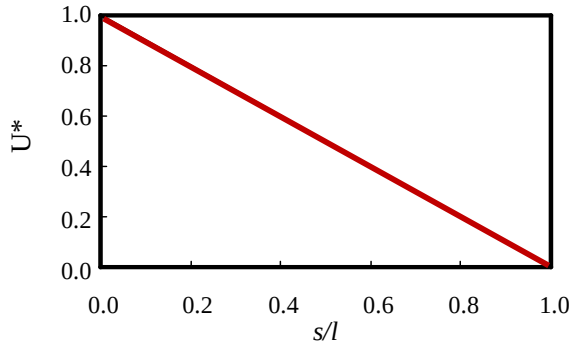

(c) U* distribution

Fig. 2. 3 Linearization of Index U*

U* defined below decays linearly.

$$
\begin{aligned}
U^* &\equiv 1-\frac{U}{U'} \\
&= 1-\frac{\left(\boldsymbol{K}_{AA}\boldsymbol{d}_A+\boldsymbol{K}_{AC}\boldsymbol{d}_C\right)\cdot\boldsymbol{d}_A}{\left(\boldsymbol{K}_{AA}\boldsymbol{d}_A\right)\cdot\boldsymbol{d}_A} \\
&= \frac{-\left(\boldsymbol{K}_{AC}\boldsymbol{d}_C\right)\cdot\boldsymbol{d}_A}{\left(\boldsymbol{K}_{AA}\boldsymbol{d}_A\right)\cdot\boldsymbol{d}_A} \\
&= \left(\frac{\left(\boldsymbol{K}_{AA}\boldsymbol{d}_A\right)\cdot\boldsymbol{d}_A+\left(\boldsymbol{K}_{AC}\boldsymbol{d}_C\right)\cdot\boldsymbol{d}_A-\left(\boldsymbol{K}_{AC}\boldsymbol{d}_C\right)\cdot\boldsymbol{d}_A}{-\left(\boldsymbol{K}_{AC}\boldsymbol{d}_C\right)\cdot\boldsymbol{d}_A}\right)^{-1} \\
&= \left(1-\frac{2\left(\frac{1}{2}\left(\boldsymbol{K}_{AA}\boldsymbol{d}_A+\boldsymbol{K}_{AC}\boldsymbol{d}_C\right)\cdot\boldsymbol{d}_A\right)}{\left(\boldsymbol{K}_{AC}\boldsymbol{d}_C\right)\cdot\boldsymbol{d}_A}\right)^{-1} \\
&= \left(1-\frac{2U}{\left(\boldsymbol{K}_{AC}\boldsymbol{d}_C\right)\cdot\boldsymbol{d}_A}\right)^{-1}
\end{aligned}
\tag{2.9}
$$

where $\boldsymbol{K}_{AC}$ is the degree of connectivity between Point A and Point C. Thus, index U* can be used to reveal the internal stiffness of a structure. Equation 2.10 is obtained shown as follows.

$$
U^* = \left(1-\frac{2U}{\boldsymbol{K}_{AC}\cdot\boldsymbol{S}}\right)^{-1}, \quad \boldsymbol{S}\equiv\boldsymbol{d}_A\otimes\boldsymbol{d}_C \tag{2.10}
$$

where tensor and vector notations are employed instead of matrix notation for the products. The notations $\boldsymbol{a}\cdot\boldsymbol{b}$ and $\boldsymbol{a}\otimes\boldsymbol{b}$ indicate inner and tensor products, respectively, for vectors $\boldsymbol{a}$ and $\boldsymbol{b}$. Using index notations, these direct notations are described as $a^i b_i$ and $a^i b_j$, respectively. The inner product of tensors $\boldsymbol{A}$ and $\boldsymbol{B}$ is denoted as $\boldsymbol{A}\cdot\boldsymbol{B}$, which is described as $A_{ij}B^{ij}$ using index notation. The summation convention is used in the above index notations. We call the symbol $\boldsymbol{S}$ the path displacement tensor. It can be seen that the value of U^* is unity at the loading point A and zero at the supporting point B.

We call the value of Eqs. 2.9 and 2.10 the index U*, which is described in terms of $\boldsymbol{K}_{AC}$, and which indicates the degree of connectivity between Points A and C.

2.2 Distribution of U* and Load Paths [85, 88, 89, 91, 93, 97]

An example of a U* distribution and a load path are shown in Fig. 2.4. For a flat plate with a circular hole, an in-plane forced displacement is applied. The calculated U* distribution is depicted by the potential lines for U*. Orthogonal lines referred to as "stiffness lines" are also shown. The specific stiffness line that has the smallest gradient is the ridge line on the curved surface of the potential for U*. We define this line as the "load path", because it can be regarded that the smallest gradient line of the U* surface which transfers the largest loading.

In other words, if a vector $\boldsymbol{\lambda}$ is defined by

$$\boldsymbol{\lambda} = -\mathrm{grad}U^* \tag{2.11}$$

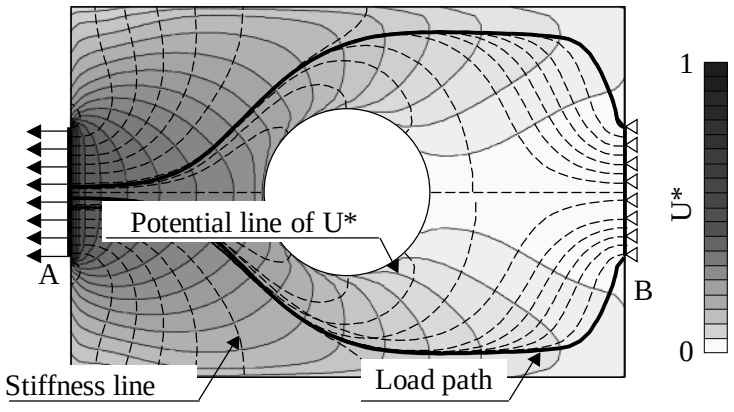

Fig. 2. 4 Distribution of U* and Load Paths

the load path is the successively traced line along the smallest $\boldsymbol{\lambda}$ value. The vector $\boldsymbol{\lambda}$ is a conservative quantity because of the following relation showing that the value $\boldsymbol{\lambda}$ of is conservative:

$$\mathrm{rot}\boldsymbol{\lambda} = \mathrm{rot}\left(-\mathrm{grad}U^*\right) = \mathbf{0} \tag{2.12}$$

In Fig. 2.4 potential lines for U* and the stiffness lines are indicated with thin solid lines and dashed lines, respectively. The two load paths are represented as thick solid lines. The effect of stress concentration is excluded along the path. This corresponds to our intuitive expectation.

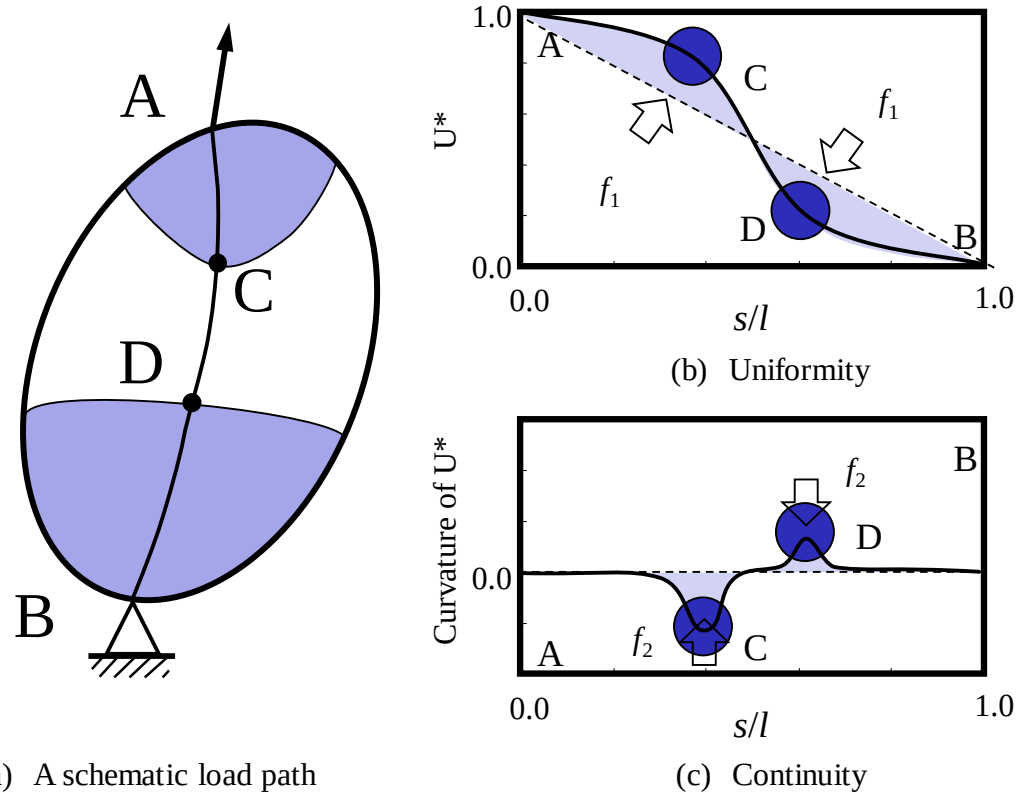

(a) A schematic load path (b) Uniformity (c) Continuity

Fig. 2. 5 Uniformity and Continuity of Load Path

2.3 Three Conditions for Structural Design [84, 89, 90, 97]

2.3.1 Uniformity of Load Path

Figure 2.5(a) schematically shows a load path in a structure with relatively stiff domains, which is indicated by shaded areas. Figure 2.5(b) denotes the distribution of U* along the load path, where *s* is the coordinate along the load path and *l* is the length of the load path. The decay of the internal stiffness can be represented at point C and point D in this figure. Homogeneity of the internal stiffness is necessary for desirable structures. The area f_1 shown in Fig. 2.5(b) is an example of measures to express the degree of uniformity for this condition.

2.3.2 Continuity of Load Path

We can recognize the discontinuities of the stiffness from a distribution curve of the

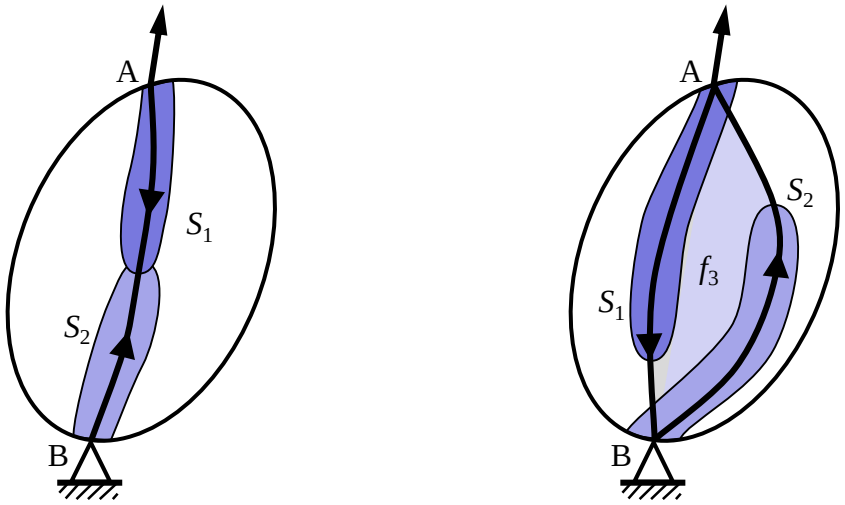

(a) (b)

Fig. 2. 6 Consistency of Load Path

curvature of U* which is the second derivative of U* with respect to *s* more precisely, as shown in Fig. 2.5(c). Continuity of the stiffness along the load path is another condition for desirable structures. The area f_2 shown in Fig. 2.5(c) is an example of measures to express the degree of discontinuity.

2.3.3 Consistency of Load Path

Figure 2.6 shows another model of a structure. The load path from the loading point A is obtained from the ridge line of the contour lines of U* distribution, S_1 in Fig. 2.6(b). The load path from the supporting point B is obtainable with the same procedure, S_2 in Fig. 2.6(b). It is worth noting that the load paths from the loading point A, S_1, and from the supporting point B, S_2, are not coincident with each other in Fig. 2.6(b).

It is desirable that the two paths S_1 and S_2 are coincident with each other in the structure, as shown in Fig. 2.6(a). Consistency of the load paths S_1 and S_2 is the third condition for desirable structures. The area f_3 shown in Fig. 2.6(b) expresses the degree of inconsistency for this condition.

2.4 Structural Optimization Using U* Index [97, 99, 122]

2.4.1 Optimization model

To validate the concept of U* being applicable to structures, an optimization process using a Genetic Algorithm (GA) in terms of U* was introduced. Figure 2.7(a) shows an initial model as an example of optimization calculations.

The objective function was determined by above-mentioned three conditions.

1) Uniformity: Uniform decay of U* along a path

2) Continuity: Smoothness of the curvature of U* along a path

3) Consistency: Coincidence between a path from Point A and a path from Point B

A design parameter is the thickness of FE model. The analytical objective function F is defined as

$$\begin{cases} F = \alpha_1 f_1^* + \alpha_2 f_2^* + \alpha_3 f_3^* \\ f_i^* = \dfrac{\overline{f}_i - f_i}{\overline{f}_i} \quad (i = 1,2,3) \end{cases} \tag{2.13}$$

where $\overline{f}_i$ is the average of f_i values in the initial generation, indexes f_i are the values of three conditions (uniformity, continuity, and consistency), and α_i is the weigh function.

2.4.2 Desirable structure

The design parameter was the thickness of each element in the flat plate model shown in

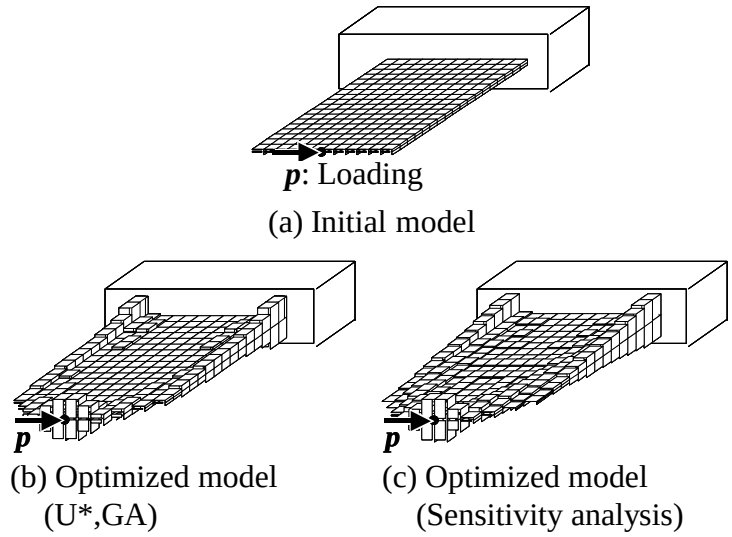

p: Loading

(a) Initial model

(b) Optimized model (U*,GA)

(c) Optimized model (Sensitivity analysis)

Fig. 2. 7 Structural Optimization

Fig. 2.7(a). The optimized structure in the 50th generation of the GA using U* is shown in Fig. 2.7(b). For comparison, the result of conventional optimization using sensitivity analysis of strain energy density is shown in Fig. 2.7(c). We can see that there is no significant difference in the thickness distribution, which verifies the effectiveness of the U* theory. During the optimization process, the thickness distribution developed once into the Michell truss pattern but eventually reached a simple pattern using the operation of intensification.

It is important to see that this objective function using U* has no relationship to the concepts of stress, strain, or strain energy density. Generally, the strain energy density is suitable for strength studies, and U* is adequate for studies of load transfer. Both are necessary to achieve structural improvements.

2.5 Review of Index U**: A Complementary Concept of Index U* [98]

The index U** has been introduced as a complementary concept to index U*. The loading condition at Point A (Fig. 2.2(a)) is changed from the forced displacement $\boldsymbol{d}_A$ to the loading $\boldsymbol{p}_A$ shown in Fig. 2.8(a). The inverse expression of Eq. 2.1 is:

$$\begin{Bmatrix} \boldsymbol{d}_A \\ \boldsymbol{d}_C \end{Bmatrix} = \begin{bmatrix} \boldsymbol{C}_{AA} & \boldsymbol{C}_{AC} \\ \boldsymbol{C}_{CA} & \boldsymbol{C}_{CC} \end{bmatrix} \begin{Bmatrix} \boldsymbol{p}_A \\ \boldsymbol{p}_C \end{Bmatrix} \tag{2.14}$$

where the quantities related to point B are not written to avoid a singularity in the rigid translation. Each tensor $\boldsymbol{C}$ with suffixes is the internal compliance. In other words, the

variable is exchanged from displacement to force, which is the same operation as the Legendre transformation.

The complementary index U** is defined as

$$\begin{aligned} U^{**} &\equiv 1-\frac{W'}{W} \\ &= 1-\frac{(\boldsymbol{C}_{AA}\boldsymbol{p}_A+\boldsymbol{C}_{AC}\boldsymbol{p}'_C)\cdot\boldsymbol{p}_A}{2\left(\frac{1}{2}(\boldsymbol{C}_{AA}\boldsymbol{p}_A)\cdot\boldsymbol{p}_A\right)} \\ &= -\frac{(\boldsymbol{C}_{AC}\boldsymbol{p}'_C)\cdot\boldsymbol{p}_A}{2W} \\ &= -\frac{\boldsymbol{C}_{AC}\cdot\bar{\boldsymbol{S}}}{2W}, \qquad \bar{\boldsymbol{S}} \equiv \boldsymbol{p}_A \otimes \boldsymbol{p}'_C \end{aligned} \tag{2.15}$$

where W is the complementary strain energy stored in the entire body when Point C is free (Fig. 2.8(a)), and the value W' is the complementary strain energy when Point C is constrained (Fig. 2.8(b)). Notation $\boldsymbol{p}'_C$ denotes the force that should be applied to Point C

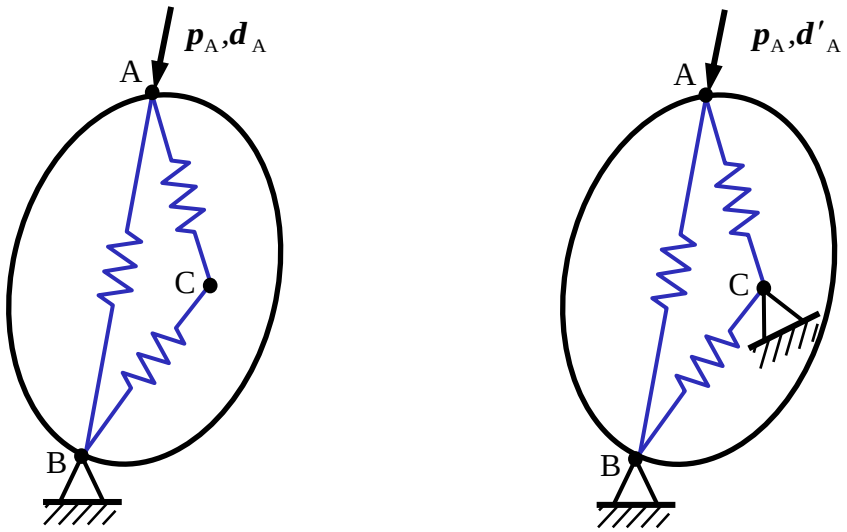

(a) (b)

Fig. 2. 8 Index U**

in order to constrain it.

Index U* and its complementary index U** for the load transfer analysis have been introduced so far. Based on the definition of two indexes, it can be found that indexes U* and U** are generated from the ratio of strain energies and complementary strain energy, respectively. From the viewpoint of thermodynamic potentials, they correspond to the particular isothermal state of Helmholtz free energy and Gibbs free energy.

2.6 Comparison of U*, U**, and Stress Distributions

2.6.1 Stress and U Distributions [84, 90]*

As we mentioned in Chapter 1, although it is difficult to express the load transfer by means of the stress distribution, the U* or U** analysis can solve the problem of the stress concentration. In fact, as shown in Fig. 2.9(a), the maximum principal stress distribution of the frontal part of a truck compartment is presented. The absolute values of the principal stresses in the middle plane of each panel are shown. The cab is supported at the roof side rail and the vertical loading is applied at the front left side bracket. Large stress values are observed around the holes, and hence, we cannot discuss the load transfer or load path from the pattern of the stress distribution. However, the distribution of U*, in Fig. 2.9(b), shows the load transfer clearly. We can see that the loading is transferred through the horizontal beam.

From Figs. 2.7 and 2.9, we can summarize that by the usage of indexes U* and U** we can obtain a reasonable design for a structure without the effect of stress concentrations. When using the index U* and GA in structure optimizations, we can obtain a result with higher stiffness and lower stress in distributions. It is not the aim to use indexes U* and U** to decrease the stress distribution, but it is a by-product obtained automatically. Moreover, if using indexes U* and U** to make structural designs, we can avoid cracks and fractures by decreasing the stress distributions in the global point of view. When considering the localization effects, the stress concentrations should be dealt with case by case which is not the main job of indexes U* and U**.

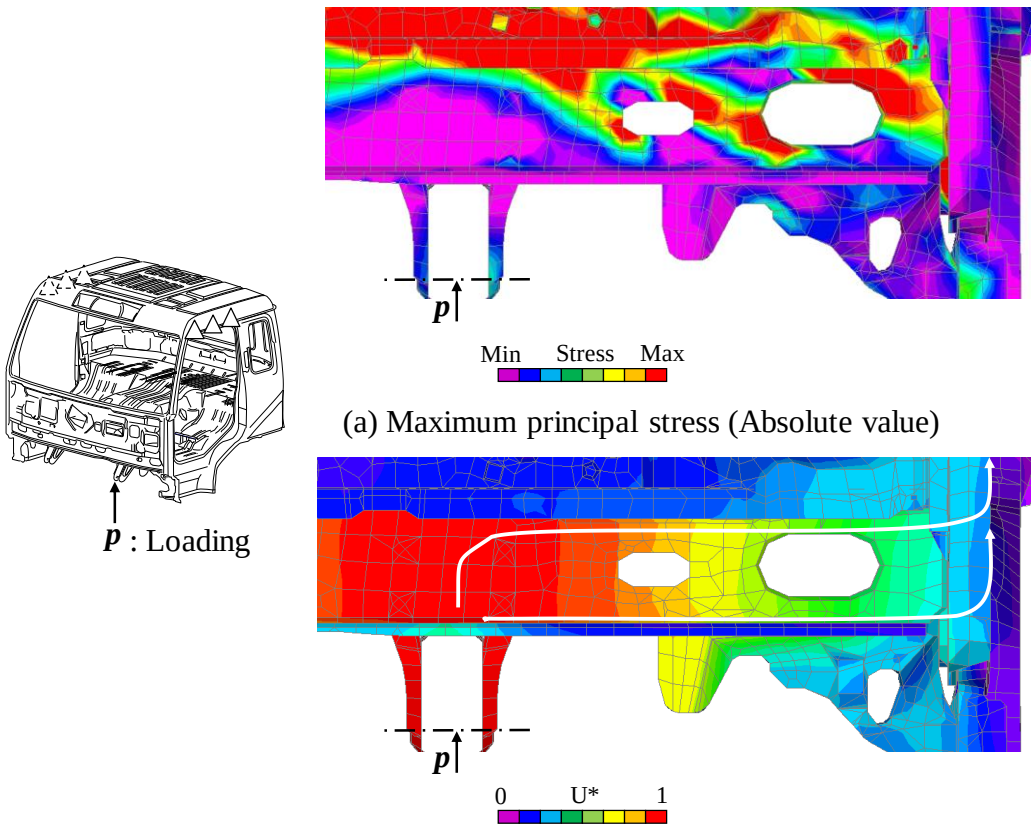

(a) Maximum principal stress (Absolute value)

(b) Distribution of U*

Fig. 2. 9 Distribution of Principal Stress and U (Frontal View)**

2.6.2 Distributions of U and U***

The calculation results for U* and U** indices are compared for a simplified aircraft wing model as shown in Fig. 2.10, where the wing length is 8,000mm, and the thickness of the surface panels and the bulkheads is 2mm. The distributions seen in these two figures for U* and U** correspond fairly well to each other.

Another calculation results for U* and U** are compared for a plate model with a hole

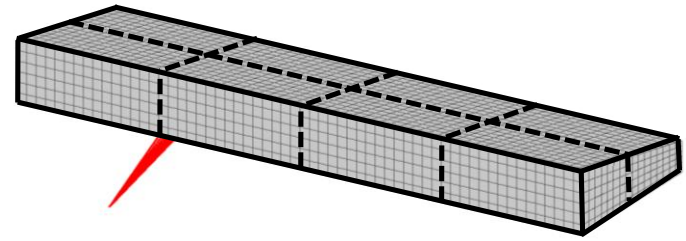

(a) Model

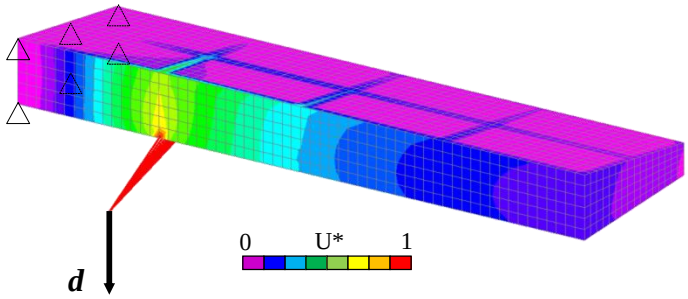

(b) Distribution of U*

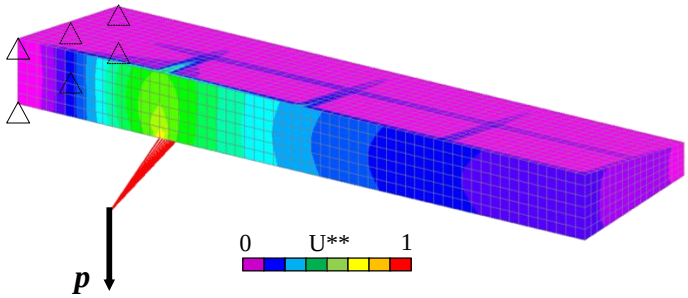

(c) Distribution of U**

Fig. 2. 10 Distribution of U* and U in Simplified Airplane Main Wing**

[98] as shown in Fig. 2.11. The number of finite elements is 2,200, and MSC.Nastran [123] is used for the calculation. The distributions seen in these two figures also show a fairly well correspondence to each other. Although small differences are observed, this is inevitable due to the different definitions of the load transfer.

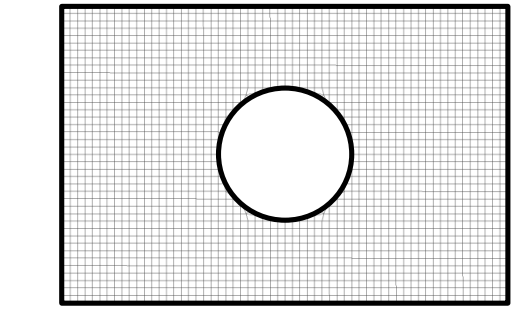

(a) Model

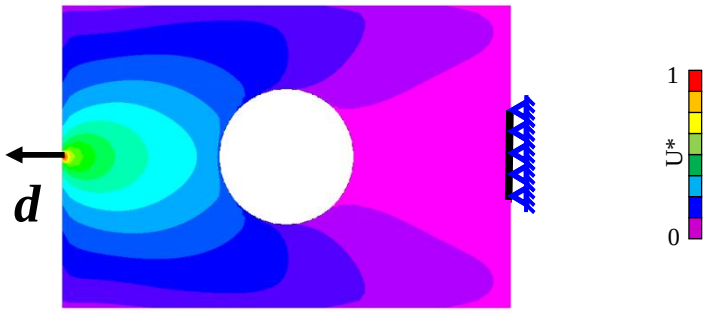

(b) Distribution of U*

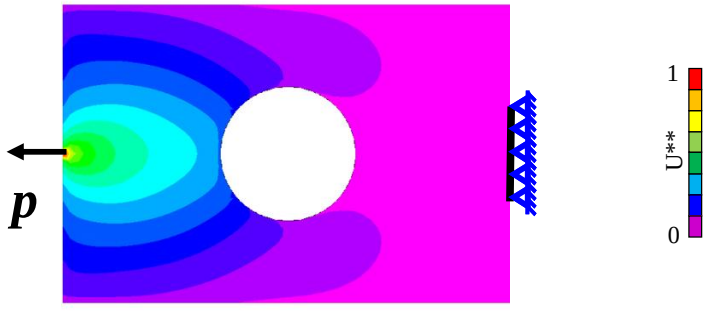

(c) Distribution of U**

Fig. 2. 11 Distribution of U* and U in Plate with Circular Hole**

When a flat panel is under distributed loading condition shown in Fig. 2.12, the U* and U** distributions are presented [98]. The number of finite elements is 5,400. The stiffen cross-members are highlighted in dark color shown in Fig. 2.12(a). The results reveal the advantageous of using index U** to make the load transfer and load path analyses under distributed loading conditions. For crash analyses, the distributed force caused by the inertial force is important. For this reason, U** is used in the present study to allow for a future extendibility. Summation Indexes U*sum and U**sum [124]

*2.6.3 Definitions of Indexes U*sum and U**sum*

Generally, in structures, parts strongly connected to a loading point and those connected to a supported point are different. When a stiff member extends to a certain point and

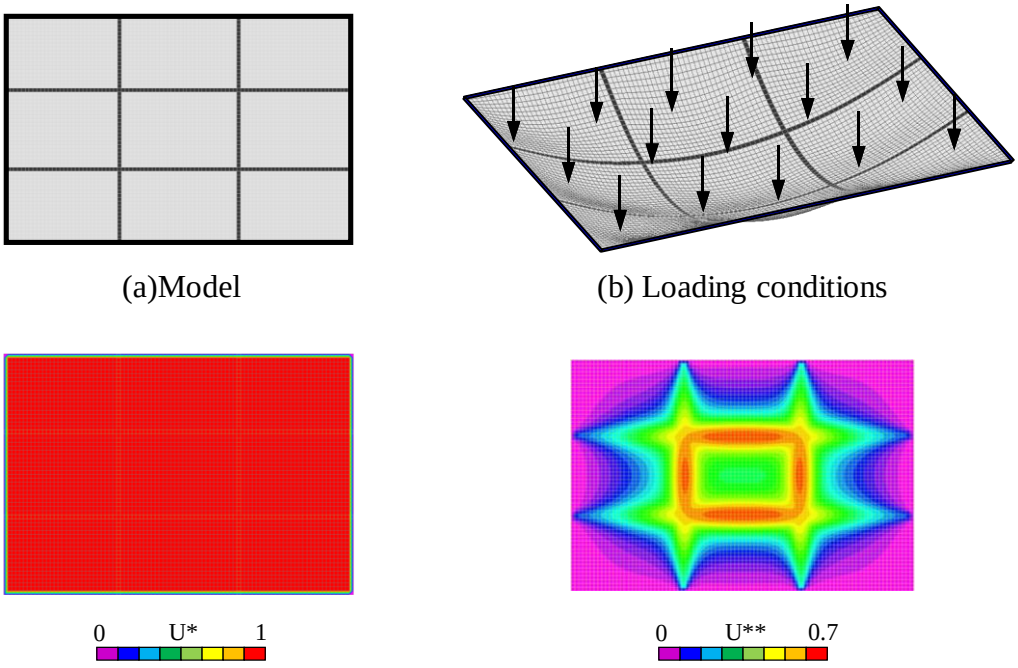

(a)Model (b) Loading conditions

(c) Distribution of U* (d) Distribution of U**

Fig. 2. 12 Comparison of U* and U Distributions**

vanishes at that point, such a member is not always supported by the supporting point. In other words, the load path from the loading point A and the load path from the constraint point B do not coincide in general, as shown in Fig. 2.6(b). The degree of connectivity between a loading point and an arbitrary point is expressed by the ordinary U* distribution. The degree of connectivity between a supporting point and the arbitrary point can be depicted by exchanging the loading point and the supporting point. These U* distributions generally have no relation to each other.

If we take the summation of these U* distributions, we would have the following index. A simple linear spring and the U* distributions are shown in Fig. 2.13(a). The U* distribution from the loading point A decreases linearly, and U* from the supporting point B becomes a symmetrically decreasing line, because of the exchange of the loading point and the supporting point. The summation of these U* distributions becomes a horizontal line having the value 1. Since a simple spring can be regarded as the optimum structure that conveys a uniform loading, the value 1 of the U* summation can be thought as an indication of ideal load transfer. We denote the summation of U* as "U*sum". From the same manner, the summation of U** is proposed and denoted as “U**sum”. Due to the definition of index U** the summation value of U**sum may be equal or smaller than U*sum.

*2.6.4 Histograms of Indexes U*sum and U**sum*

As mentioned above, U* itself takes a value between 0-1. Hence, the value of U*sum takes a value between 0-2. To depict the U*sum histogram [124], the calculated values of

U*sum are taken on the abscissa and divided into several intervals, and the nodes number frequencies in these intervals are plotted on the ordinate. In an actual expression, the frequency is normalized to the density function.

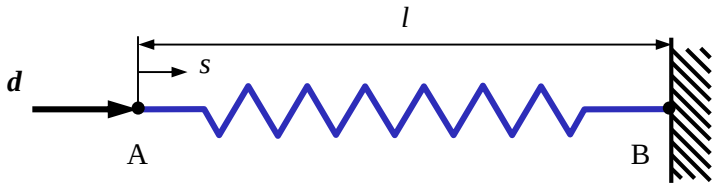

(a) Spring model

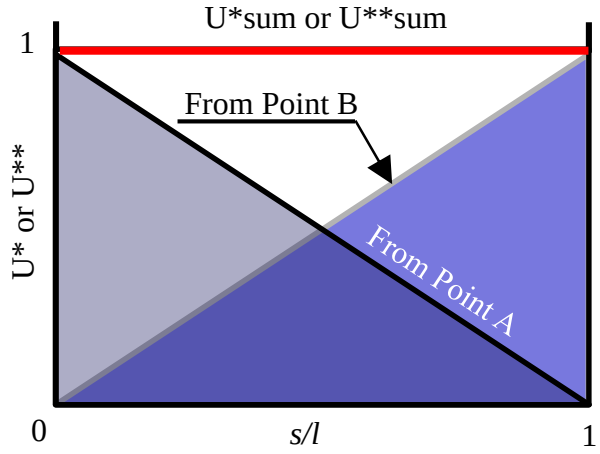

(b) Distribution of U*sum or U**sum

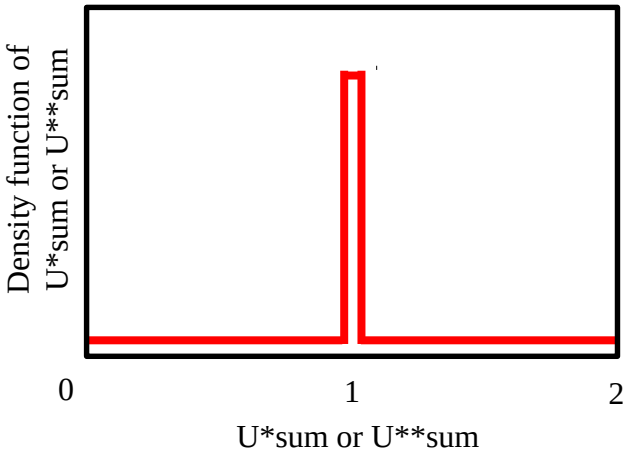

(c) Histogram of U*sum or U**sum

Fig. 2. 13 Definition of Summation of Index U*sum or Usum**

For a simple spring, the histogram is shown in Fig. 2.13(c) as a single peak. This shows an example of an ideal structure. If the structure is not one-dimensional, distributed load paths can be seen in structures as shown in Fig. 2.14. In these cases, U*sum = 1 is not always preferable, but in general, U*sum with a value lower than 1 is desirable, because distributed load paths are more effective. Apart from the average values, a histogram with a sharp peak is preferable, because the uniformly distributed U*sum that characterizes a small variance histogram is desirable. The similar conclusions can be derived for the index U**sum and its histogram.

Consequently, a histogram with a low average and small variance is desirable for ideal structures.

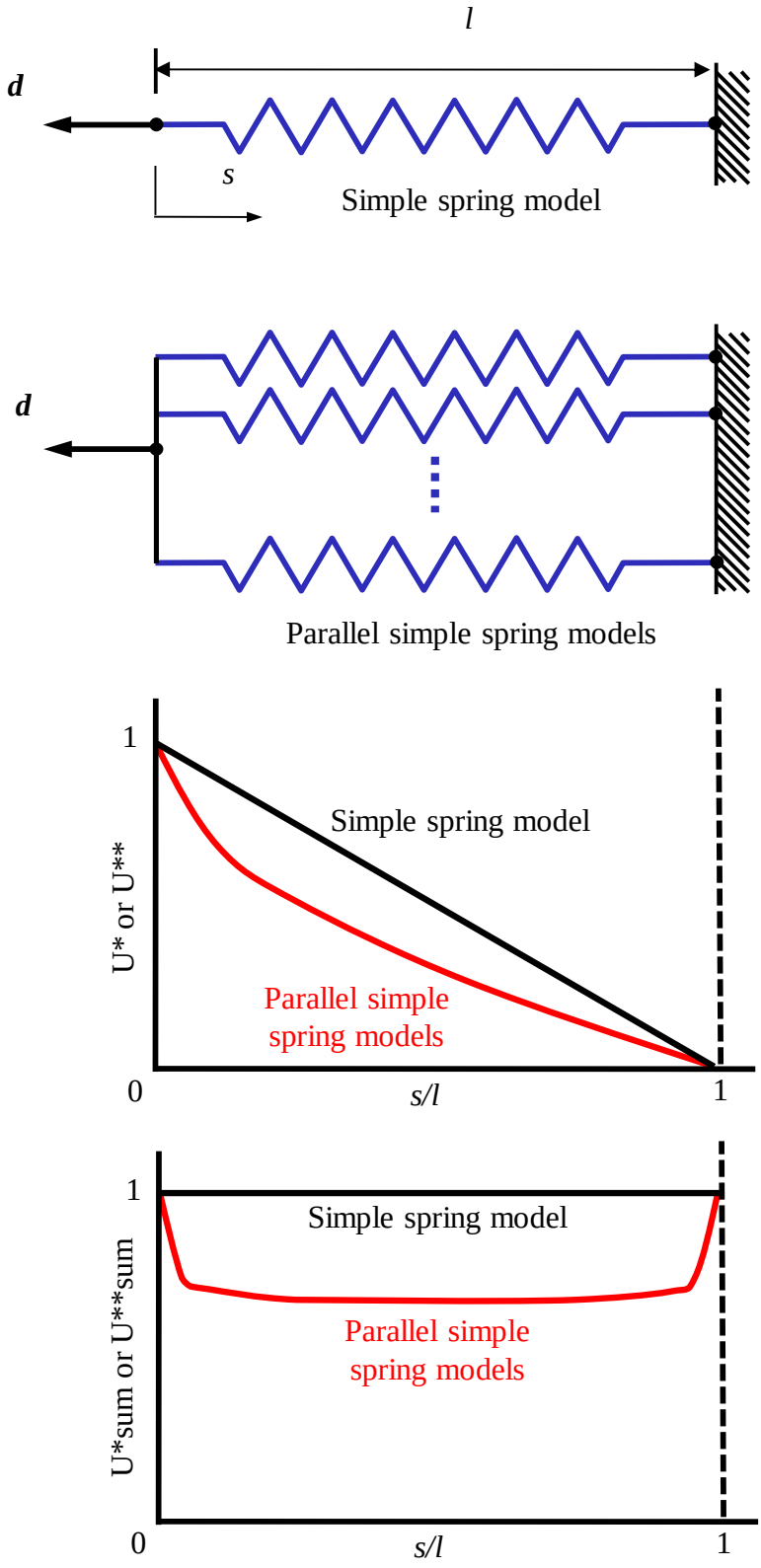

Fig. 2. 14 Uniformity of U* or U and U*sum or U**sum**

3. Methodology of Load Transfer and Load Path Analysis for Vehicle Structures under Impact

3.1 Background

The schematic diagram shown in Fig. 1.4 illustrates the load transfer from the front end of a vehicle to its body. Also, a lot of time has been spent in understanding the load transfer in the design stage of vehicle bodies, and such sketches are often found in documents for body structure designs. However, after the development of a vehicle body, verification of these ideas is difficult because of the lack of a method or tool to present the load transfer or realization of the load paths as shown in Fig. 2.4.

The examples shown in Figs. 2.9, 2.10, 2.11, and 2.12 are linear static analyses. However, for nonlinear crash analyses, it is difficult to apply the U* and U** calculation directly. A method to express the load transfer and load paths should be proposed to show quantified values for nonlinear crash problems. For this purpose, at first we need to consider *When*, *Where*, and *How* to apply the linear U* and U** analyses to the collision problems.

The conventional studies and theories have been reviewed so far. From this chapter, originalities and new findings will be mentioned and introduced.

3.2 Vehicle Structures

There are many kinds of automotives such as SUV (Sport Utility Vehicle), sedan, van, wagon, MPV (Multi-Purpose Vehicle), pickup, cargo trucks, etc. The schematic pictures of two vehicles are shown in Fig. 3.1. A cab structure of a heavy duty truck and a sedan car are studied numerically under frontal collision. Because the structure of the truck cab is simple in structures and supported by the rear cargo, load path analyses using indexes U* and U** can be applied statically without the effect of inertial forces. The most general sedan car is investigated including the effect of inertial forces.

As mentioned in Chapter 1, when the passenger cars are under frontal collision, the compartment structure 'Safety Cage' is required to have minimum deformations for the safety of the occupants. The impact energies are absorbed based on the deformation of front-ends and rear-ends. In contrast, most of the impact energies of trucks shown in Fig. 3.1(b) are absorbed by based frames.

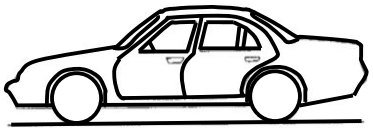

(a) Sedan

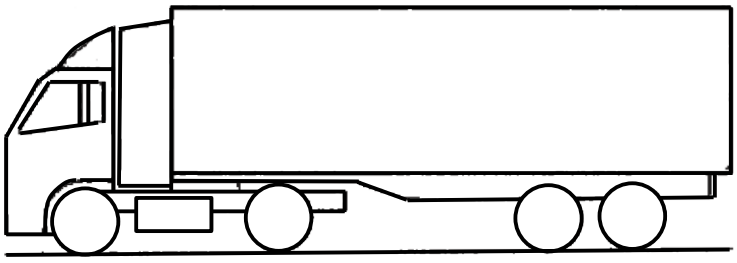

(b) Heavy Duty Truck

Fig. 3. 1 Vehicle Structures

Thus, for the safety of the occupants, the main part of the compartment ‘Safety Cage’, as shown in Figs. 1.2(b), 3.2, and 3.3 should be maintained in the linear elastic condition. The linear U* and U** analyses can be applied to the main part of the compartment. Regarding to the structural differences of passenger vehicles and heavy duty vehicles, the proper assumptions for the load transfer and load path analyses are proposed. Firstly, a truck cab under frontal collision is studied as a typical example for heavy duty vehicles in the early crash stage. Meanwhile, studies of the truck cab are the very first attempts to introduce the conventional static U* and U** analyses into dynamic problems. Secondly, a passenger car under frontal collision is investigated as a typical example for passenger vehicles. Several new methods and approaches for each type of vehicles are proposed to employ the static U* and U** analyses.

3.3 Calculation Method for Heavy Duty Vehicles (Trucks)

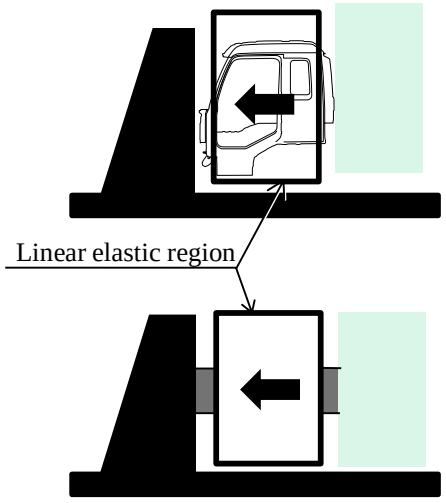

Fig. 3. 2 Truck Cab under Frontal Collision

3.3.1 Dynamic-Static Method

In the study of trucks, we do not intend to trace the time history of the load transfer. Our purpose is to express the load transfer in the initial crash stage for the linear elastic region that is shown in Fig. 3.2. We call this method a “dynamic-static method”.

There is a considerable difficulty in deciding the exact input loading that occurs at the instant of the vehicle body is in contact with the barrier. The vehicle body touches the barrier within an extremely small area at an instant of the collision. Since the contact region between the front end and the barrier is not a large flat area, determining the loading condition is difficult. To avoid this difficulty, the deformation of the front end is calculated using the crash simulation code LS-DYNA [121], and the obtained deformations at several instances during the initial stages of crash are extracted. Afterward, the extracted deformed model for each sample time is calculated using linear elastic analysis code NASTRAN [123] to obtain the U* and U** distribution.

Thus the load transfer is statically calculated for each deformed model that is extracted at each time step during the initial crash stage. As shown in the subsequent Sections, the difference in the U* and U** distributions for each time step is not large, although the distribution of the barrier reaction changes by a large amount even in the initial crash stage. Therefore, we can obtain the aspect of the load transfer in the initial crash stage from any of these U* and U** distributions.

3.3.2 Substitution Method

The second step in applying static U* and U** analyses to a dynamic collision phenomenon is the treatment of non-linear domain. For the safety of occupants, the main part of the compartment (*Safety Cage*) needs to be maintained in the linear elastic region, which is schematically shown in Figs. 1.2(b), 3.2 and 3.3. Extracting the linear elastic region that remains in the initial crash stage, we can apply linear U* and U** analyses to this main part of the compartment. For a model that is extracted at a sample time, substituted properties are assigned to reproduce the material and geometrical nonlinearities for the U* and U** analyses.

We can introduce the following two kinds of "substitution method": substitution-stress method and substitution-modulus method.

(1) Substitution-Stress Method

The stresses that are calculated by the dynamic crash analysis are applied to the linear

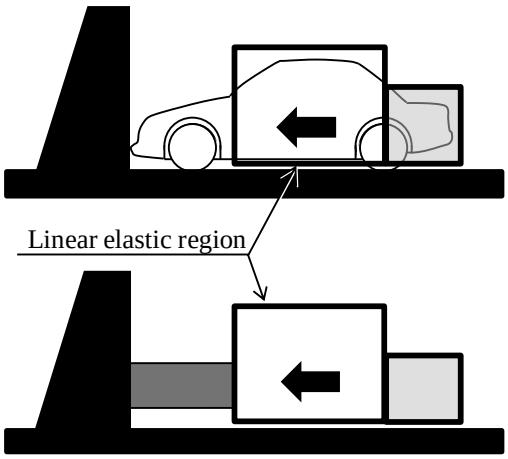

Fig. 3. 3 Passenger Car under Frontal Collision

region in a static calculation along the boundary between the nonlinear and linear region. In other words, as the equivalent effects caused by the nonlinear region, the substitution stresses are applied to the linear region along the interactive boundary. The substitution stresses are schematically shown in Fig. 3.4. Although the substitution-stress method can rigorously reproduce the nonlinear effects in the linear region, data input for the calculations becomes complicated

(2) Substitution-Modulus Method

The substitution-modulus method involves substituting a hypothetical linear modulus for the nonlinear regions. The substitution modulus is determined in Eq. 3.1.

$$E_s = E_i / m, \qquad (m = 1, 2, \ldots) \tag{3.1}$$

where E_i is the initial modulus and m is an arbitrary parameter. Figure 3.5 shows the definition of E_s and m. Comparing this method with the substitution-stress method, although this method provides an approximate approach, the calculation is not complicated. In the present analysis, the substitution-modulus method is used. When taking different values of parameter m, different values of substitution moduli are

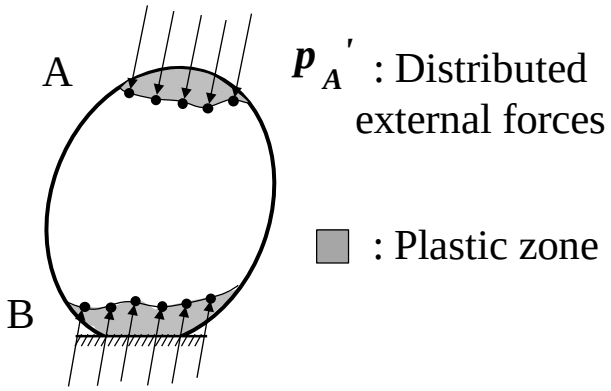

Fig. 3. 4 Substitution Stress Method

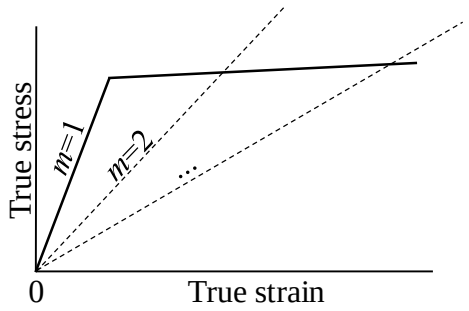

Fig. 3. 5 Substitution Modulus

obtained as shown in Fig. 3.5.

It is necessary to notice that the illustration of dash lines in Fig. 3.5 corresponds to the substitution moduli with different arbitrary value of parameter *m*. In dynamic calculations, the unloading process does not refer to the dash lines but according to the slope of initial elastic modulus.

It is impossible to estimate the correct value of the parameter *m* for each element. Fortunately, the nonlinear areas of the body panels are not so large in the initial stage of

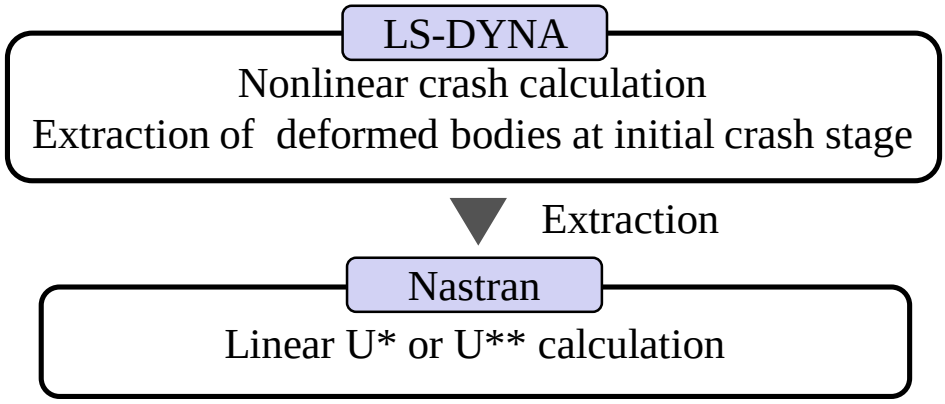

Fig. 3. 6 Calculation Procedure

the impact, as schematically shown in Fig. 3.2. Moreover, U* or U** distribution does not indicate the absolute value but the ratio of the load transfer. Hence the load transfer in the cab depends only slightly on the values of the substitution modulus or parameter *m* as discussed in the subsequent Chapters. The parameter *m* has a small effect on the load transfer, but above all, we can choose the most appropriate value of *m* and determine it as the standard condition for the cab during the initial crash phase.

3.3.3 Calculation Procedure

The process of the calculation is shown in Fig. 3.6. The software codes LS-DYNA and Nastran are used for dynamic and static calculations, respectively.

3.4 Calculation Method for Passenger Vehicles (Passenger Cars)

3.4.1 Separation Structure Method

In the investigation of passenger cars, dynamic-static method is also used to employ the static U** analysis. As mentioned in Section 3.2, an optimal structure of the passenger compartment ‘Safety Cage’ should be mainly elastic during the crashing. From this point of view, we propose an assumption that in the early crash stage (before large deformation appears in passenger compartment) the passenger compartment can be realized as an elastic body. Thus, the load path analysis is applicable for the passenger compartment.

For dynamic simulations, a simplified numerical model is invented based on the above assumption. The original numerical model which was developed based on the

experimental data is also analyzed. In the new numerical model, the properties of substructures in the whole passenger compartment are defined as elastic materials. The properties of rear structures are defined as rigid bodies, due to the minor deformation during the whole impact stages. This approach is called separation structure method. The boundary between the elastic passenger compartment and rear rigid structures will be defined in the next chapter.

3.4.2 Relative Displacement Method

Instead of the substitution modulus method used in the study of trucks, the relative displacement method is proposed for U** calculation of passenger cars. The relative displacement is defined as the variation of distance between each node in the passenger compartment (A_i) and the reference node in the rear structures (B) shown in Fig. 3.7. The definition of the reference node depends on the numerical model. In this study, the reference point is defined as the last node in the centerline of the rear rigid structure with steel properties, which height is the same as floor panels. In dynamic analysis, the relative displacement data of each node are obtained. Then the relative displacement is applied to the deformed model to obtain the equivalent distributed force which can

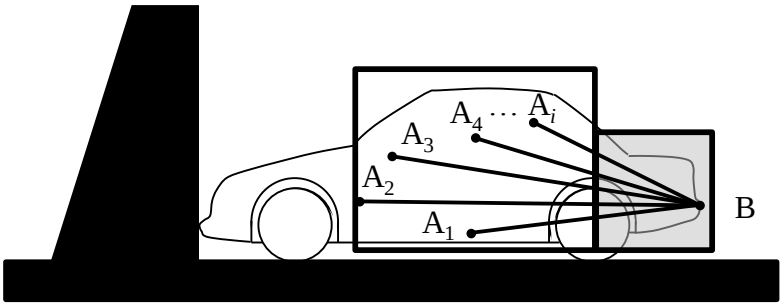

Fig. 3. 7 Relative Deformation

generate the same relative displacement. Then the equivalent distributed force are applied to make U** analyses.

In the present study, an alternative fixation condition is proposed for dynamic calculations to instead of the conventional condition which is free in 6 degrees of freedoms for the sake of simplicity in applying the relative displacement method. Except the degree of the freedom along the impact direction, other 5 degrees of freedoms are constraint in the rear rigid structures in the dynamic impact. The simplification of constraint conditions avoids the rigid rotation in the dynamic results which means that the motion of the reference node (B) only along the impact direction.

3.4.3 Calculation Procedure

The calculation procedure in analyzing passenger car models is the similar as the procedure shown in Fig. 3.6.

3.5 Summary

The following is the summary of the proposed methods for avoiding the difficulty concerning the expression of the load transfer in vehicle structures during frontal collisions.

(1) Large Elastic Volume

For the safety of occupants, the main part of the compartment should be maintained in the linear elastic condition in which the linear U* and U** analyses can be applied.

(2) Dynamic-Static Method

At the moment of impact, the body contacts the barrier at one point. It is meaningless to think about the load transfer under such conditions. Using the crash simulation, however, we can obtain the slightly deformed body under the frontal loading during the initial crash phase. Extracting the deformed body obtained from the dynamic analysis, the U* and U** distributions can statically be calculated.

(3) Substitution-Modulus Method

For a truck model that is extracted at a sample time, a substitution modulus is introduced to reproduce the material and geometrical nonlinearities for the U* and U** analyses.

(4) Separation Structure Method

For a passenger car model, the properties of substructures in the whole passenger compartment are defined as elastic materials, and the properties of rear structures are defined as rigid bodies in both dynamic and static analyses in the initial phase of collision.

(5) Relative Displacement Method

In the load transfer analysis of passenger cars, the relative displacement method is proposed to make static U** analyses of passenger compartments.

In the above approaches, we can show that the time history and the substitution modulus have small effects on the load transfer during the initial crash stage. However, we can select the most appropriate sample time *t* and substitution modulus parameter *m* in the initial crash stage. By using indexes U* and U**, the conventional imaginary figure that is shown in Fig. 1.4 could finally be actualized for the benefit of structural engineers to understand the load transfer in a vehicle body during collision.

4. Calculation Model and Boundary Conditions

The models of a heavy duty truck (UD. Truck) and a passenger car (Dodge Neon 1996) are analyzed in this study. Due to the impact characteristics of the truck and passenger car models, different boundary conditions and assumptions are proposed for the investigation of the load transfer and load paths analyses. Initially, the truck cab model is investigated using the dynamic-static method and substitution modulus method. Then passenger car models are studied.

4.1 Heavy Duty Truck Model

To perform a linear analysis using U* and U**, the behaviour of a truck compartment shown in Fig. 4.1 is calculated in an extremely early stage of a frontal collision. The

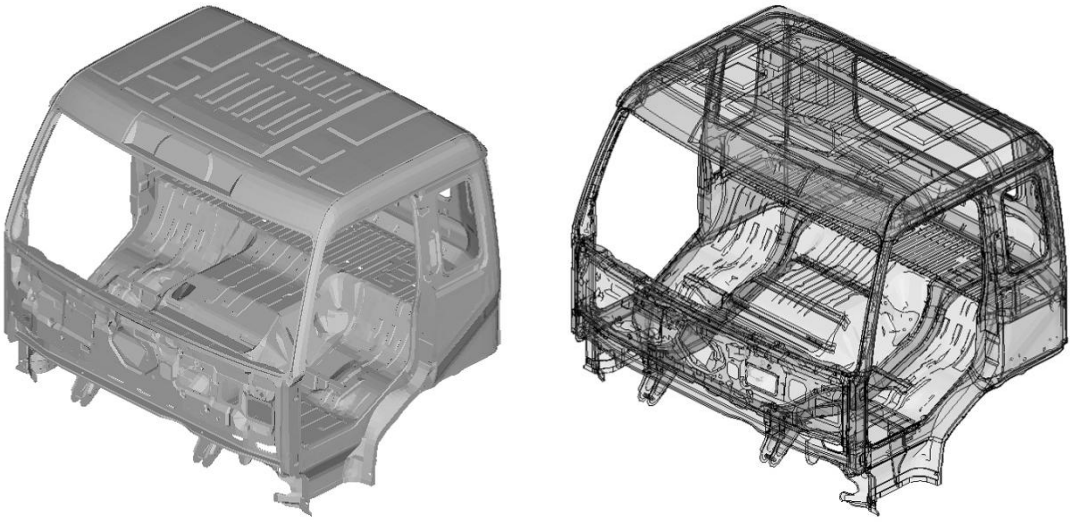

Fig. 4. 1 Heavy Duty Truck

Table 4. 1 Parameters of Truck Cab Model

Impact speed (m/s)	15.6
Rear mass (kg)	5,000
Element number	73,346
Yield stress (MPa)	300
Poisson's ratio	0.3
Mass density (kg/m^3)	7,830
Initial elastic modulus (GPa)	200

finite element (FE) model of the truck compartment is developed based on UD. Truck, and related parameters of the FE model are derived from validated experimental data.

For the dynamic analysis, the inertial force of the steel panels of the cab is taken into account. The inertial forces of the occupants, seats, windscreens, and doors are ignored because these effects are considered to be small compared with that of the steel panels in the extremely initial stage of the crash. On the other hand, for the static U* and U** analysis, inertial forces are excluded. The related parameters for dynamic and static analyses are represented in Table 4.1.

In the dynamic analysis, the rear end of the cab is postulated to be fixed to the rear cargo mass for simplicity as shown in Fig. 4.2, where the terminology *v* means impact speed. Elasto-plastic material properties (MAT24 [LS-DYNA]) are used for the truck cab steel

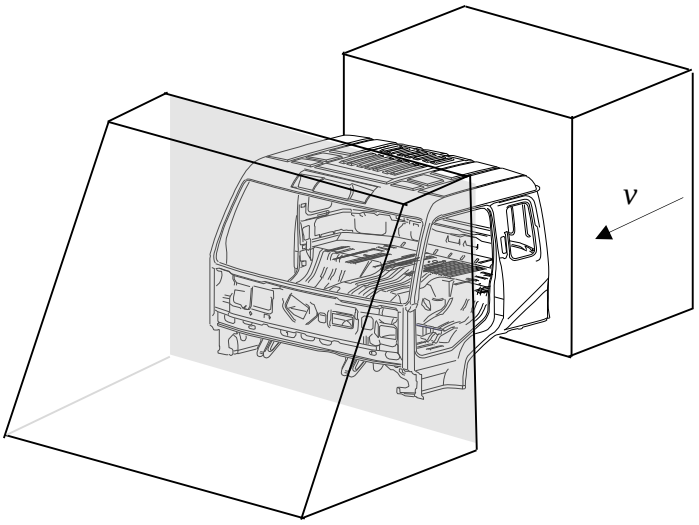

Fig. 4. 2 Boundary Conditions of Truck Cab

panels. The assumed bilinear stress-strain curve is shown in Fig. 4.3, where the parameter *m* is the ratio of initial (E_i) and substitution (E_s) elastic modulus.

In the static calculation, the moduli of plastic regions obtained by dynamic calculations are substituted into the extracted model for U* or U** calculation manually. To avoid the effects of the wave propagation to output data from dynamic calculations, the displacement of truck cab in each stage recorded in dynamic simulations is employed as

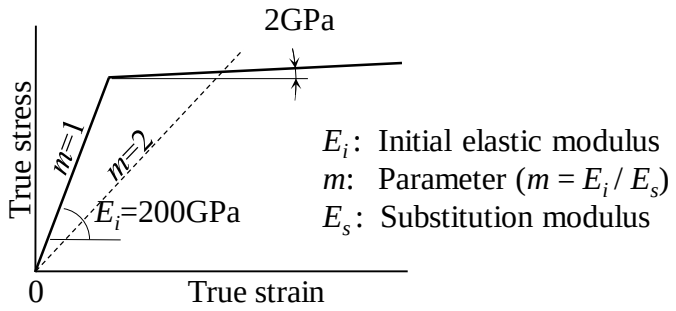

Fig. 4. 3 Stress Strain Curve

the input data for static U* or U** calculations. Thus, for U** calculation, the distributed loadings are regarded as the equivalent forces to generate the same displacements. For U* or U** calculation, the fixation of truck cabs is applied to the rear ends which are postulated to the rear cargo mass.

4.2 Passenger Car Model

Using index U**, the load transfer and load paths of a passenger car shown in Fig. 4.4 is

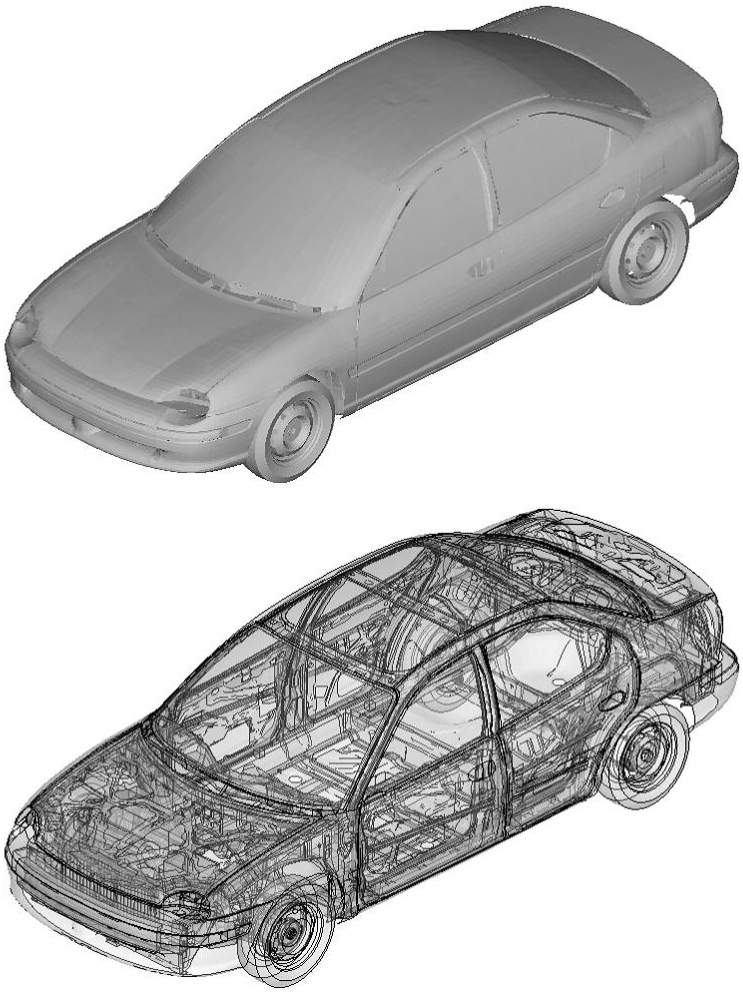

Fig. 4. 4 Passenger Car

calculated in an early stage of a frontal collision. The finite element (FE) model of the passenger car is obtained from National Crash Analysis Center (NCAC) which was

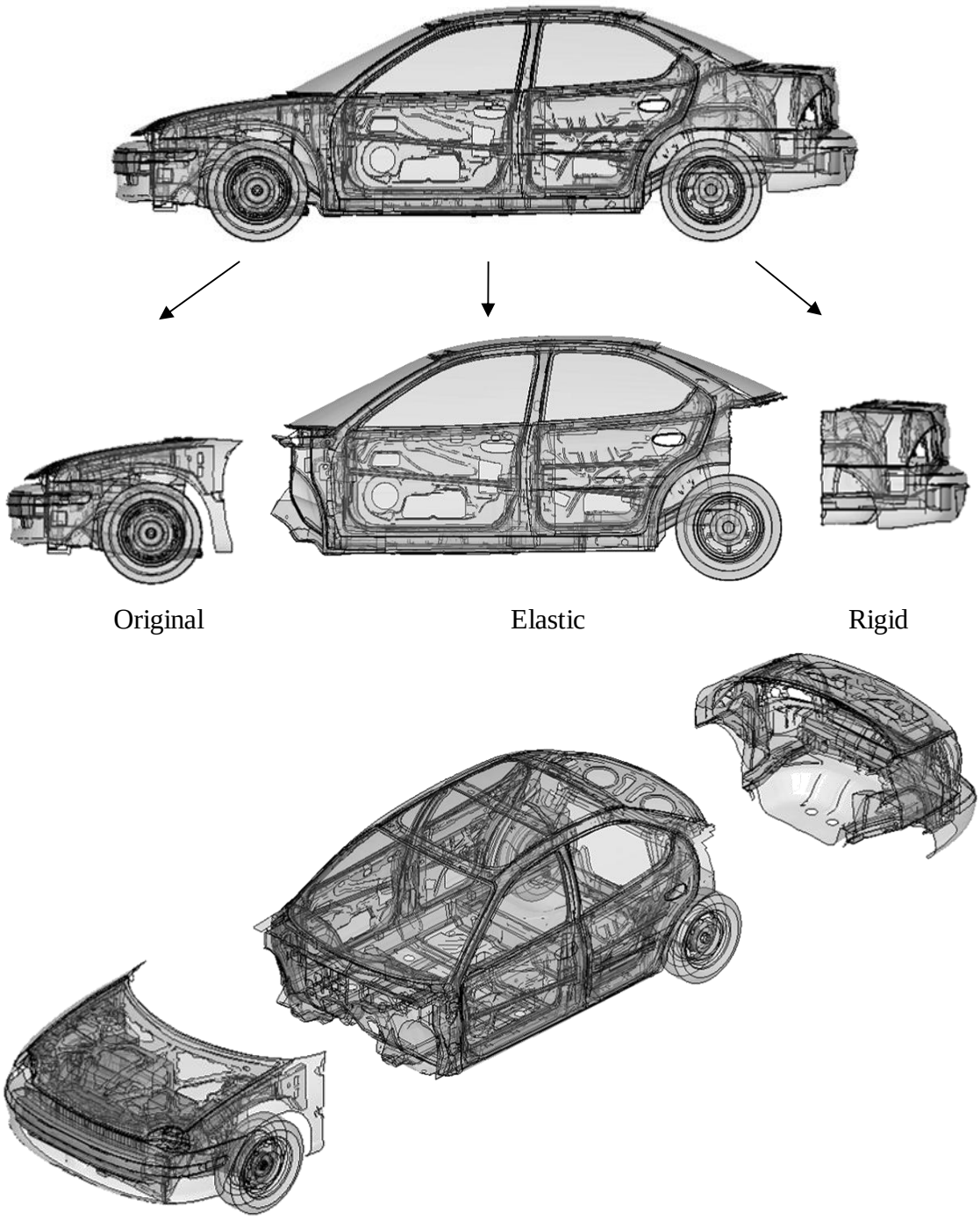

Fig. 4. 5 Approaches of Passenger Car

developed based on Dodge Neon ver. 1996. The FE models of NCAC are open for the academic usage.

As mentioned in Chapter 3, the simplified numerical model is generated which includes the elastic approach for the passenger compartment and the rigid approach for rear structures. Based on the schematic figure shown Fig. 3.3, the detail illustration of three regions (original, elastic, and rigid regions) is shown in Fig. 4.5. The frontal structures, including engine, front-ends, tires, bumper, frontal suspensions, fans, clutch, brakes and so on, is defined the same as the original numerical model. The middle structures of the passenger compartment are assumed to be elastic bodies, and the related elastic parameters are obtained from the original definitions. The elastic body starts from dash panel, scuttle panel, and frontal bulkhead and ends to the vertical edge of the geometric center of rear suspensions in which parts of side structures, rear window shield, and bulkhead brace assembly are included. The latter structures of rear structures are regarded as rigid bodies in which elastic moduli are amplified 1,000 times larger for the sake of simplicity. The rear tires which are not shown in Fig. 4.5 are defined as elastic bodies.

For the dynamic analysis, the inertial force of the whole vehicle structures is taken into account. The impact speed is 15.6 m/s. The element number of the numerical models is 270,768. Figure 4.6 shows schematically that the passenger car impacts to a flat rigid barrier. The nodal data of relative displacement connecting frontal and middle parts in vehicle structures are output to obtain equivalent distributed forces for static calculation.

As mentioned in Chapter 3, the displacement data is used to obtain the equivalent distributed forces which can lead to the same displacements. Then, in the U** static analysis the distributed forces are input to the extracted models. The fixation is applied to the edge between elastic and rigid bodied for U** calculations.

4.3 Calculation Environment

4.3.1 Dynamic Impact Calculation

In the dynamic calculation, commercial software code LS-DYNA (Version 970, Revision 5434a, 32 bit, Single precision) is performed in Windows XP Professional. The calculation platform is Dell PowerEdge server (T605). Commercial software Altairs HyperWorks (Version 9.0 & 10.0) is used as the Pre/Post processor.

In the calculation of the truck cab (Nissan Diesel), the total CPU time is 47 minutes 51 seconds for 15 ms numerical simulations. In the calculation of the passenger car (Dodge

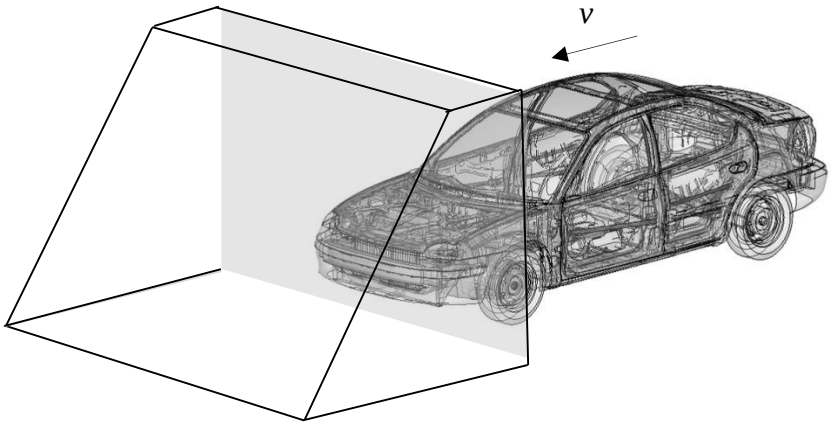

Fig. 4. 6 Frontal Impact of Passenger Car

Neon), the total CPU time is 26 hours 19 minutes 16seconds for 150 ms numerical simulations.

4.3.2 Static U and U** Calculation*

In the static calculation, commercial software code MSC. MD.Nastran (Version 2.0, 64 bit, Double precision) is performed on Windows XP Professional 64bit to output the

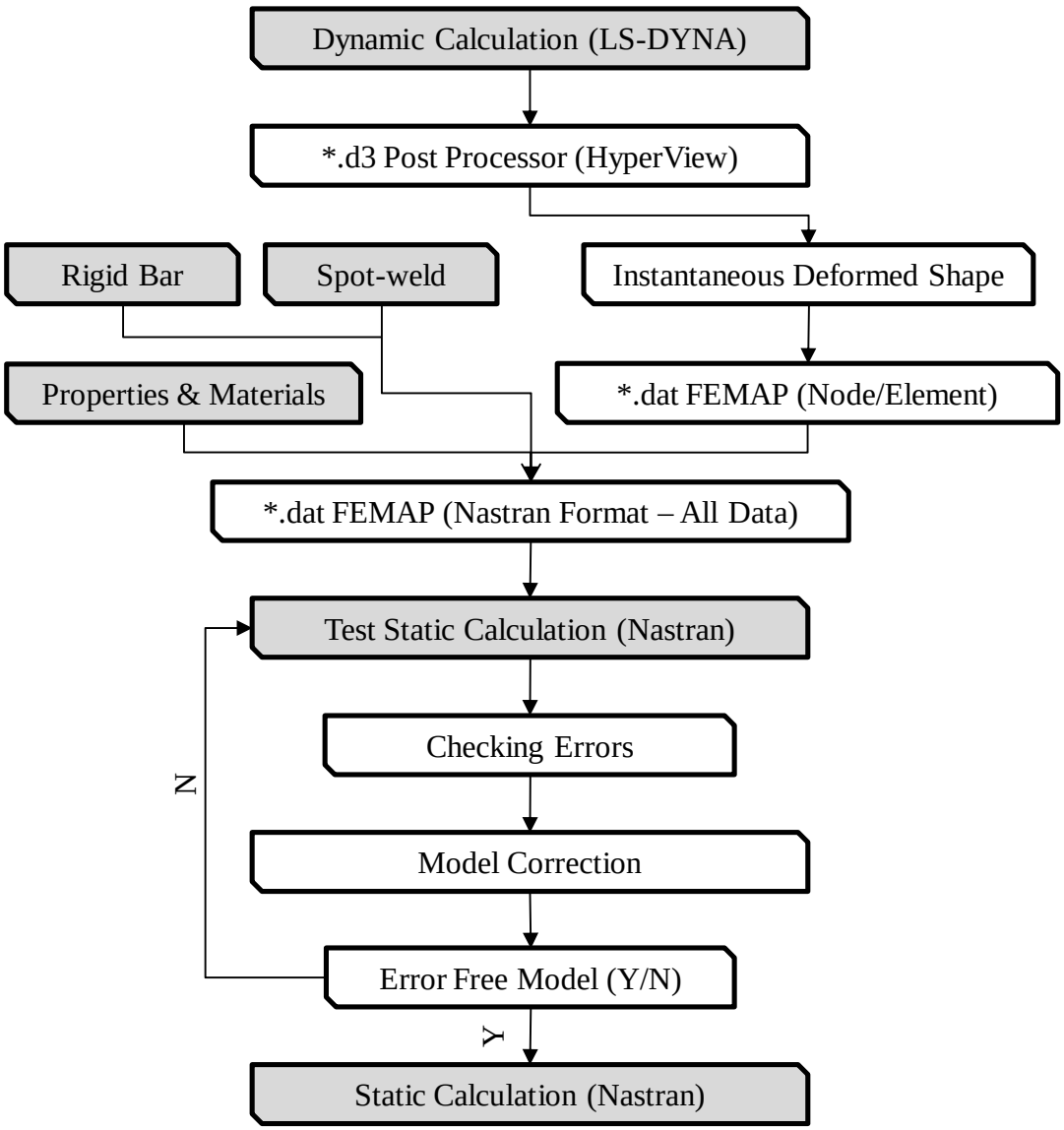

Fig. 4. 7 Model Conversion

internal stiffness and internal compliance for the U* and U** analysis. The calculation platform is HPC Workstation (HPC5000-XH216TA). Commercial software FEMAP with NX.Nastran (Version 9.3 & 10.1.1) is used as the Post processor to visualize the U* and U** distribution.

In the U* and U** calculation, self-made programs and manually operations are included to obtain the necessary input data for static load path analyses and U* or U** results. Thus the calculation time of load path analyses is not summarized here.

4.4 Model Conversion

As mentioned in Chapter 3, the static analysis of the load transfer and load paths is based on the extracted deformed model from dynamic numerical simulations. However, due to the inevitable differences of numerical models between LS-DYNA format and Nastran format, it is necessary to make a conversion of numerical models. The process of the model conversion is shown in Fig. 4.7. Based on the most effective and popular Pre-Post commercial software HyperWorks, most of the conversion of the model's properties and material definitions can be mapped accurately and converted automatically, such as 2D and 3D elements and metal properties. However, the properties of springs, spot-welds, rigid-bars, and non-metal properties cannot be converted properly by any available commercial software packages. Thus, the semi-manual conversion is operated to obtain an accurate model for static calculation. The detail process of semi-manual conversion is

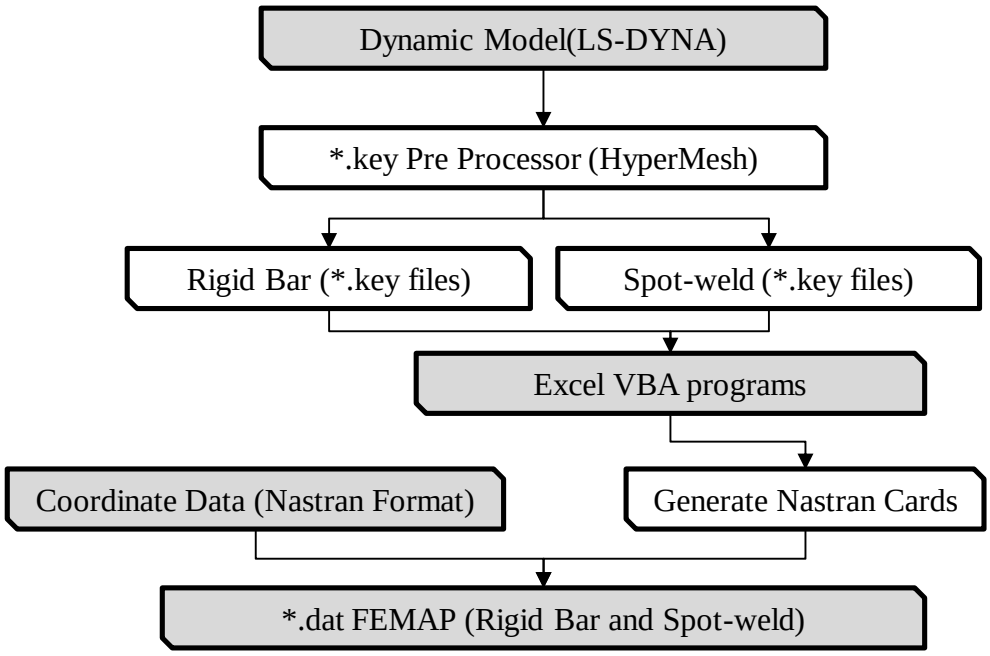

Fig. 4. 8 Spot-Weld and Rigid Bar Convention

plotted in Fig. 4.8. The definition of the detail mapping conversion can be found in the related references [121, 123].

5. Dynamic Crash Results

5.1 Results of Truck

For the dynamic simulation, commercial code LS-DYNA is used. The numerical crash simulation of the truck cab is performed till 15ms. During the dynamic simulation process, the deformed structure is extracted at any given instant to reproduce a model for U* and U** analyses. The deformation in each typical stage is exhibited in Fig. 5.1. From Fig. 5.1, it can be found that within 5ms the deformation of passenger compartment is relatively small. Moreover, the distribution of plastic strains in the middle plane of panels is shown in Fig. 5.2. The plastic regions are increasing gradually as the crash progressed. Except the tunnel structure working as crushable zones to absorb impact energies, other main structures present small plastic regions which disperse the impact forces to the rear rigid body structures.

Based on the numerical simulation of the truck cab, the variation of the distance between A-pillar and B-pillar is shown in Fig. 5.3. The positions of point A and point B are determined based on the geometric center of A-pillar and B-pillar, respectively. The distance between A-pillar and B-pillar is keeping constant within 7ms, which reveal that there is no effect of doors within 7ms. Thus, the static U* and U** analyses are applicable for examining the load transfer and load paths in the truck cab without doors in the extreme initial crash stage. In contrast, the distance is decreasing after 7ms. Therefore, to avoid the effect of large deformations and rotations, the load transfer and

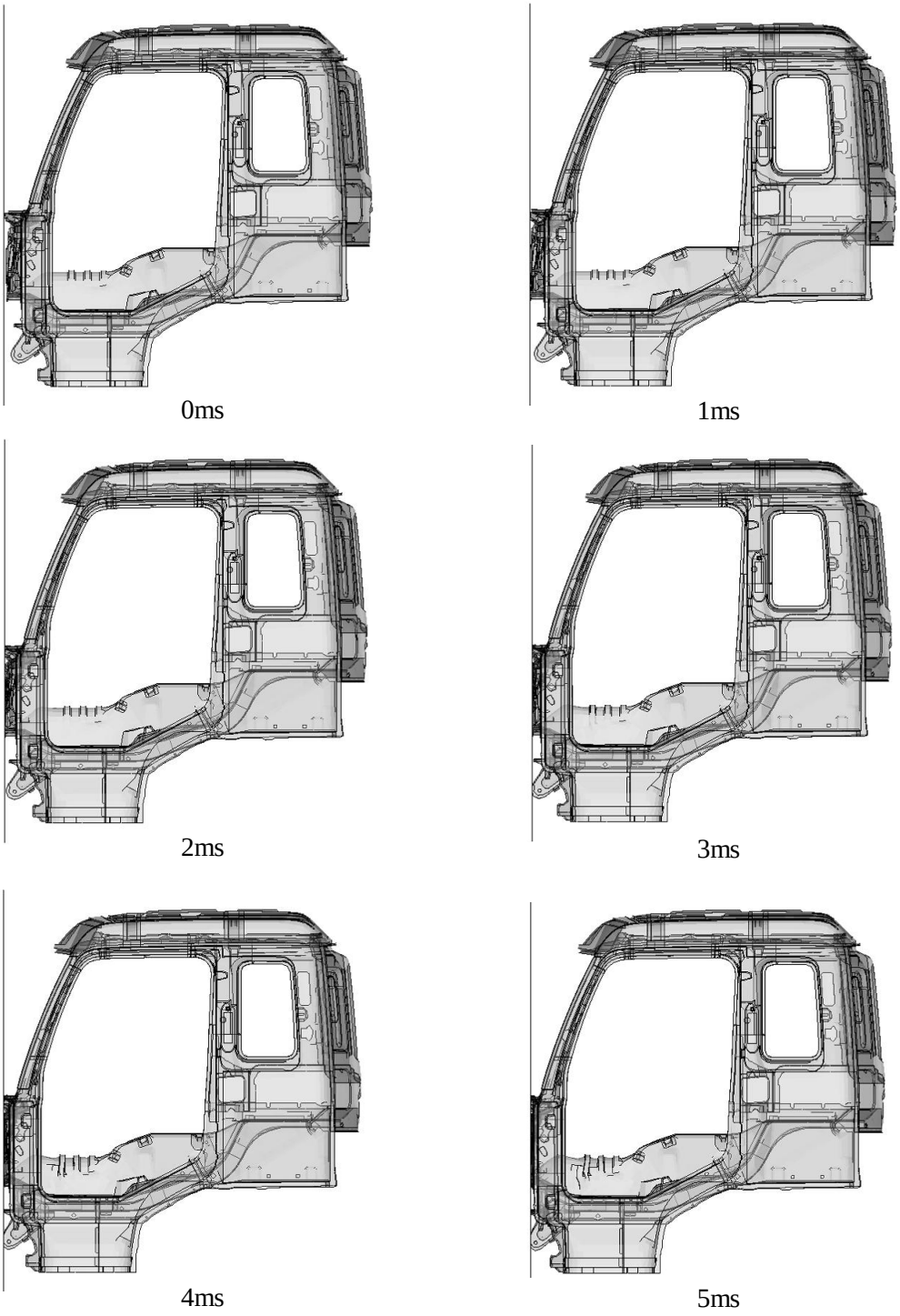

Fig. 5. 1 Deformation of Truck Cab under Frontal Impact

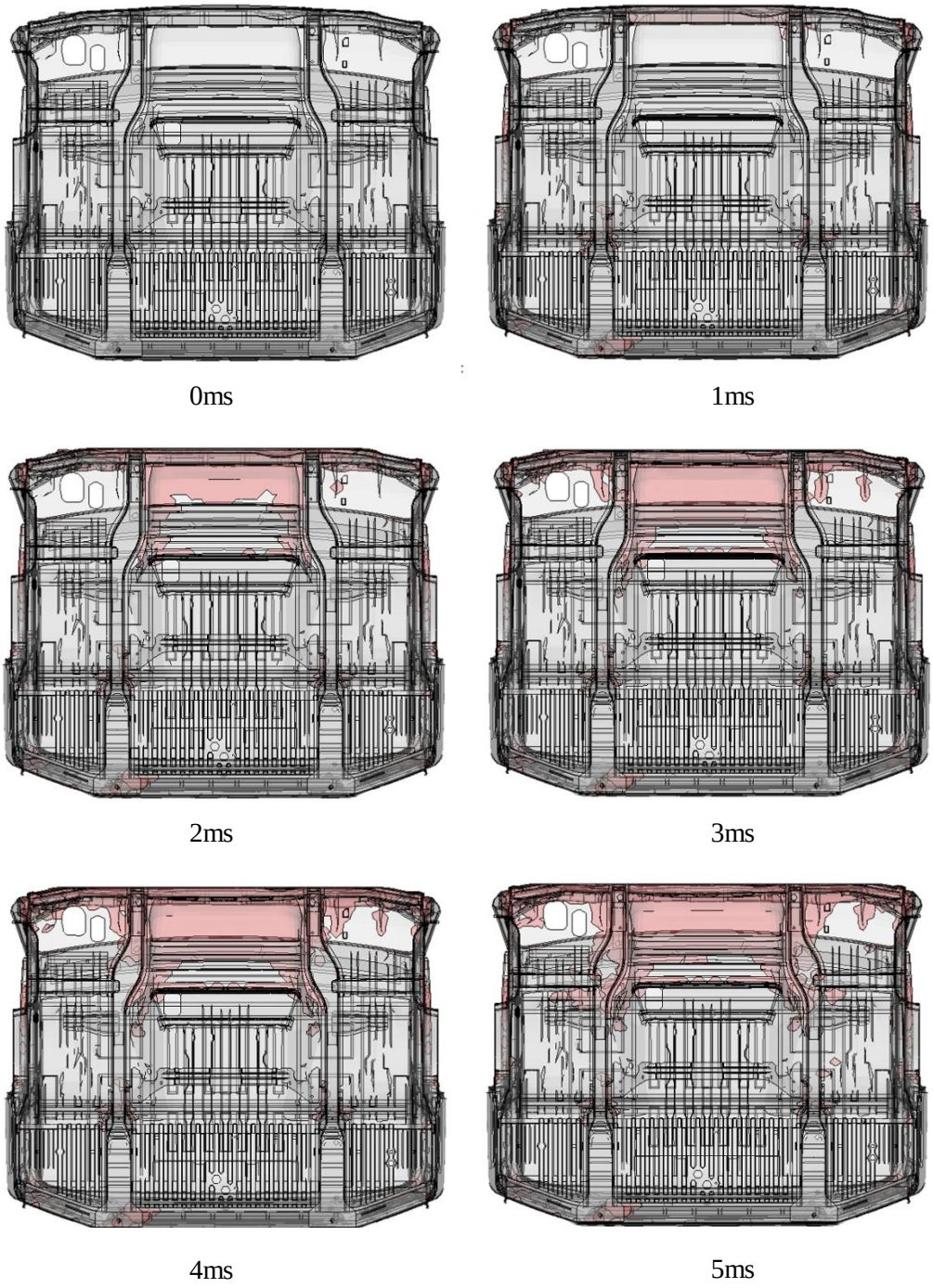

Fig. 5. 2 Distribution of Plastic Strain in Truck Cab

load path analyses of the truck cab model are studied in the extreme initial crash stage within 7ms. In the present study of the truck cab model, the load transfer and load paths are investigated at 1ms, 2ms, 3ms, 4ms, and 5ms.

5.2 Results of Passenger Car

5.2.1 Original Boundary Condition

The original car model provided by National Crash Analysis Center (NCAC) is analyzed numerically, and the simplified model mentioned in Chapter 4 is also calculated. The whole crash process of passenger cars is analyzed numerically till 150ms. A comparison

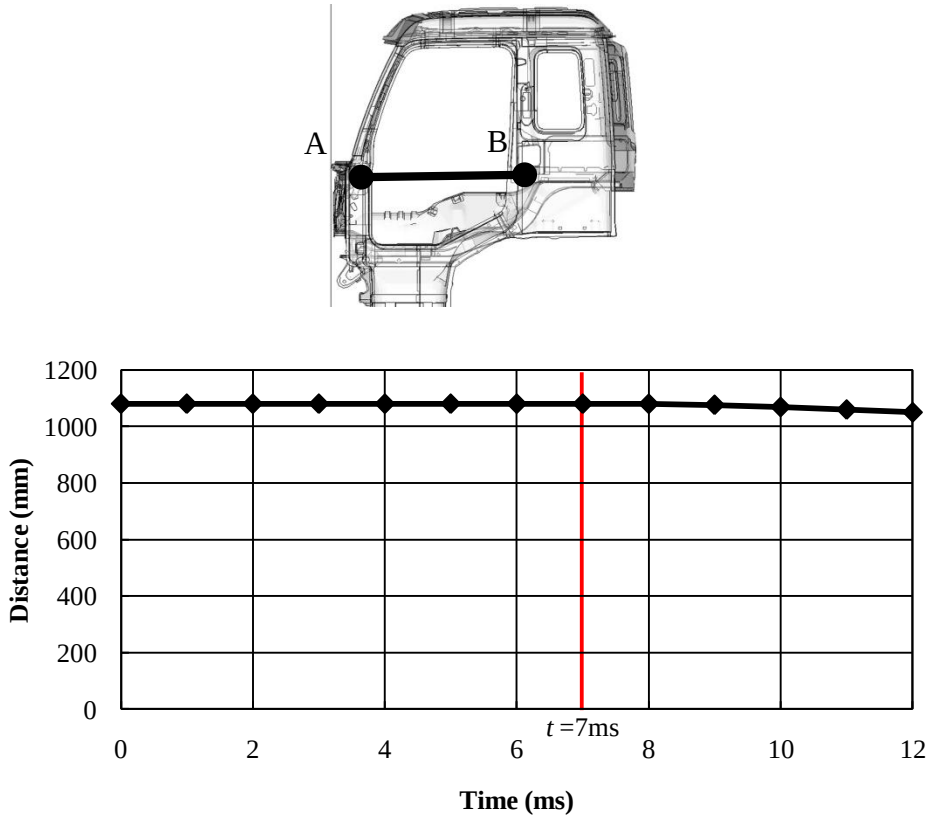

Fig. 5. 3 Variation of Distance between A-Pillars and B-Pillars

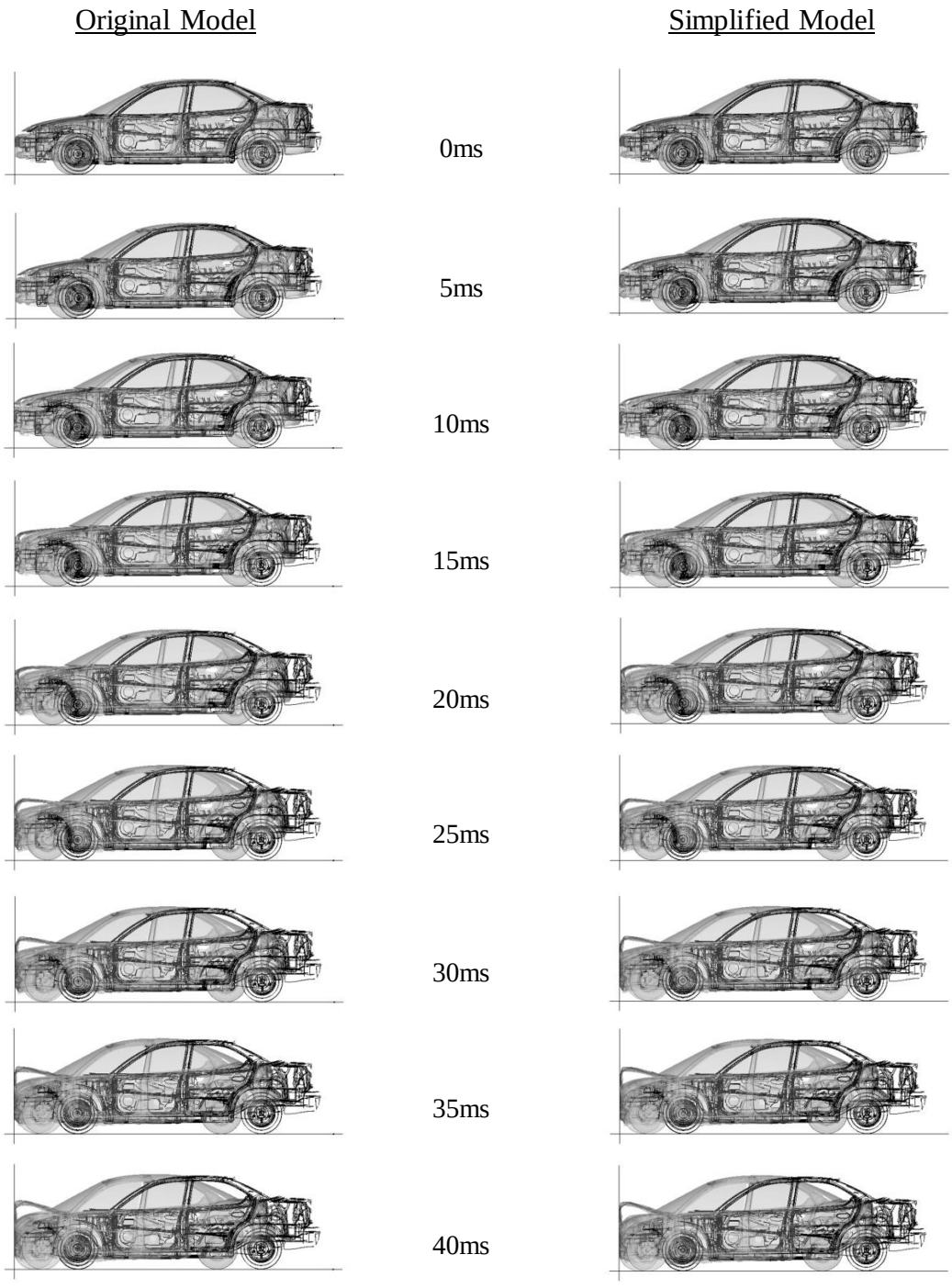

Fig. 5. 4 Comparisons of Simulation Results (0-40ms)

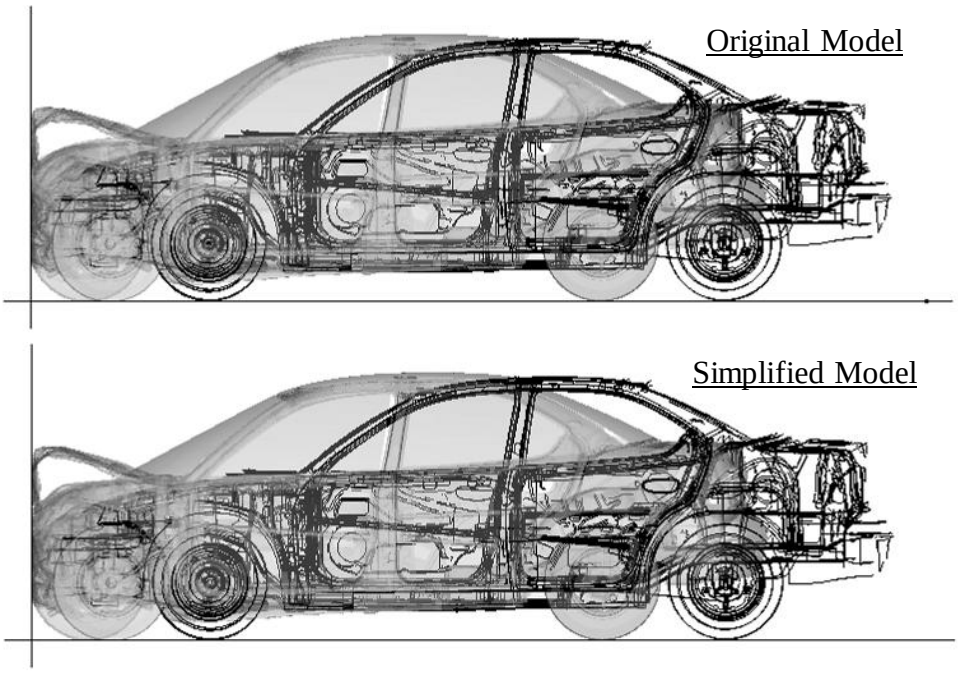

(a) 40ms

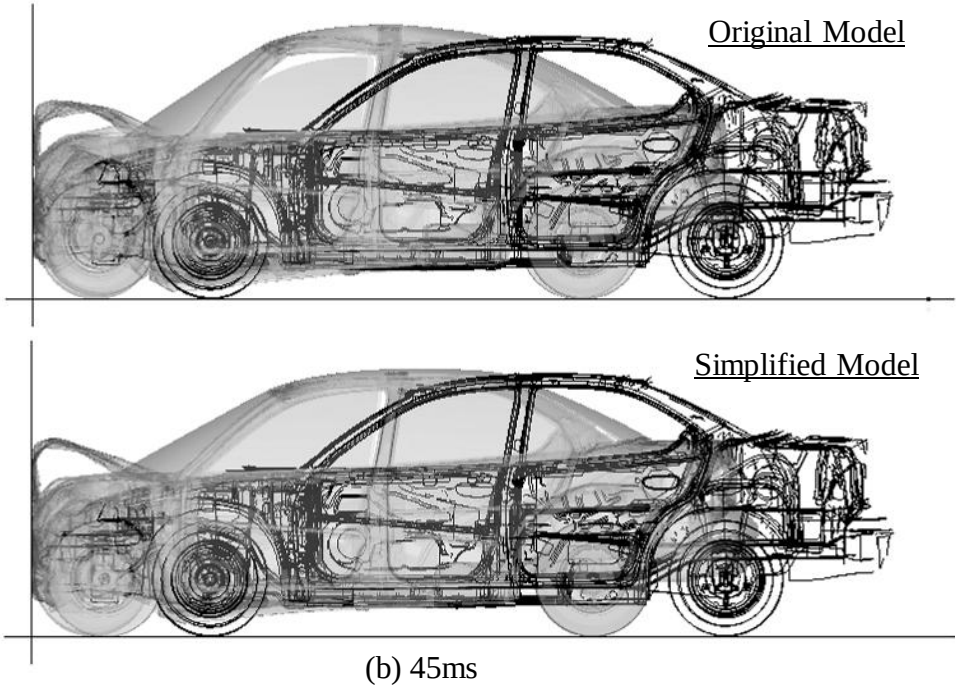

(b) 45ms

Fig. 5. 5 Comparisons of Simulation Results (40-45ms)

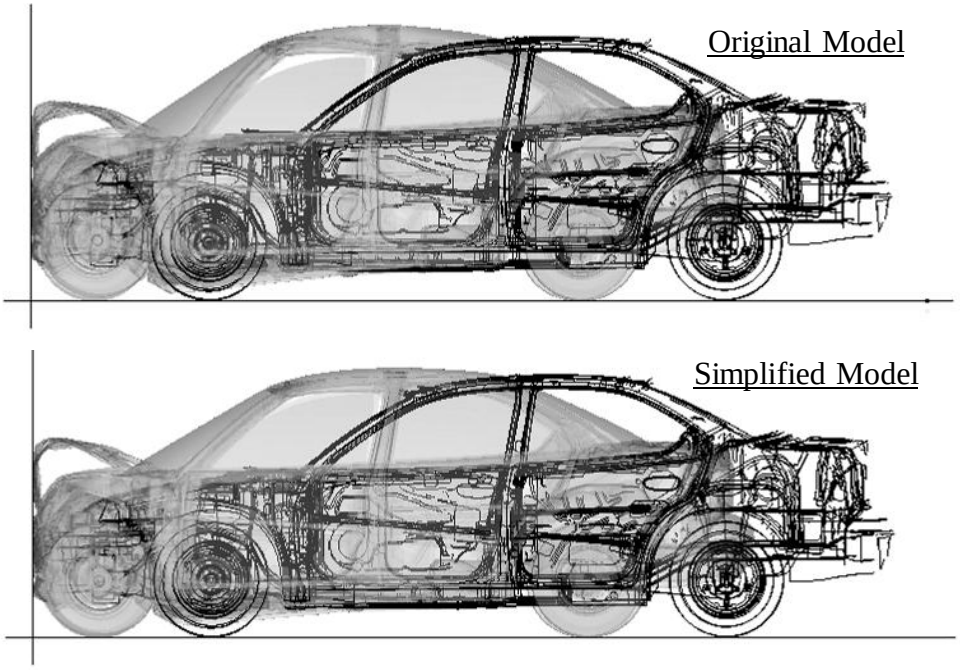

Fig. 5. 6 Comparisons of Simulation Results (100ms)

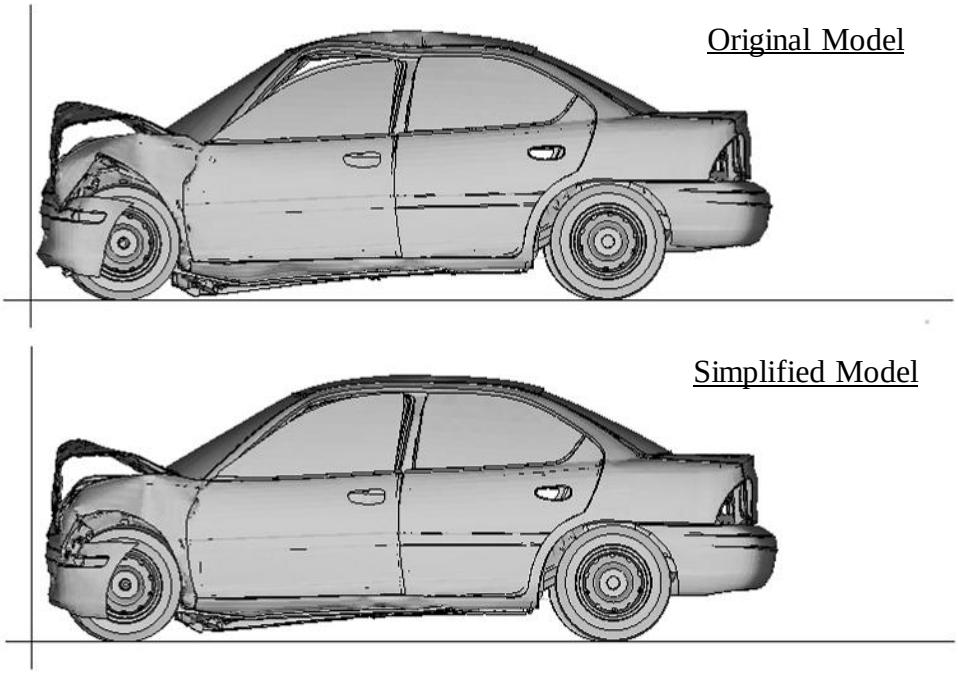

Fig. 5. 7 Comparisons of Numerical and Experimental Results (150ms)

of the crash deformation till 40ms is shown in Fig. 5.4. From Fig. 5.4, it can be seen that the approach of the simplified car model shows a perfect agreement with the original model within 40ms.

But after 40ms, the deformation between original model and simplified model becomes different as shown in Fig. 5.5. From Fig. 5.5(b), the deformation of roof panels can be observed clearly that the deformation of original model is larger than the simplified one. The comparison of 100ms between original and simplified models is shown in Fig. 5.6. The simplified model appears less deformation than the original model.

The final deformed shapes of original and simplified numerical results are shown in Fig. 5.7. Compared with the results shown in Fig. 5.7, it can be found that the elastic approach of the passenger compartment and the rigid approach of rear structures lead to a difference in the final deformation of roof panels.

Thus, aiming to obtain valid results of the load transfer and load paths, the proper stages for U** calculations is suggested within 40ms. The sophisticated comparison and determination are made based on the variation of crashing data.

The crash behaviours of both simplified model and original model are compared. In Fig. 5.8, the comparison of the GC rigid mass displacement is presented. It can be found that in the initial stage of crash (we manually defined that from 0-30ms is the initial crash stage of the Neon model) there is no difference in the GC rigid mass displacement. But in

the middle and end stage of impact, the simplified model has a less displacement than the original model. The comparison of velocities is demonstrated in Fig. 5.9. From Fig. 5.9, it can be found that the difference of the GC rigid mass velocity between the simplified model and the original model. Except the initial crash stage, the variation of the

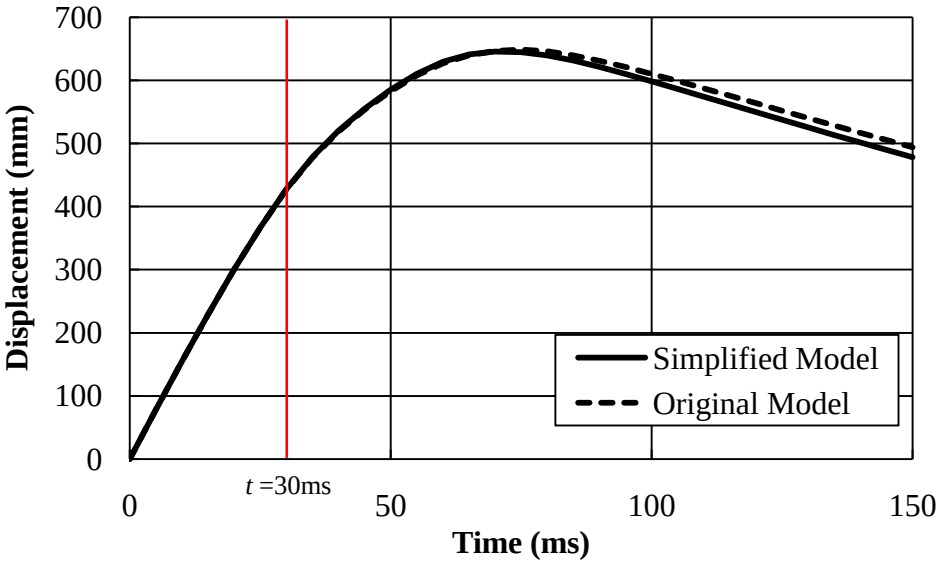

Fig. 5. 8 Comparison of Displacement

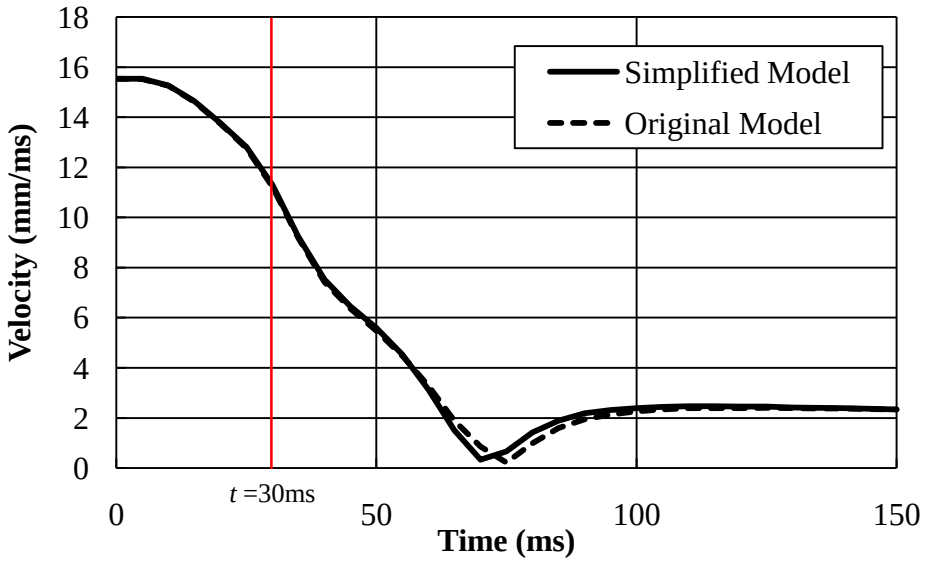

Fig. 5. 9 Comparison of Velocity

simplified model decreases more rapidly. The comparison of the GC rigid mass acceleration is interpreted in Fig. 5.10. The GC rigid mass acceleration in simplified model appears a higher variation than the simplified model after the initial crash stage. Meanwhile, the comparison of the internal energy is shown in Fig. 5.11. The value of internal energy in the simplify model is higher than the value in the original model after the initial crash stage.

As the results obtained from Figs. 5.8, 5.9, 5.10, and 5.11, there are obvious differences between the simplified model and the original model after the initial crash stage, which also can be observed from the deformation shape shown in Figs. 5.4 and 5.5. Although the difference is inevitable because of the elastic approach of the passenger compartment and rigid approach of rear structures, the simplified model and original model demonstrate a reasonable coherence within the initial crash stage when the passenger compartment mainly remains elastic.

Thus, aiming to obtain an accurate variation of the load transfer and load paths in the passenger compartment, it is necessary to make the static U** calculation in the initial crash stage. The precise boundary of initial crash stage will be defined based on the distribution of plastic regions and the deformation of the passenger compartment. The distribution of plastic regions in the original model (at 5ms, 10ms, 15ms, 20ms, 25ms, 30ms, 35ms, 40ms, 45ms, and 150ms) is shown in Fig. 5.12. It can be found that after 30ms the distribution of plastic regions is increasing drastically.

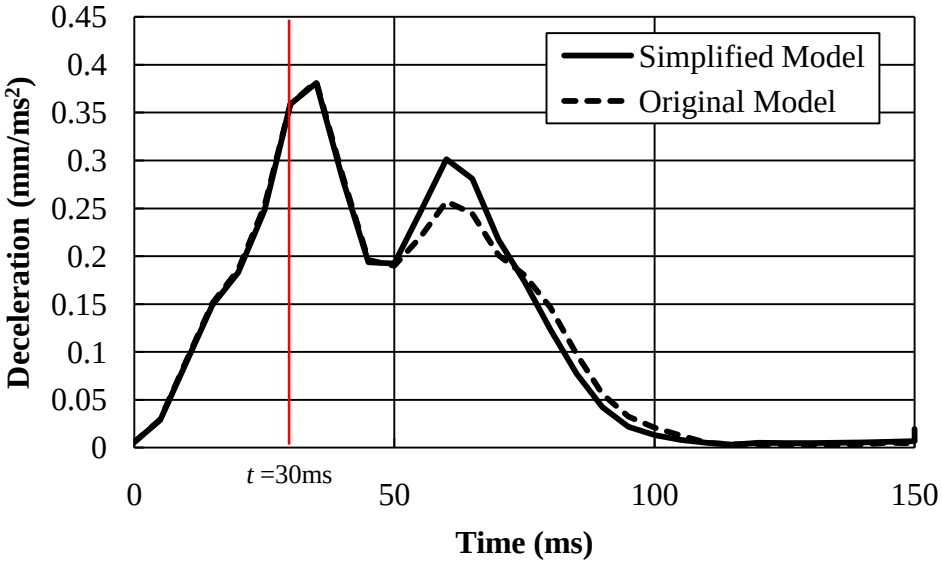

Fig. 5. 10 Comparison of Acceleration

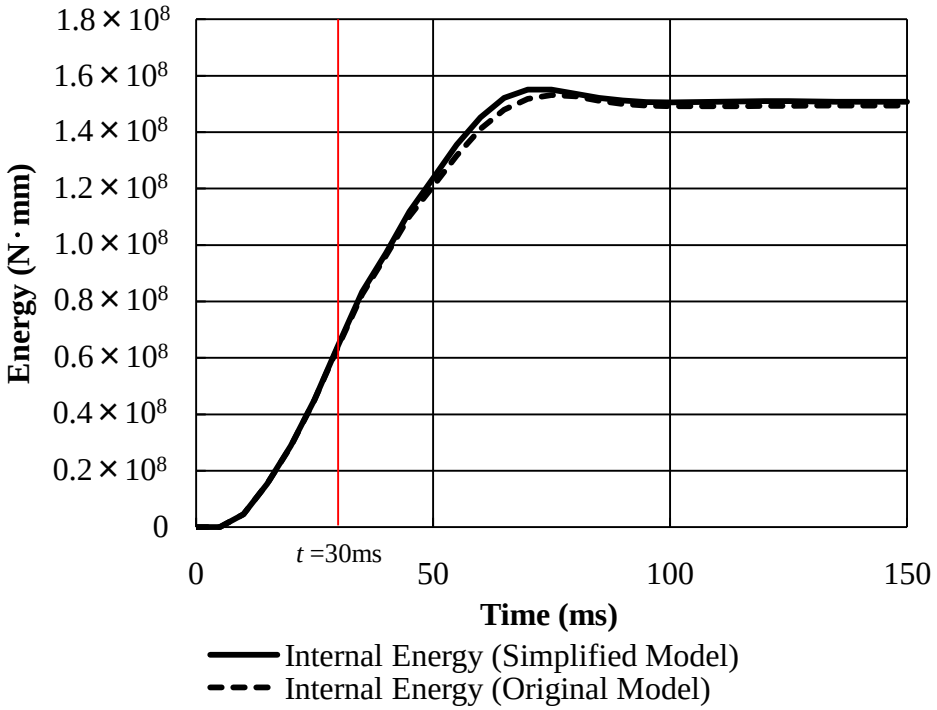

Fig. 5. 11 Comparison of Internal Energy

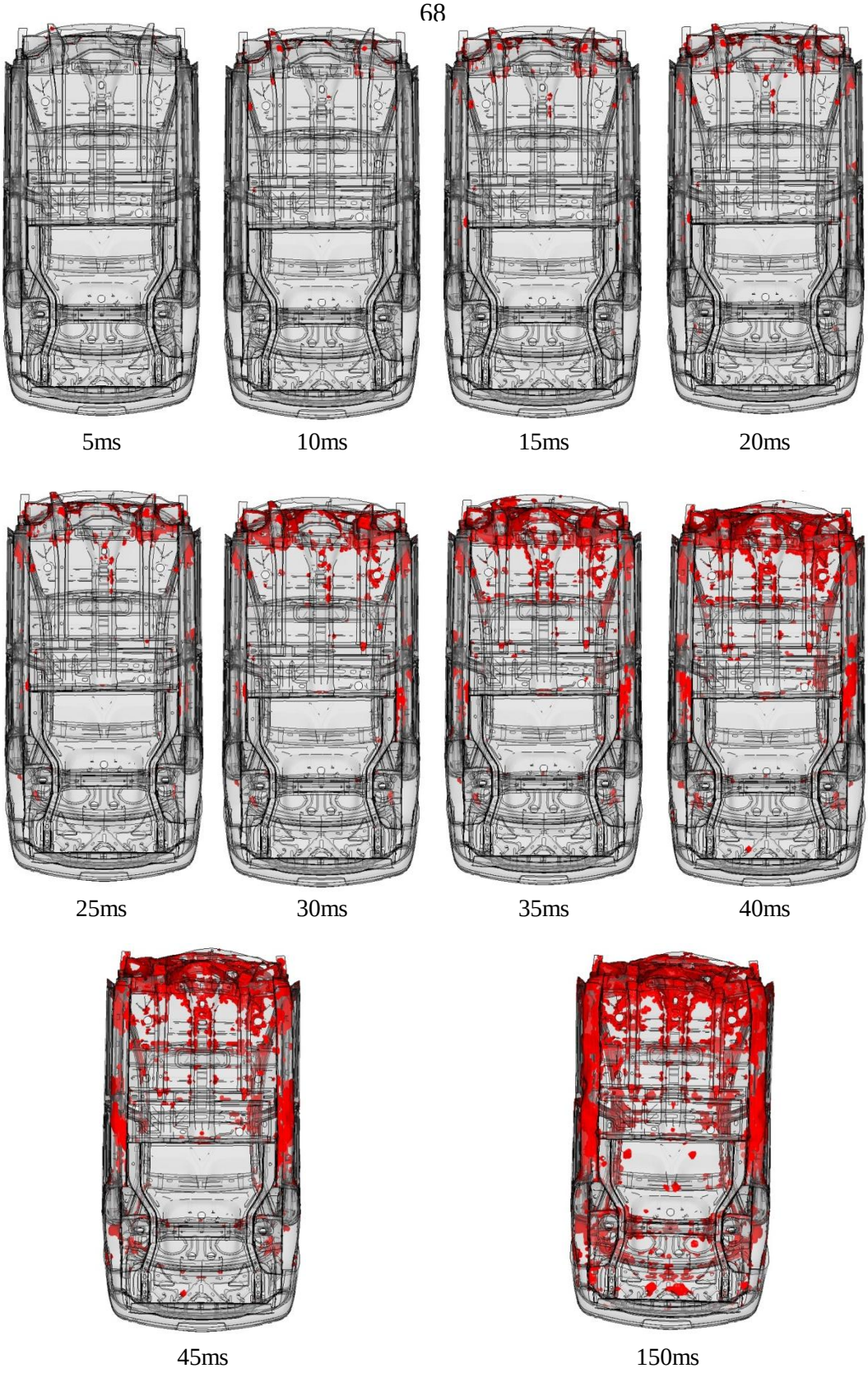

Fig. 5. 12 Distribution of Plastic Strain in Original Passenger Car

Moreover based on the numerical simulation of the simplified model, the variations of the distance between A-pillar and B-pillar and the distance between B-pillar to C-pillar are plotted in Fig. 5.13. According to the crossing points of beams in doors and the geometric center of A-pillar, B-pillar, and C-pillar, the positions of point A, point B, and point C are determined, respectively. The distance between A-pillar and B-pillar is decreasing rapidly after 30ms and keeping nearly constant after 90ms. In contrast, the distance between B-pillar and C-pillar is almost constant except a small disturbance around 70ms. Thus, aiming to avoid the effect of large deformations and rotations, the load transfer and load path analyses of the simplified model are studied in the initial crash stage within 30ms. In the present study of the passenger car model, the load transfer and load paths are investigated at 15ms.

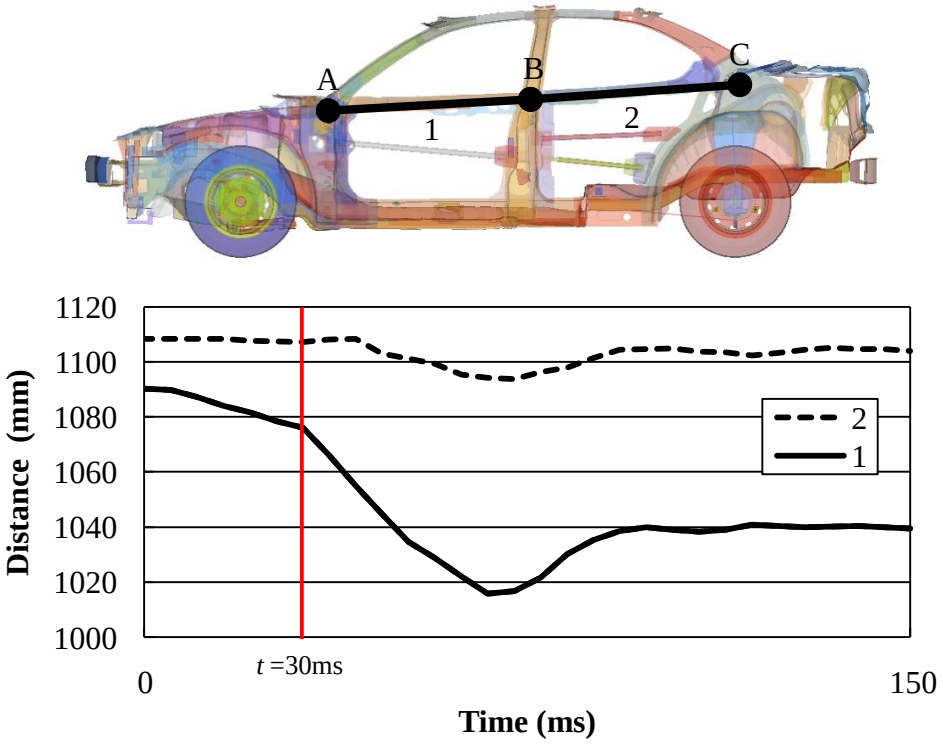

Fig. 5. 13 Variation of Distance between A-B Pillars and B-C Pillars

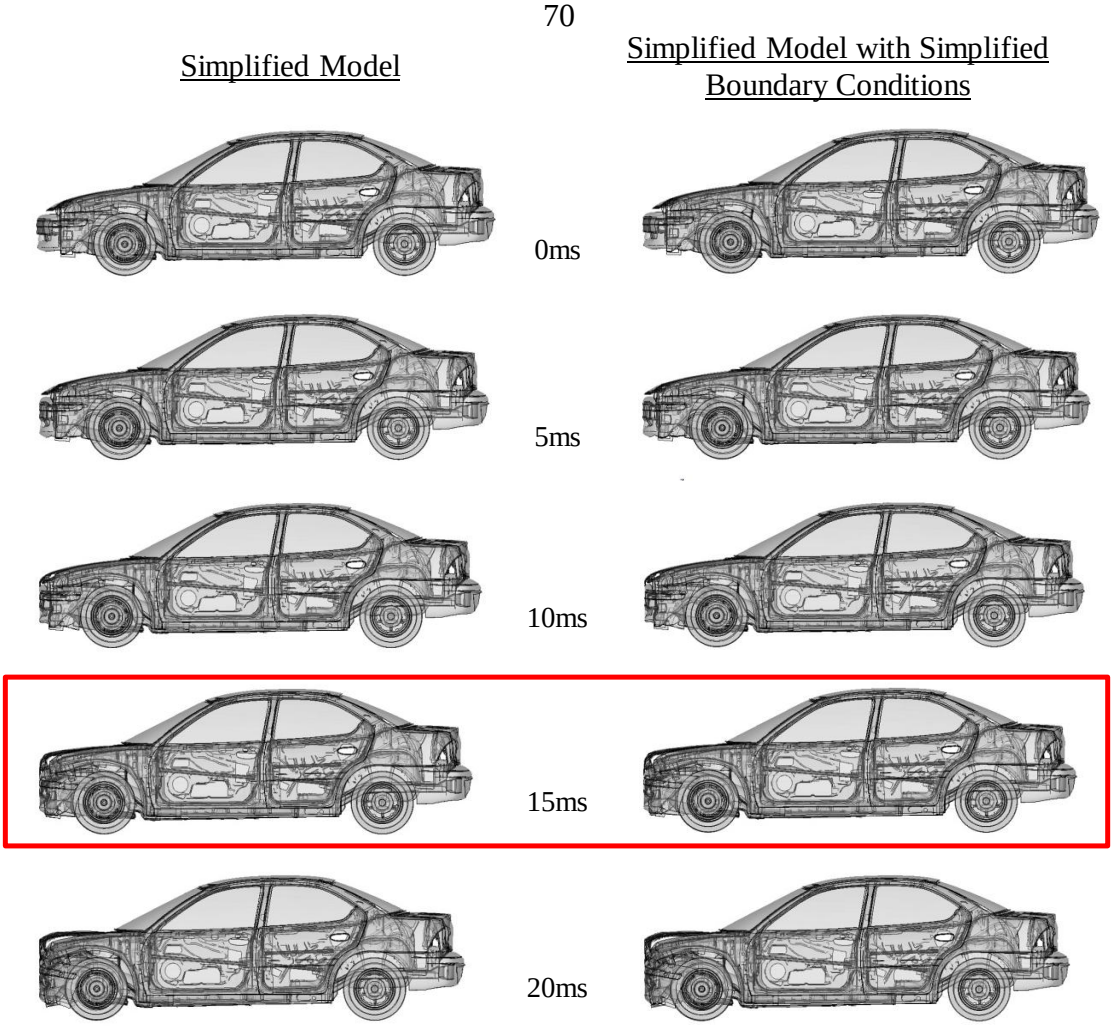

(a) Small difference of deformed shapes (0-15ms)

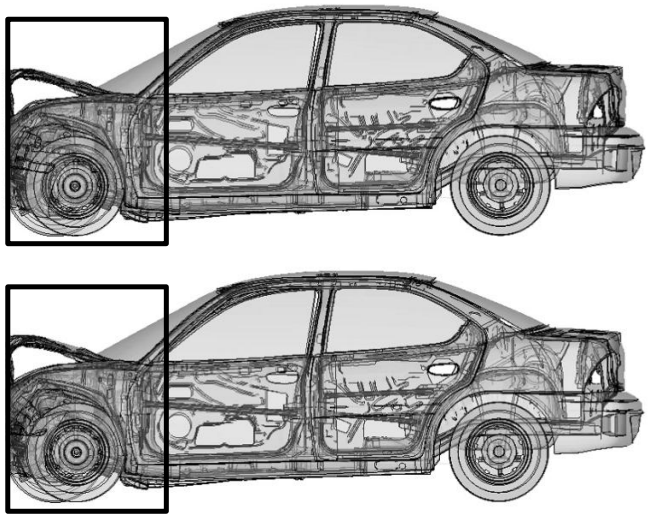

(b) Difference of deformed shapes (40ms)

Fig. 5. 14 Comparison of Deformed Shapes

5.2.2 Simplified Boundary Condition

As mentioned in Chapter 3, for the sake of simplicity a simplified condition is used to obtaining the relative displacement in the present stage of this study to investigate the load transfer at 15ms. The dynamic crash results are shown in Fig. 5.14. From Fig. 5.14(a), it can be found that the difference in deformed shapes analyzing by between the conventional condition and the simplified one at 15ms. Thus, we can summarize that at 15ms the results obtained by the simplified condition can be used for the load transfer and load paths analyses.

It is unavoidable that as the crash progress the differences in deformed shapes can be observed shown in Fig. 5.14(b). In Fig. 5.14(b), the highlight regions present the difference in deformed shapes at 40ms.

In the calculation of simplified boundary conditions, it is assuming that the dashboard structures subject to frontal loadings. When inversing the loading and constraint conditions in the numerical calculations, the deformed dashboard structures are constraint due to the minor deformation shown in Figs. 5.13 and 5.14. Such an approach of boundary conditions should be treated carefully in determining the loading and constraint regions. In the present study, the dashboard structures and other substructures connecting with front ends are defined as constraint regions in the cases of consistency analyses.

6. Static Load Path Analysis for Truck Cab Structures Using Index U**

6.1 Small Differences of U** Distribution with Regard to Sample Time *t* and Parameter *m*

*6.1.1 U** Distribution in Floor Panels*

The method presented in Chapter 3 assumes that the load transfer is hardly affected by the sample time *t* and nonlinear parameter *m*. To verify this assumption, we calculate the U** distribution for different values of *t* and *m* for the floor panel. The results are depicted in Fig. 6.1 showing the bottom views of the floor panel.

As expected, almost the same distribution of U** is observed for every combination of *t*

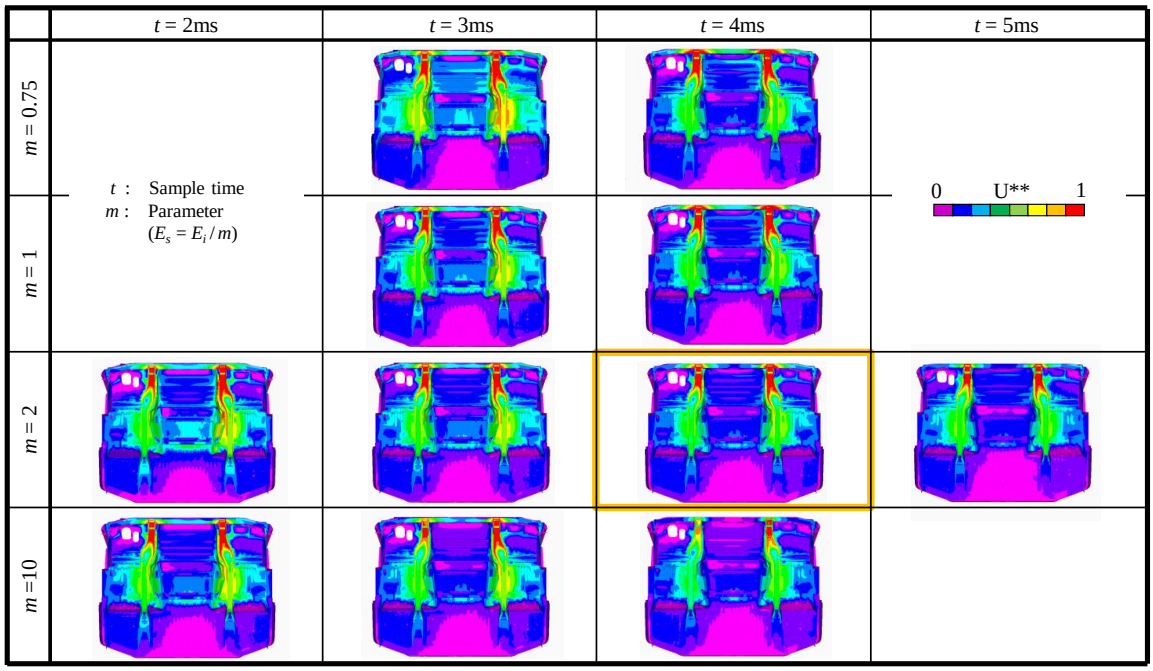

Fig. 6. 1 Small Differences of U Distribution**

and *m*. On the other hand, it is obvious that the distributions of the barrier loading vary considerably in these cases. However, since the frontal structure is moderately collapsed, only the behaviour of the load transfer in the elastic structure is being maintained during the initial crash phase. Here, again, it should be remembered that the U** distribution does not indicate the absolute value of the load transfer but shows the ratio of the load transfer only.

Although we can hardly find any differences between the cases in Fig. 6.1, we can choose the most suitable combination of a sample time *t* and a parameter *m* in the initial crash stage. From Fig. 6.1, we can determine that the combination of *t* = 4ms and *m* = 2 is the most appropriate one, and we refer to this as the "m2-4msU**" index. This index can be used as the standard condition of the load transfer for the estimation of the new stiffeners in the truck cab. However, it is preferable to determine the standard condition *m* = 2 and *t* = 4ms for the comparison of the change in the load transfer before and after reinforcement of a cab.

The necessity of the precise definition of the condition "m2-4msU**" is emphasized from the designation of *m* = 2 and *t* = 4ms. The value of *m* and *t* will be investigated in future studies to express the nonlinear behaviour more appropriately. We cannot use the tangent modulus instead of the value of *m*, because the extremely small elastic constant introduces very small loading in U** analysis.

6.1.2 Small Difference in Floor Cross-Sections

The U** distributions for two cross-sections (x_2 = 450mm and x_2 = 750mm) of the floor panel are shown in Fig. 6.2, where the value m = 2 is used based on the results of Fig. 6.2. We can see again from this figure that the behaviour of the load transfer is almost independent of the sample time t during the initial crash stage. Moreover, we can observe that the two main members play important roles for the load transfer.

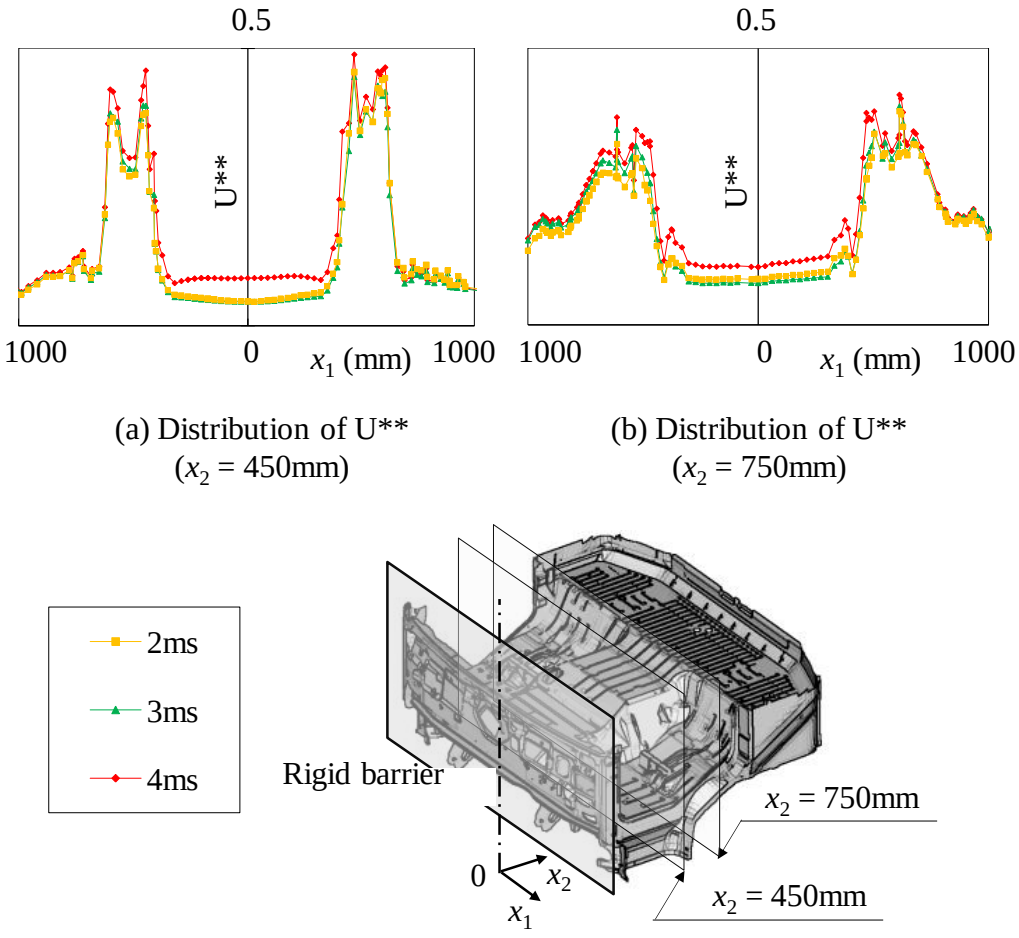

(a) Distribution of U** (x_2 = 450mm)

(b) Distribution of U** (x_2 = 750mm)

Fig. 6. 2 Cross-Sectional Distribution of U (m=2)**

*6.1.3 U** Variations along Load Paths*

The U** values along the corners of the main floor member are presented in Fig. 6.3. We can see again that the U** distribution along each path depends little on the sample time *t* during the initial crash stage, where *s* is the distance from the front end along the path and *l* is the total length of each path.

As we mentioned in Chapter 3, the U* or U** distribution along a load path should decay uniformly and continuously. From this point of view, we can say that the U** values in Fig. 6.3 decay uniformly, and that the conditions of uniformity and continuity for the desirable structure are almost being satisfied along the main member. However, at the

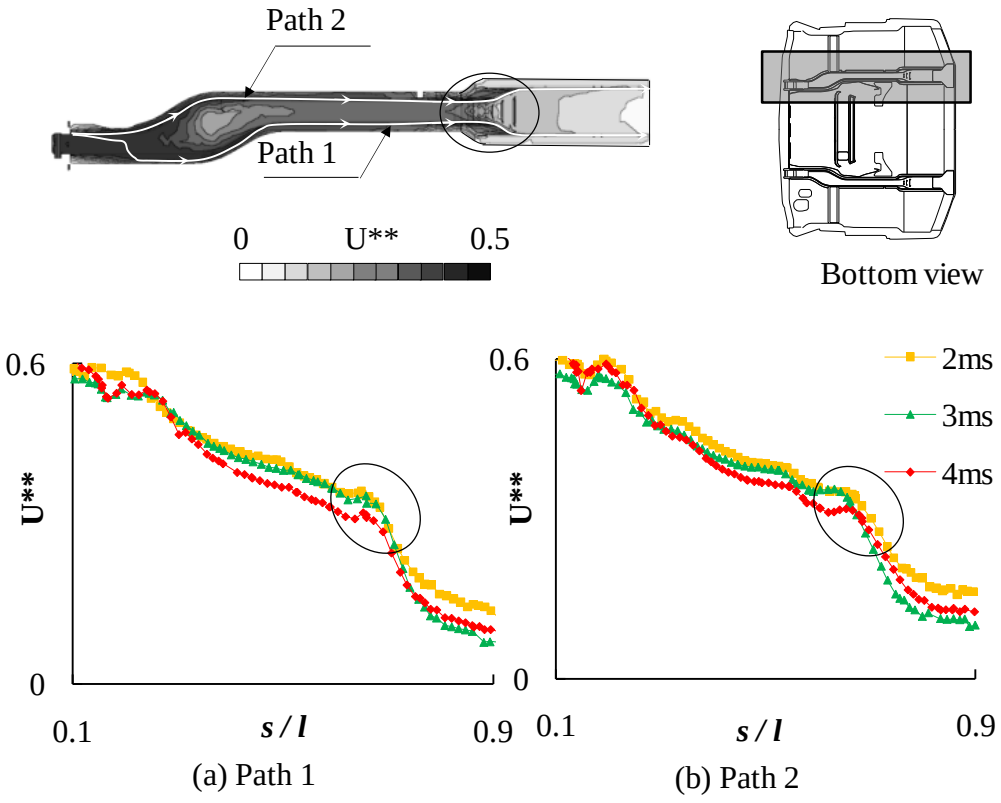

Fig. 6. 3 Decay of U along Load Paths (*m*=2)**

area indicated by the circles in Fig. 6.3, the condition of continuity is slightly disturbed, and the smoothness of the load transfer is not maintained.

Thus, using the U** distribution, we can quantitatively analyze these structural problems, as demonstrated in the above example.

6.2 Load Transfer and Load Paths in Floor Structures

6.2.1 Load Paths along Floor Main Members

The load path for the main floor member is shown in Fig. 6.4. Observing the high "m2-4msU**" index values or the load path on the corner of the cross-section, we can

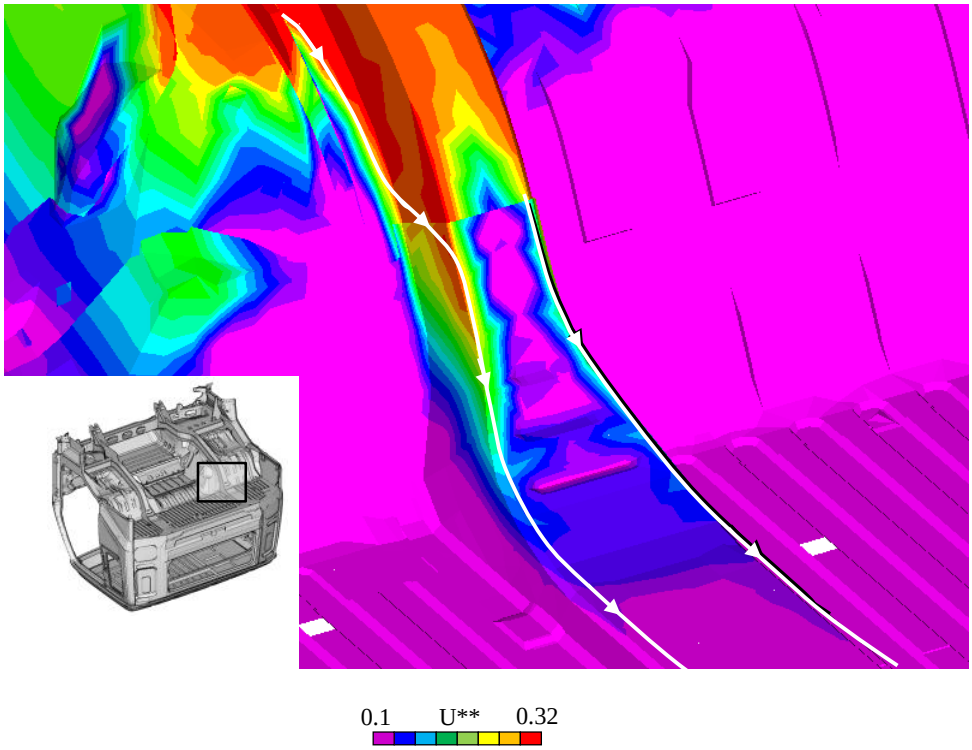

Fig. 6. 4 Distribution of "m2-4msU" and Load Paths**

conclude that the corner of the member plays an important role in the load transfer. By introducing cross-sections with multi-corners shown in Fig. 6.5, additional load paths are added, and the stiffness in the main members is increased. Thus, it can be found that the structural design with multi-corners in a predominant member is preferable and effective for the load transfer.

6.2.2 Load Transfer in Floor Structure

The distribution of "m2-4msU**" for the floor structure is shown in Fig. 6.6(a). The frontal loading is introduced to the main member, and the shear effect of the side floor panel transfers the loading to the side sill. It is important to use the side floor panel as a flat shear panel. A comparison of the max principal stress distribution and "m2-4msU**" distribution is shown in Fig. 6.6(b), in which the absolute values of the principal stresses on the middle surfaces of floor panels are used. If we use this stress distribution instead of U** to examine the load transfer, the effect of the tunnel center panel is overestimated, and that of the main member is underestimated, as shown by the circles.

As shown below, the stress distribution is useful for the study of strength, and on the

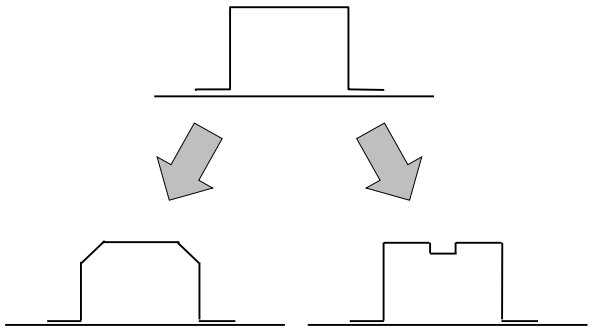

Fig. 6. 5 Multi-Corner Cross-Sections

other hand, U** is useful for the study of load transfer. Summarizing the above, we can say the following:

- Stress distribution: for the investigation of the strength
- U** distribution: for the investigation of the load transfer

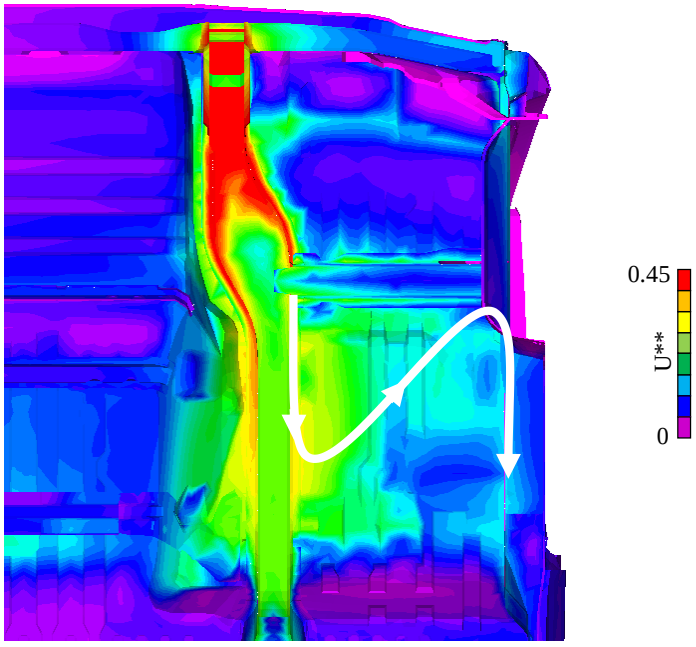

(a) Distribution of "m2-4msU**"

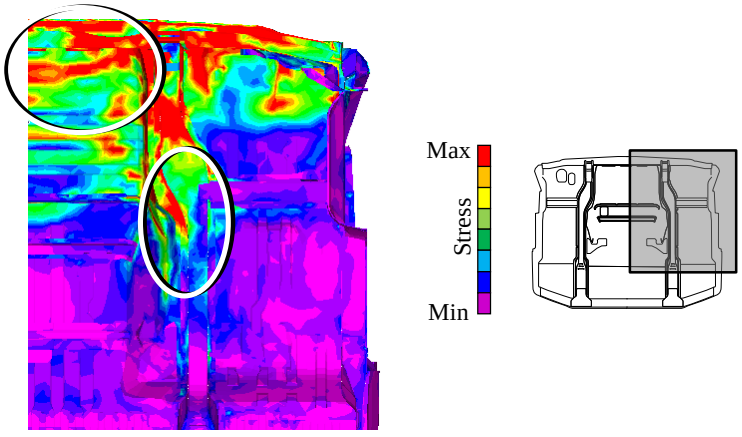

(b) Distribution of maximum principal stress

Fig. 6. 6 Load Transfer in Floor Structure

Thus, both the conventional stress distribution and the present U** distribution should be used for the study of the total performance of structures. The stress distribution is useful for the study of strength, and on the other hand, U** is useful for the study of load transfer. Thus, both the conventional stress distribution and the present U** distribution can be used for the study of the total performance of structures under frontal collisions.

6.2.3 Load Transfer in Tunnel Structure

As we see in Fig. 6.6(a), the tunnel center panel has little effect on the load transfer. "m2-4msU**" distribution for the tunnel structure in its diagonal view is shown in Fig. 6.7. It can be observed that the tunnel wall is playing an important role together with the main member for the load transfer. This observation is suggesting the necessity of a stiffener member which effectively conveys the loading from the wall surface of the tunnel into

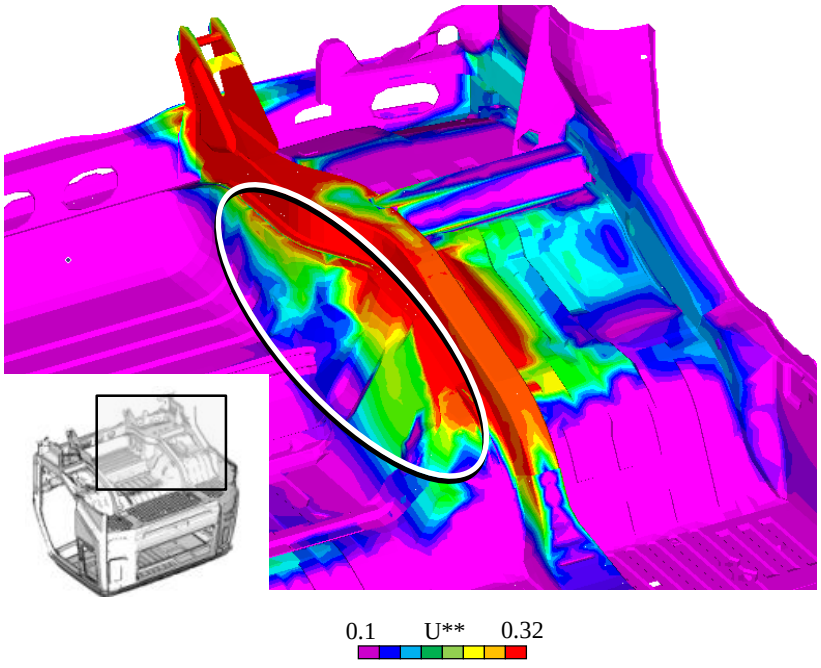

Fig. 6. 7 Distribution of "m2-4msU" (Tunnel Wall)**

the rear part of the cab.

6.2.4 Load Transfer in Side Sills and Cross Members

When the parameter *m* equals to 2, the distributions of U** in the side sill are shown in

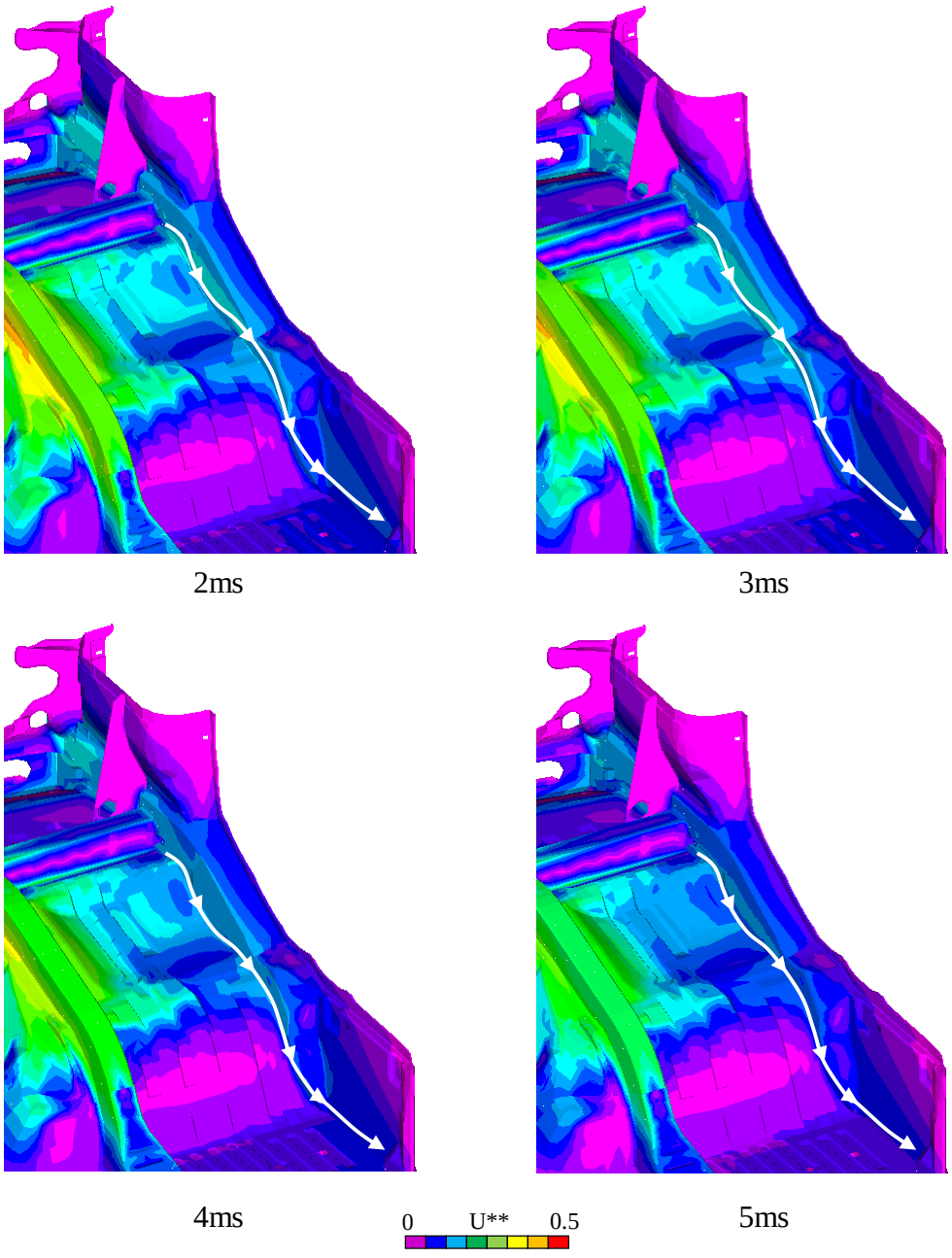

Fig. 6. 8 Distribution of U and Load Paths (*m*=2, Side Sills)**

Fig. 6.8. From Fig. 6.8, we can find that the side sill also plays some roles in transferring loads to the rear structures in each time step. The cross member connecting between the main member and the side sill transfers some loading successfully to the side sill. The load path in the side sill and the cross member is plotted in Fig. 6.8. Observing on the value of U**, the quantity of the load transfer through cross-member to the side sills is less than that of the main member. Thus, the load path in the cross-member is regarded as a secondary load path.

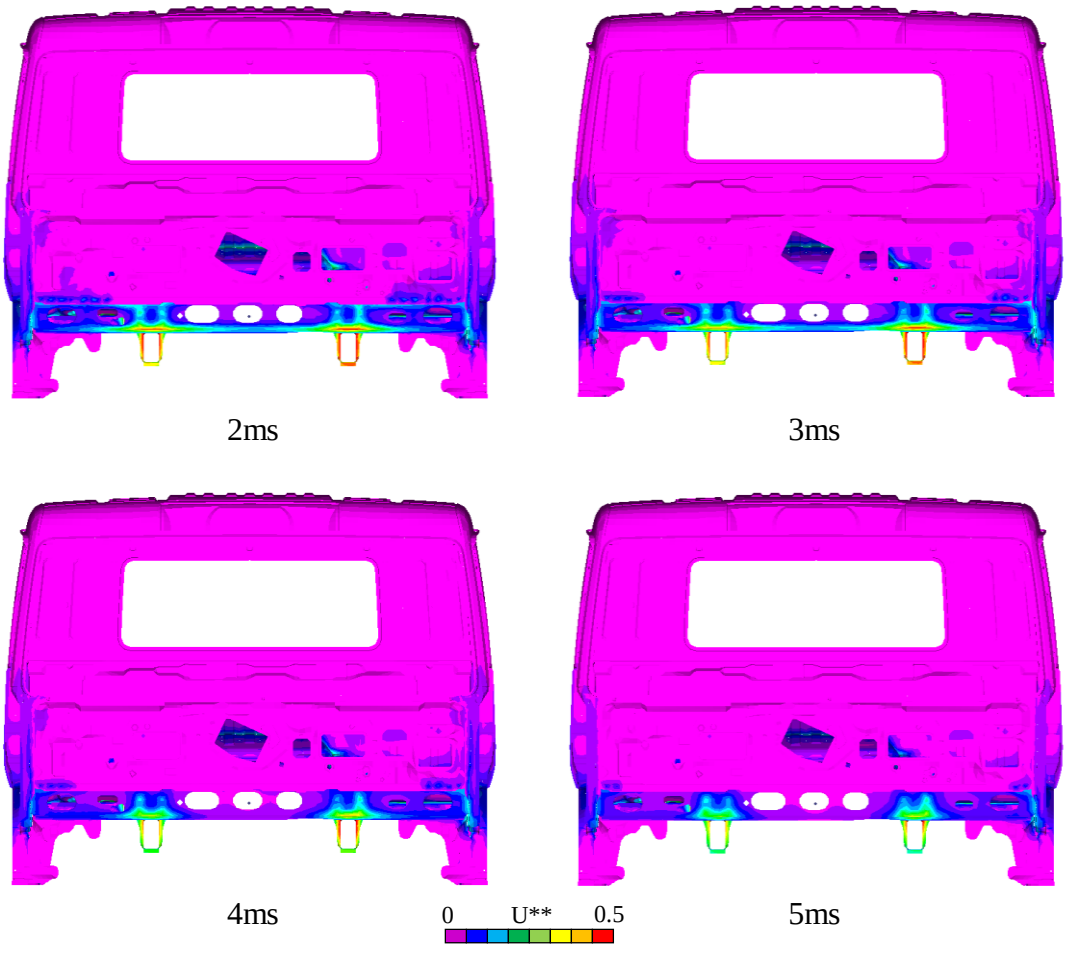

Fig. 6. 9 Distribution of U (*m*=2, Frontal Panel)**

6.3 Load Transfer in Front Panel

The U** distribution of the front panel is presented in Fig. 6.9. Based on the deformation shown in Fig. 5.1, the front panel is under distributed loading after contacting with the frontal rigid barrier, and the loading area changes rapidly at initial crash stages. The results of Fig. 6.9 reveal that the front panel has little effect in the load transfer. The intrinsic reason can be understood easily because of the minor effect of flat panels in resisting perpendicular distributed loadings. Thus, a stiffer design should be applied to

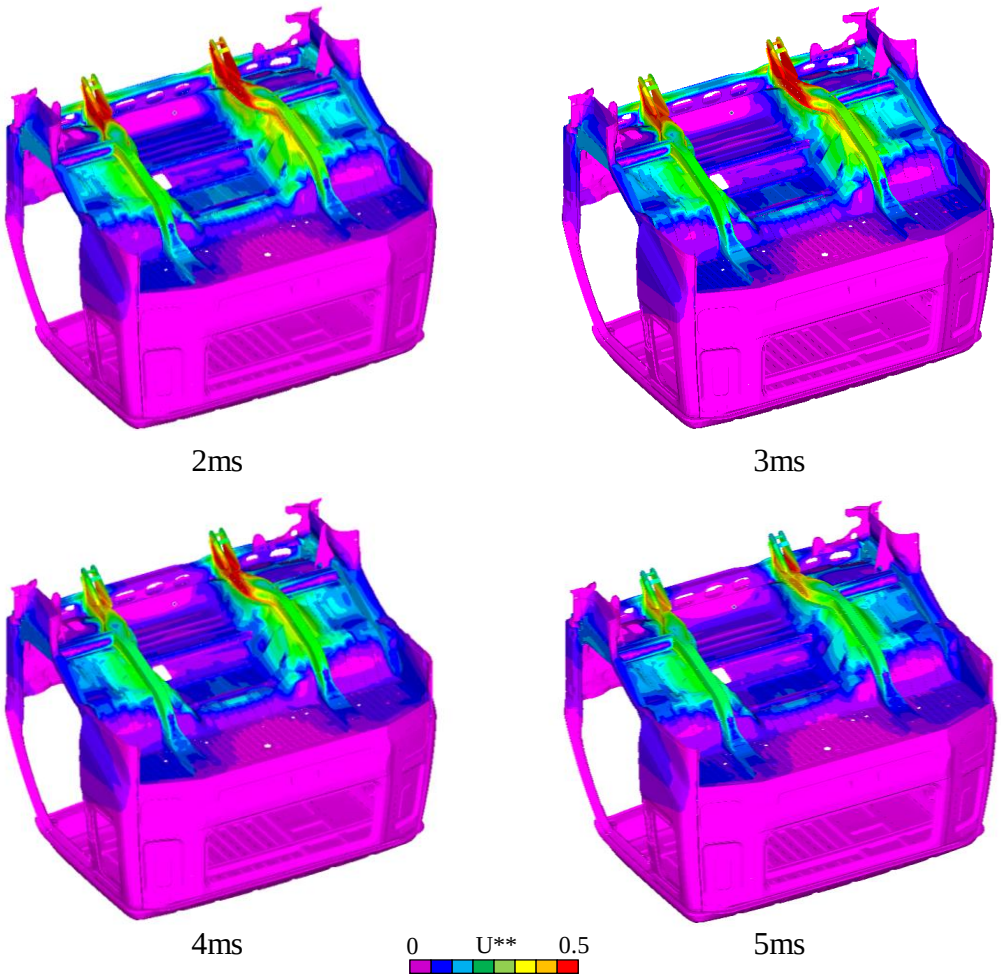

Fig. 6. 10 Distribution of U (*m*=2, Floor Panel)**

the front panel to improve its ability of transferring loads. Moreover, due to significant variation of the loading area it is necessary to examine the load transfer and load paths at 4ms when loadings become stabilized.

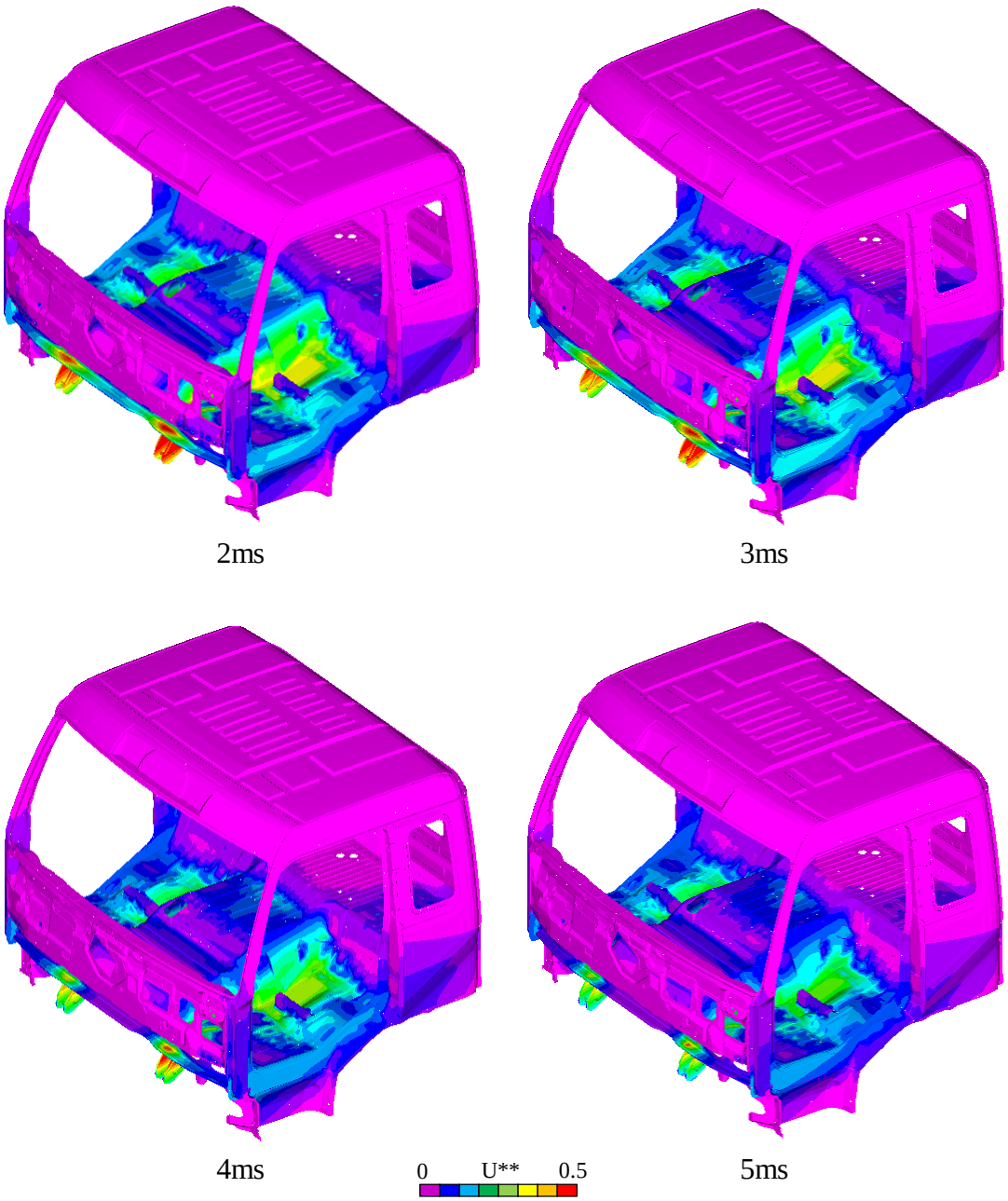

Fig. 6. 11 Distribution of U (*m*=2, Roof)**

Roles of the main members and the side sills are clearly shown in the overall views of the floor structures in Fig. 6.10.

6.4 Load Transfer in Roof Panel

The U** distribution of the truck cab in the isometric view is shown in Fig. 6.11. Observing Figs. 6.10 and 6.11, although frontal structures demonstrate outstanding abilities in the load transfer, the roof panel has minor effect in transferring the impact loads. The U** values of A-pillars are also very small compared with the frontal cross-member. We can say that because of a little effect of the frontal panel and the minor effect of A-pillars in the load transfer, the roof rail structure does not show its proper ability in the load transfer.

6.5 Summary

The new index U** is applied to express the load transfer in heavy-duty truck cabs during the initial crash phase, and the following results are obtained. It should be noted that the concept of the stress is not used here.

(1) Since the main part of a compartment should be maintained in the linear elastic condition for the safety of occupants, a linear static analysis of U** is applicable to the main part of a truck cab.

(2) A deformed cab body at the initial crash stage is obtained by a dynamic simulation. The deformed body is extracted and the U** distribution for this body can be statically calculated. In this process, a method of the substitution modulus is applied to reproduce the material and geometrical non-linearities for the load path U** analysis.

(3) The most appropriate index "m2-4msU**" is proposed as the standard condition for the load path U** analysis for the estimation of the effect of newly designed stiffeners in the cab.

(4) The predominant load paths are observed along the main floor member, and the load transfer based on the shear effect of the floor panel is demonstrated. The tunnel wall is playing an important role together with the main member for the load transfer. The side sill also plays some roles in transferring loads to the rear structures in each time step. The load path in the cross-member is regarded as a secondary load path. The roof rail structure does not show its proper ability in the load transfer.

(5) The frontal panel and the roof panel do not show proper abilities in the load transfer. It is found that at 4ms frontal loadings become stabilized. The load transfer and load paths analysis of the cab structure should take 4ms for U** calculations.

7. Static Load Path Analysis for Truck Cab Structures Using Index U*

7.1 Small Differences of U* Distribution

In Chapter 6, we calculated the U** distribution with different values of the duration time *t* and the parameter *m* for the floor panels as shown in Fig. 6.1. In Fig. 6.1, every figure is a bottom view.

As shown in Fig. 6.1, in the initial crash stage, nearly the same distribution of U** can be observed with regard to every set of *t* and *m*. The load transfer in the elastic structure is maintained almost unchanged during the initial crash phase.

In this chapter, to compare with the above mentioned U**, the U* distribution is calculated for the same model. Fig. 7.1 shows the results of the calculations. In these calculations, referring to the results of Fig. 6.1, we fix the value *m* for *m* = 2.

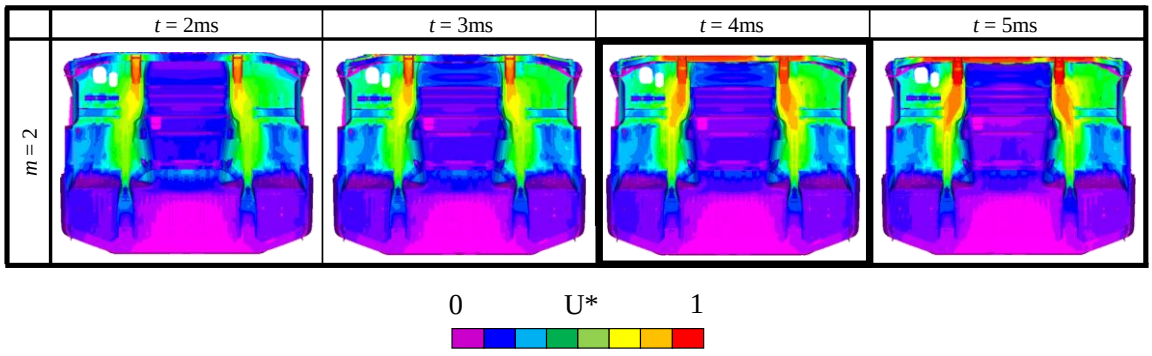

Fig. 7. 1 Small Variation of U* Distribution from Frontal Barrier (*m*=2)

Comparing U* in Fig. 7.1 with U** in Fig. 6.1, we arrive at the same conclusion as Chapter 6 that the difference in load transfer with respect to the time *t* is small. The reasons for this small difference are the small nonlinear areas, the uniformly deformed frontal surface, and the non-dimensional expression of U** values.

The frontal part of a main member contacts to the barrier at just before 3ms for the present cab, therefore the sample time is preferable to be taken after 3ms. The values of *m* = 1 and *m* = 10 mean the extraordinary cases. Between these two extraordinary conditions, we can see the difference of the U** distribution is small. Therefore, we can determine that the combination of *t* = 4ms and *m* = 2 is the most suitable set, and we refer to the U* value with this combination as the index "m2-4msU*".

This index can be used as the standard condition of the load transfer for the comparison of the change in the load transfer before and after reinforcement of a cab.

We cannot use the tangent modulus instead of the value of *m*, because the extremely small elastic constant introduces very small loading in U** analysis. The values of *m* and *t* will be investigated in future studies to express the nonlinear behaviour more appropriately.

7.2 Load Transfer in Floor Structure

The U** values and the U* values along the corners of the main floor member are shown in Fig. 7.2. According to these results, we can observe that the difference in shape between U* and U** distributions is almost the same, where *s* refers to the distance from

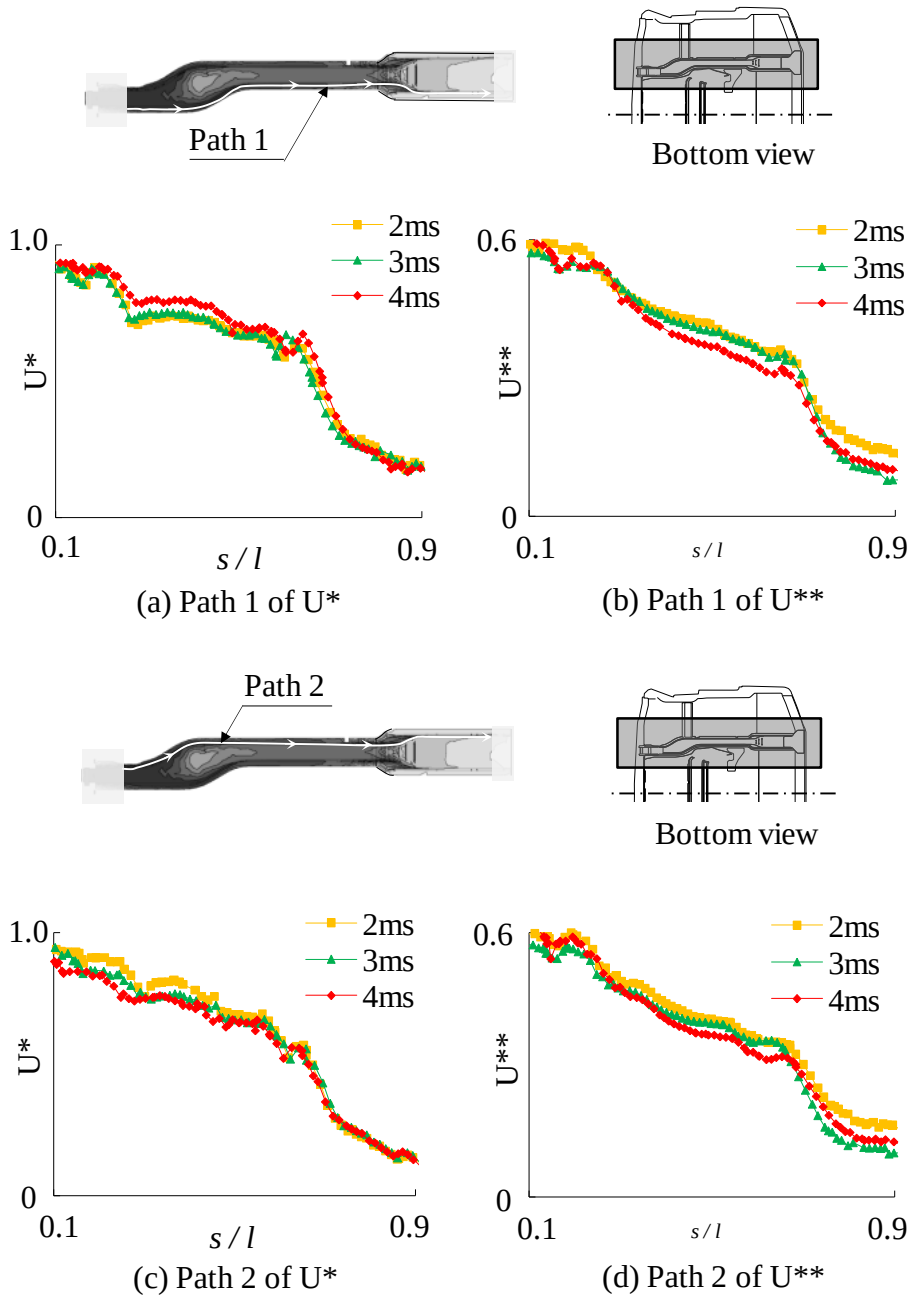

Fig. 7. 2 Decay of U* along Load Paths (*m*=2)

the front end along the path and l is the total length of each path. However, the absolute value of each is different. The U* value is higher than U** by about 1.6 times. This difference is inevitable because of the difference in their definitions.

For a desirable structure, as shown in Fig. 2.5, the U* distribution along a path should decay uniformly and continuously. Observing the uniform decay of U* in Fig. 7.2, we can say the main members almost satisfy these conditions of uniformity and continuity.

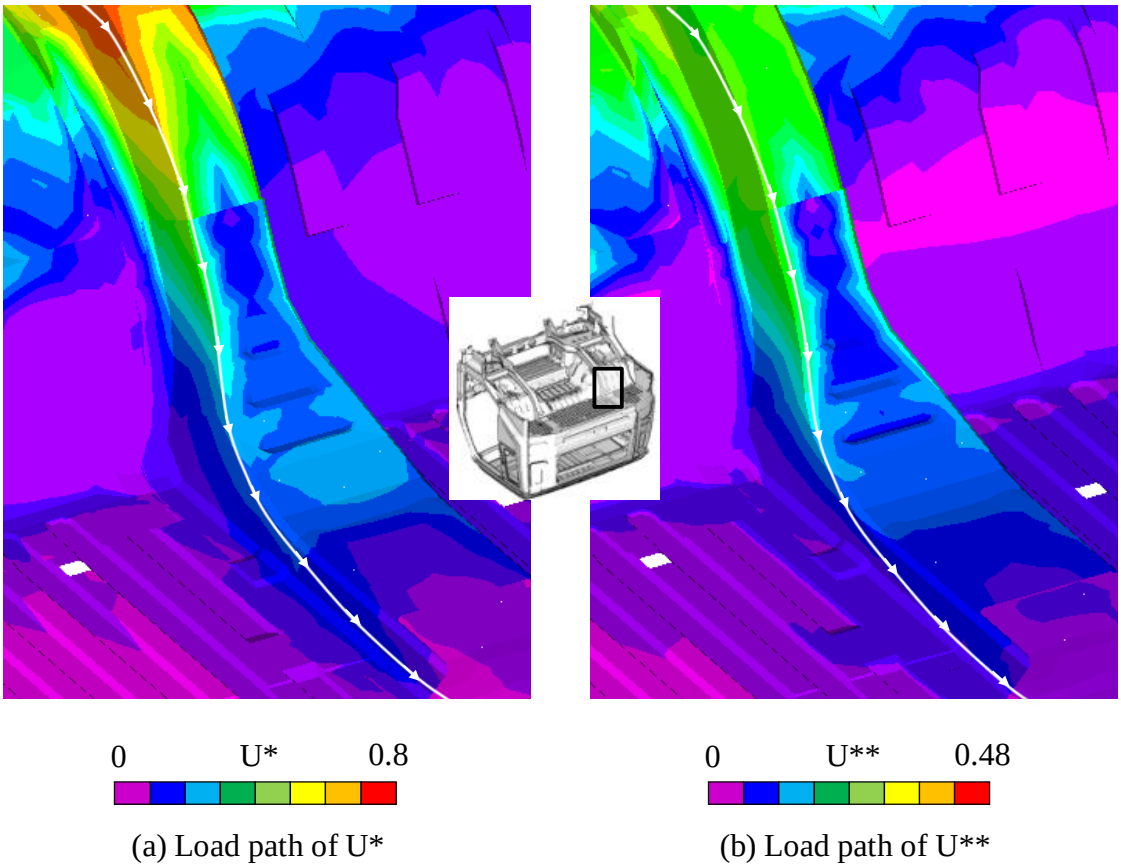

(a) Load path of U* (b) Load path of U**

Fig. 7. 3 Distribution of "m2-4msU*" and Load Paths

7.3 Comparison of Load Transfer and Load Path in Floor Structure (Comparison of U* and U**)

7.3.1 Load Path along Main Members

For the main floor member, the load path of U* distribution is shown in Fig. 7.3(a). From the high values of U* observed at the corners of the main floor member, we can see that the corner of a member plays an important role in the load transfer.

7.3.2 Load Path in Floor Panels

In Fig. 7.4(a), the distribution of "m2-4msU*" for a cross-section (x_2 = 750mm) of the front floor panel is shown. The data for U** are also shown for comparison in Fig. 7.4(b).

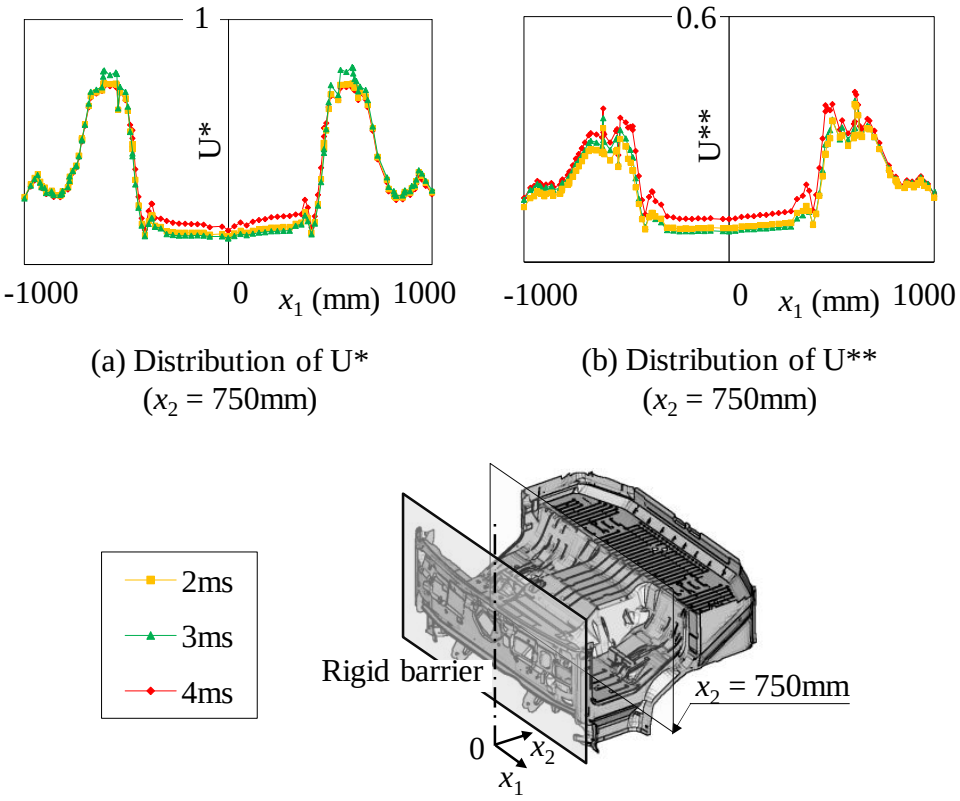

(a) Distribution of U* (x_2 = 750mm)

(b) Distribution of U** (x_2 = 750mm)

Fig. 7. 4 Cross-Sectional Distribution of U* and U (*m*=2)**

As we observe above, the value of U* is almost 1.6 times larger than that of U**. However, in Figs. 7.4(a) and 7.4(b), the difference seems larger than 1.6 times.

Moreover, in Fig. 7.5 a comparison between the U* distribution and U** distribution of floor panels is shown. The result of Fig. 7.5 also shows that there are differences in distribution in the floor panels. Based on observation of U* distribution, frontal floor panels are reasonable in the load transfer and transfer loads to side sills. In contrast, according to the U** distribution, middle floor panels transfer loads from main members to side sills.

The reason why Figs. 7.4 and 7.5 present differences in distributions is as follows.

For the value of U**, when an arbitrary point (Point C in Fig. 2.8) is constrained, the contact surface with a barrier is deformed, because the contact condition is a specified force. This is the condition for a honeycomb barrier collision. Meanwhile, the application of the index U** is more suitable for passenger cars. Thus, the index U** will be used in the study of passenger cars shown in the Chapter 9. In contrast, for the calculation of U*, as the contact condition is a forced deformation, the contact surface with a barrier remains a flat surface.

For this reason, in the present case of the flat barrier collision, U* is an adequate choice. The difference appears in a weak panel that is adjacent to a stiff member. However, as shown in the results above and below, both indexes show almost the same distribution.

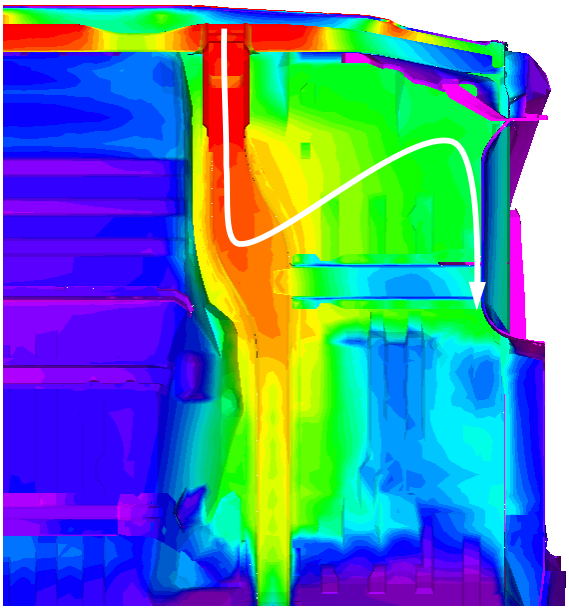

(a) m2-4msU*

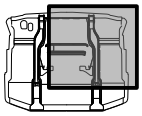

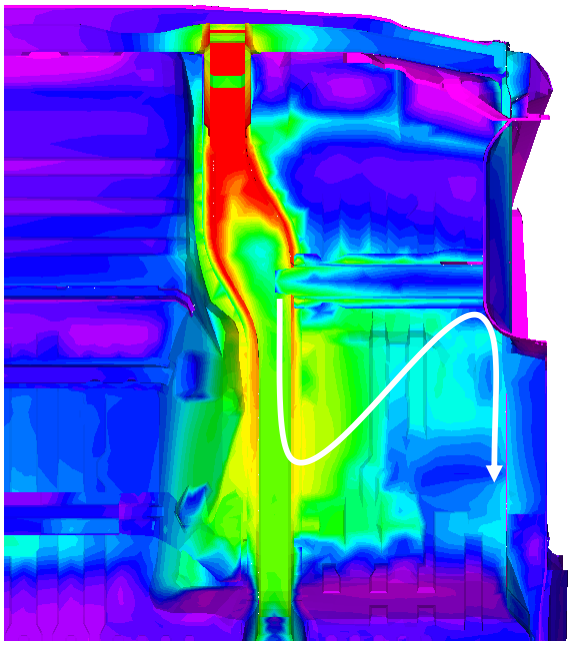

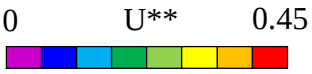

(b) m2-4msU**

Fig. 7. 5 Load Transfer in Floor Structure (m2-4msU* and m2-4msU)**

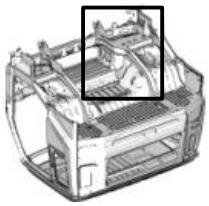

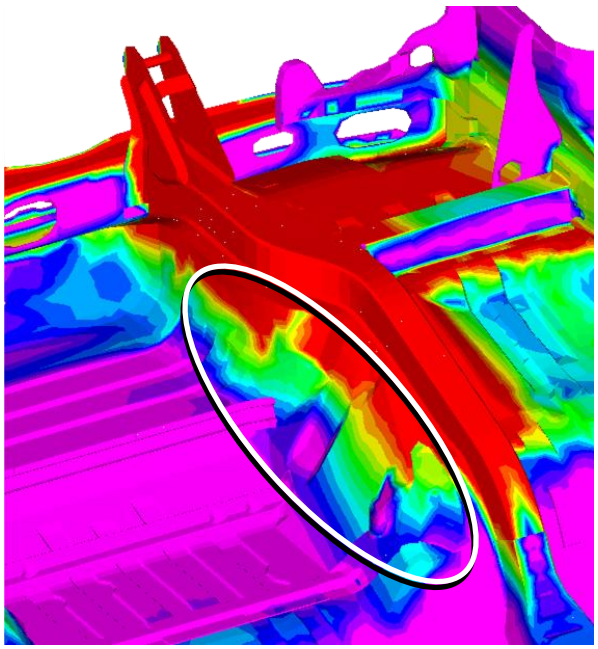

0.15 U* 0.55

(a) m2-4msU*

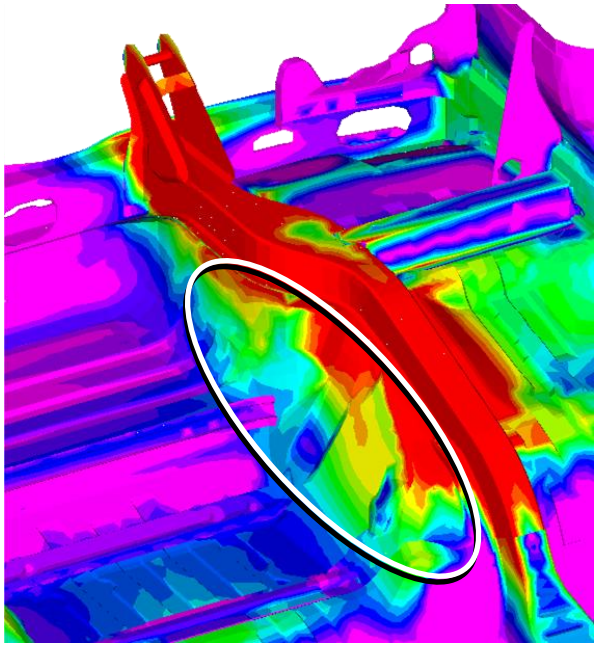

0.05 U** 0.3

(b) m2-4msU**

Fig. 7. 6 Load Transfer in Tunnel Wall

7.3.3 Load Transfer in Tunnel Structure

As far as Figs. 7.4 and 7.5 are concerned, the effectiveness of the tunnel center panel is insignificant in load transfer. However, when observing U* (Fig. 7.6(a)) of tunnel structure, we can find that the tunnel walls play a crucial role in load transfer together with the main members. This has been already shown in Fig. 7.6(b) which is the same as Fig. 6.7 in Chapter 6.

It is necessary to introduce a stiffener as an additional load path from the surface of the tunnel wall to the rear part of the cab.

7.3.4 Load Transfer in Side Sills and Cross Members

The U* distribution in side sills is shown in Fig. 7.7(a). Compared with the U** distribution shown in Fig. 7.7(b), side sills are also working as important members in the load transfer. Both cross members and frontal floors structures distribute the impact forces to side sills, which shows no difference compared with U** distribution, which shows the effectiveness of the cross-member in the load transfer. The reason has been explained in Section 7.3.2.

The load paths in side sills and cross members are plotted in Fig. 7.7. Similar phenomenon can be observed in Fig. 6.8 that the quantity of the load transfer through cross-members and side sills is less than main members. Thus, load paths in these two structures are regarded as secondary load paths.

7.4 Load Transfer in Front Panel

Figure 7.8(a) shows the U* distribution of the front panel. Compared with the U** distribution of the front panel shown in Fig. 7.8(b), it can also be found that the front panel show little effect in the load transfer, although the U* distribution in the contact regions (loading points A) are much higher than that of U** distribution. This is inevitable because of the definition of index U* where the value of U* equals unit at loading points mentioned in Chapter 3.

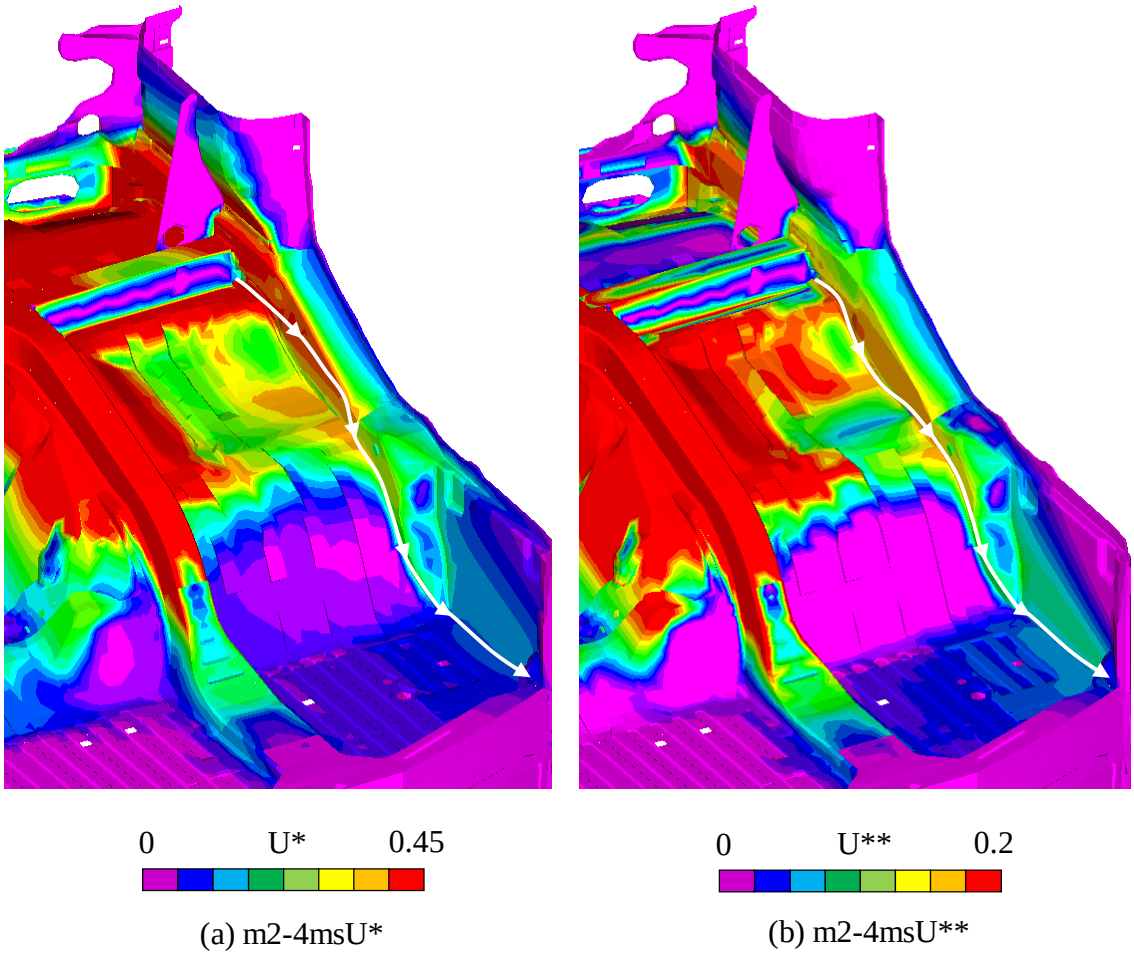

(a) m2-4msU* (b) m2-4msU**

Fig. 7. 7 Load Transfer in Side Sills

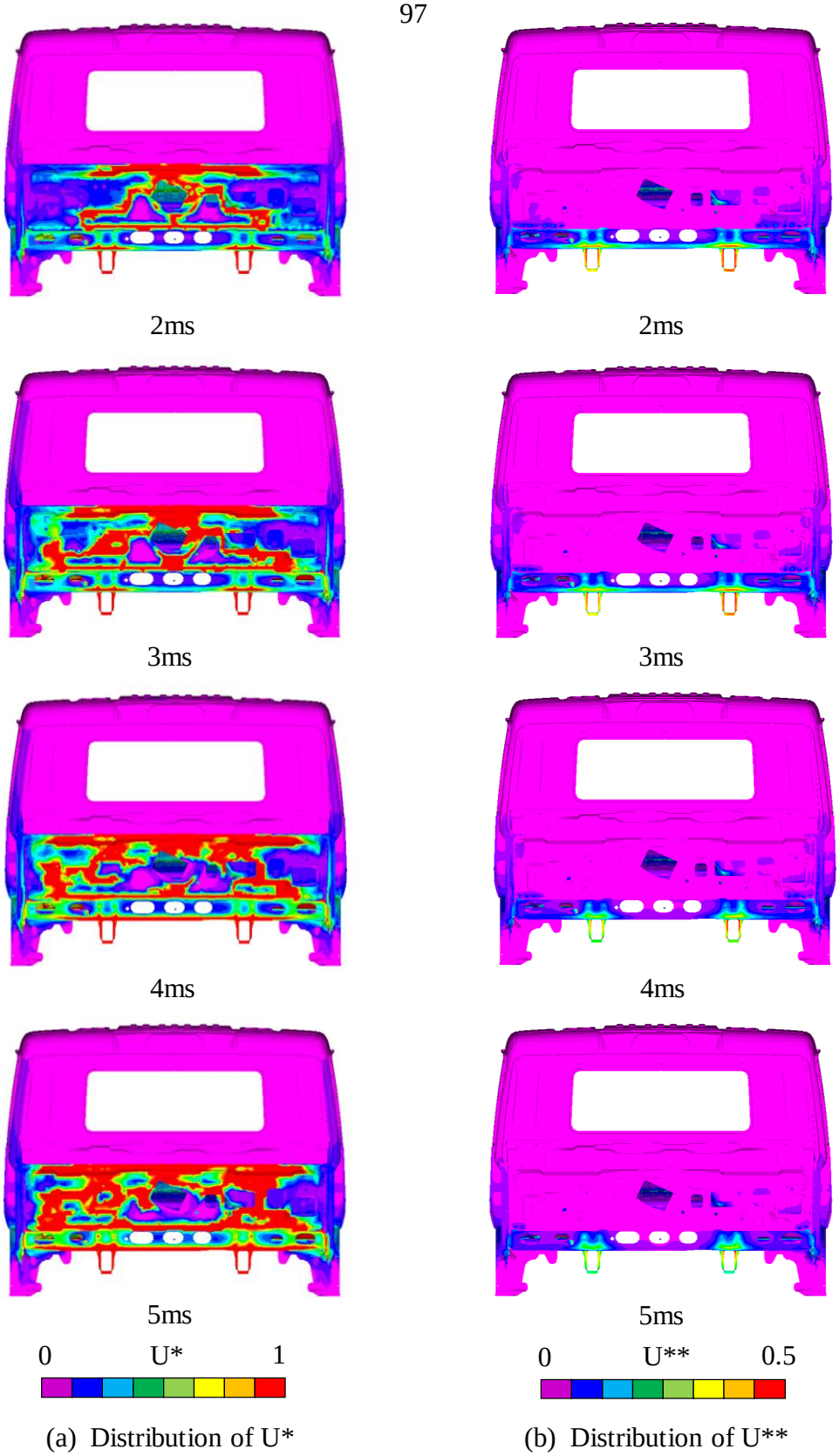

(a) Distribution of U* (b) Distribution of U**

Fig. 7. 8 Distribution of U* and U (Frontal Panel)**

Thus, it is suggested that a stiffer design should be proposed to the front panel to improve its ability of transferring loads.

7.5 Load Transfer in Roof Panel

The isometric view of U* distribution is shown in Fig. 7.9. From Figs. 7.8 and 7.9 we can obtain the same results as mentioned in Chapter 6 that the roof panel do not show its

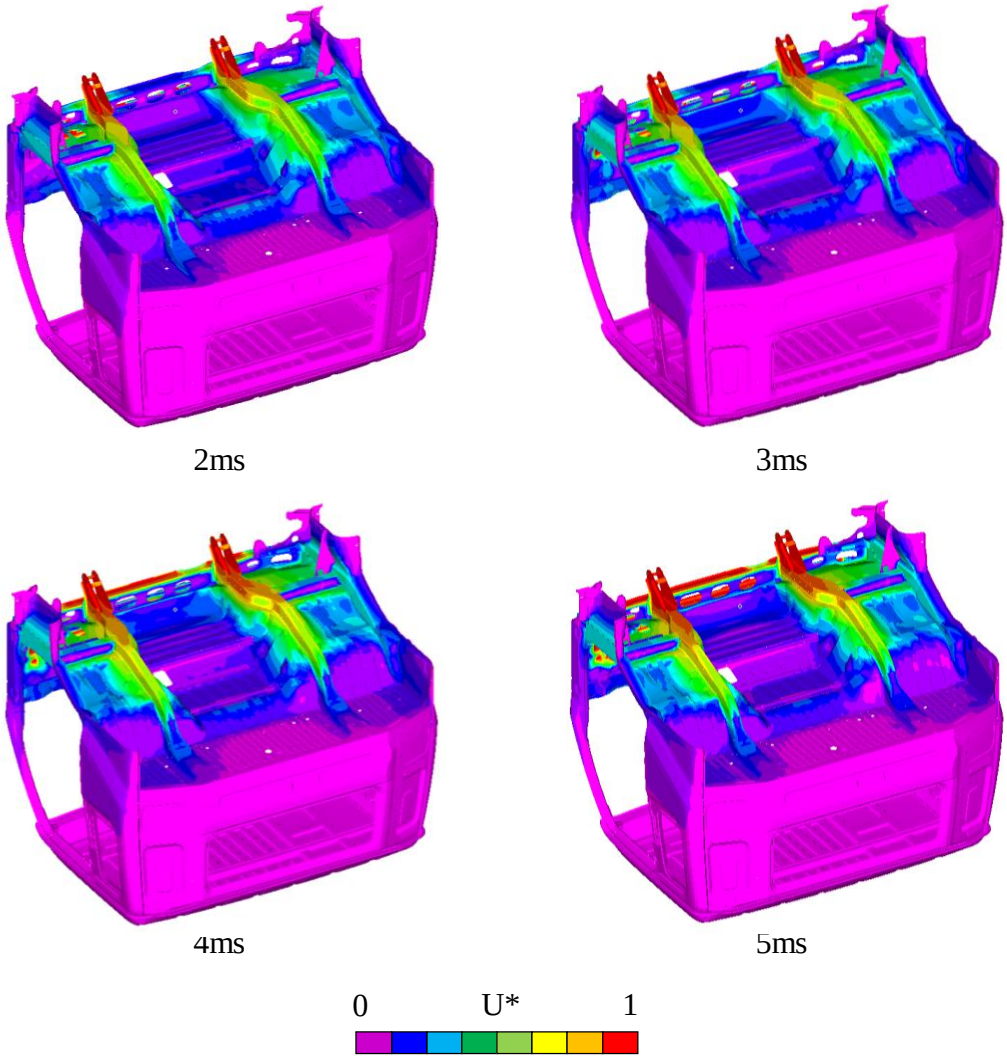

Fig. 7. 9 Distribution of U in Floor Panels**

proper ability in the load transfer. The reason of little effect is because of the little effect of the front panel and the minor effect of A-pillars in the load transfer. Therefore, stiffeners are necessary to be added in the front panel and A-pillars to improve their abilities in the load transfer.

7.6 Load Transfer in Floor Structure and Comparison of U* and U**

Fortunately, we can say that there is no significant difference between U* and U** distributions, although the absolute value of U* is larger than U** by about 1.6 times.

This difference is inevitable because of the difference in their definitions. For the discussion of load paths or load transfer, in general, the ratio of the load transfers and the distribution of transferred load are more important than the absolute values. As shown above, even considering the difference between U* and U**, the load transfer in the floor structures can effectively be discussed.

For index U*, it is feasible to the flat barrier collision, since it is derived by using the displacement method. A uniformly distributed forced displacement loading condition reflects the flat barrier impact condition perfectly. On the other hand, when using index U**, it is applicable to the problems with variable barriers such as honeycomb barriers. As mentioned in the thesis, index U** is obtained by using the force method. Distributed loadings can be applied properly. In a word, the usage of indices U* and U** is depending on the boundary conditions of the structures analyzed. In the present study,

index U* is found to be reasonable for truck cab analysis, and index U** is suitable for the study of a passenger compartment.

7.7 Summary

The index U* was applied to a truck cab structure under a frontal collision during the initial crash stage to investigate the load transfer and load paths. For the comparison with our previous results involving U**, a dynamic-static method and a substitution-modulus method which had previously been introduced by the authors were used. The results are as follows:

(1) The difference in load transfer with respect to the parameter m and the time t is small. We chose the most suitable set of m = 2 and t = 4 ms, and we referred to the U* value with this combination as the index "m2-4msU*".

(2) The shape of the U* and U** distributions is almost the same. However, the absolute value of U* is greater than U** by about 1.6 times. The difference is inevitable because of the difference in their definitions.

(3) For a flat barrier collision, U* is adequate, while for the case of a honeycomb barrier collision, U** is suitable. However, both indexes show almost the same distribution.

8. Static Load Path Analysis Using Index U*sum and Histogram

8.1 Histogram of U*sum in Floor Structure

The distributions of U*sum in the floor structure shown in Fig. 8.1 are based on the summation of the U* distributions from the frontal barrier (Fig. 7.1) and from the rear end (Fig. 8.2). The histograms of U*sum are shown in Fig. 8.3. From Figs. 8.1 and 8.3, we can see again that the effect of sample time *t* is small in the initial stage of a collision.

Comparing the histograms of the ideal simple spring (Fig. 2.13(b)) and the actual floor structure (Fig. 8.3), we can see a large difference. In the present floor structure,

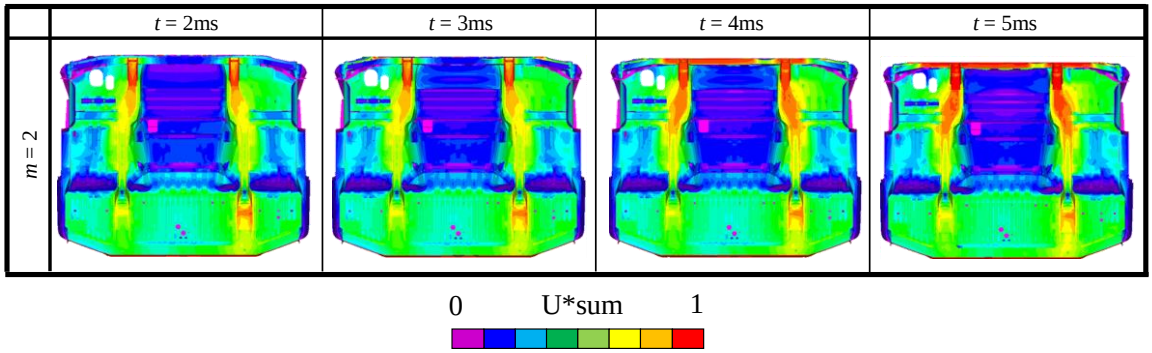

Fig. 8. 1 Small Variation of U*sum Distribution

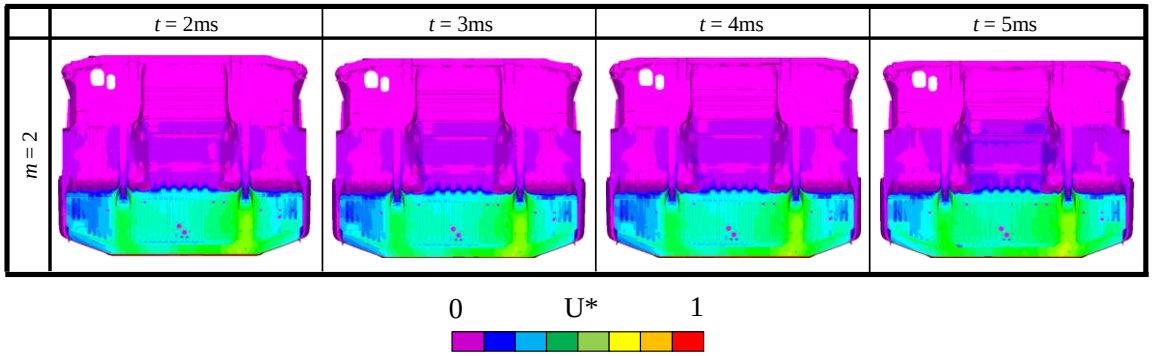

Fig. 8. 2 Small Variation of U* Distribution

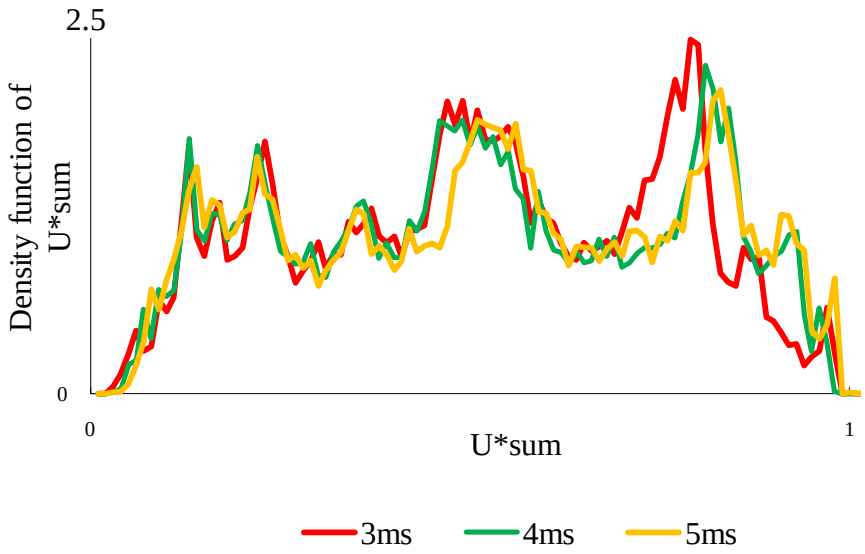

Fig. 8. 3 Histogram of Floor Structure

transferred loadings are not uniform between the members.

8.2 Load Paths and Histogram of Main Members

8.2.1 Load Paths along Main Members

For main floor members, the load paths from the loading point and the constraint point are shown in Figs. 8.4(a) and 8.4(b), respectively. From the high U* values observed at the corners of the main floor member, we can conclude that the corner of a member plays an important role in the load transfer. From the above observations, it can be said that the cross-sections with multiple corners shown in Fig. 6.5 are effective for the load transfer.

8.2.2 Histogram of Maim Members

A histogram of U*sum for m = 2 and t = 4ms is shown in Fig. 8.5 in which each histogram of the sub-structure is simultaneously represented.

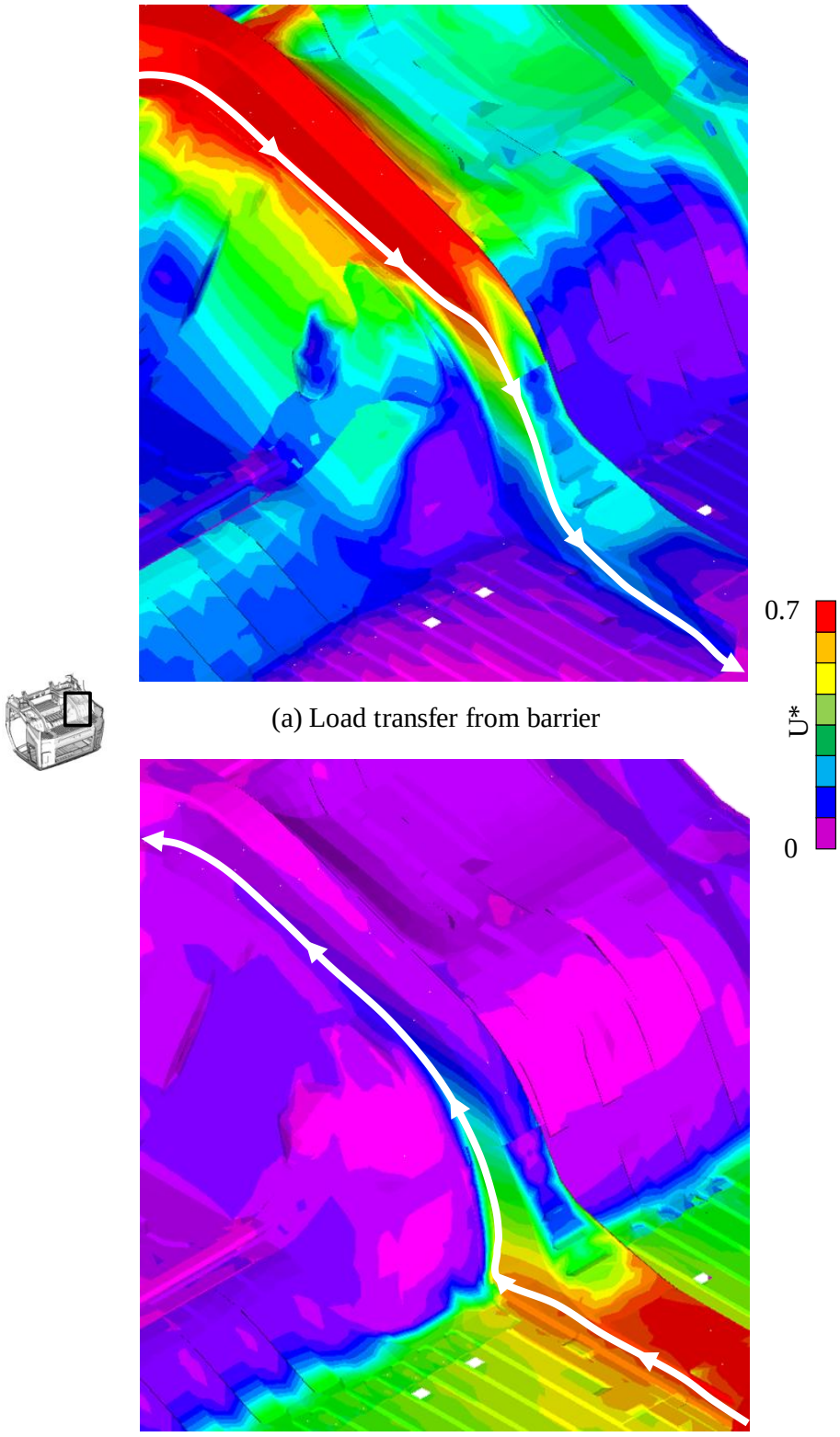

(a) Load transfer from barrier

(b) Load transfer from rear mass

Fig. 8. 4 Load Paths (m2-4msU*)

Compared with the other sub-structures, we can see that the main members have higher values, and the sharpness of the histogram for the main members shows a relatively desirable load transfer.

Meanwhile, from Fig. 8.5, we can see that the contribution of the tunnel structure to load transfer is relatively small. In the subsequent section, a more detailed investigation of the tunnel structure will be presented.

8.3 Distribution of U*sum in Tunnel Structure and Its Histogram

Although the load transfer in the tunnel structure is small, the tunnel side wall is effective in load transfer as already shown in Fig. 7.6. The histograms of U*sum for the tunnel panel and for the tunnel side wall are depicted in Fig. 8.6. From this figure, we can see that the tunnel side walls are more effectively transferring loading than the rest of the

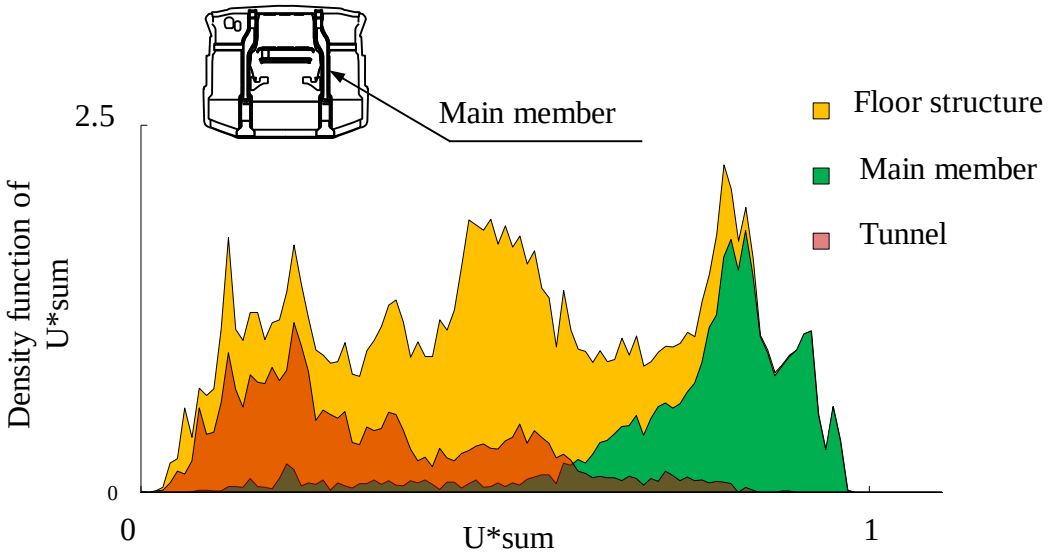

Fig. 8. 5 Histogram of Main Member and Tunnel (m2-4msU*sum)

tunnel structure. An additional stiffener is useful at the end of the tunnel side wall to convey the loading to the rear end, as shown by the circle in Fig. 8.6(a).

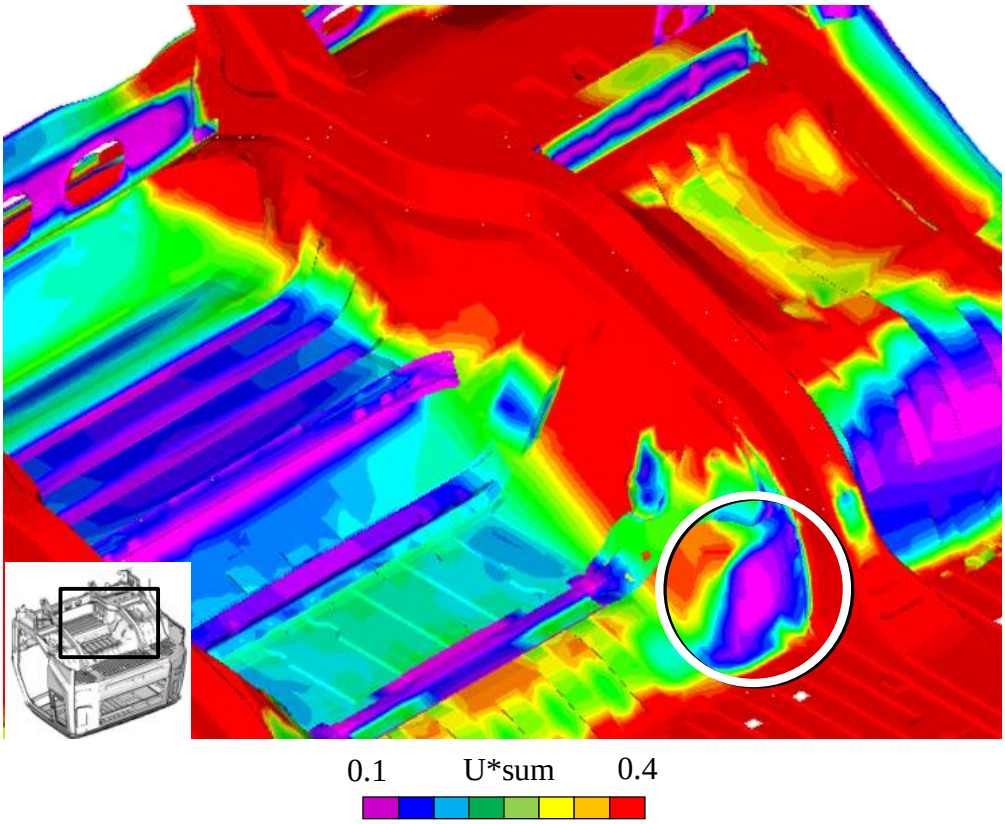

(a) Distribution of U*sum in tunnel wall

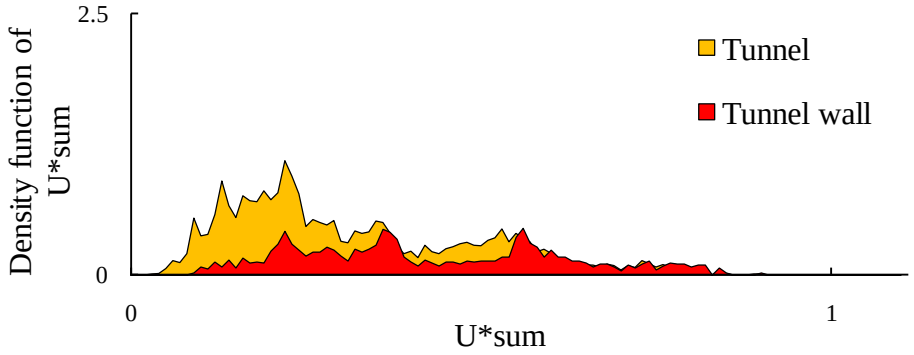

(b) Histograms of tunnel and tunnel wall

Fig. 8. 6 Distribution of U*sum and Histogram in Tunnel Wall (m2-4msU*sum)

8.4 Load Transfer in Front Floor Panel

In Fig. 8.7(a), we can see the effectiveness of the front floor panel which is also observed in Chapter 7. Comparing the front floor panel and the whole floor panel (without frame members) in the histograms shown in Fig. 8.7(b), we can recognize this fact.

8.5 Distribution of U*sum along Load Paths

U*sum of the main member is examined in the light of the description of the ideal spring shown Fig. 2.13(a). The U* distributions for load path 1 (Fig. 7.2) from the frontal loading Point A and for the same path 1 from the rear constraint Point B are shown in Fig. 8.8(a). The summation of these distributions that is U*sum along path 1 is also shown in this figure. The distribution of U*sum is close to the horizontal line with a value of 1. Consequently, two similar figures are observed for the simple spring (Fig. 2.13(a)) and for the main member (Fig. 8.8 (a)).

Moreover, in accordance with this observation, the histogram of this load path 1 shows a sharp peak near the point of U*sum = 1 (Fig. 8.8(b)). This result indicates that the main member of this cab transfers loading quite effectively. This observation is based on the U*sum distribution that is obtained along a single load path. In general, the load paths from the front end and from the rear end do not coincide. However, in the special case for which these load paths approximately coincide, it is useful to use the concept of U*sum along a path as shown here.

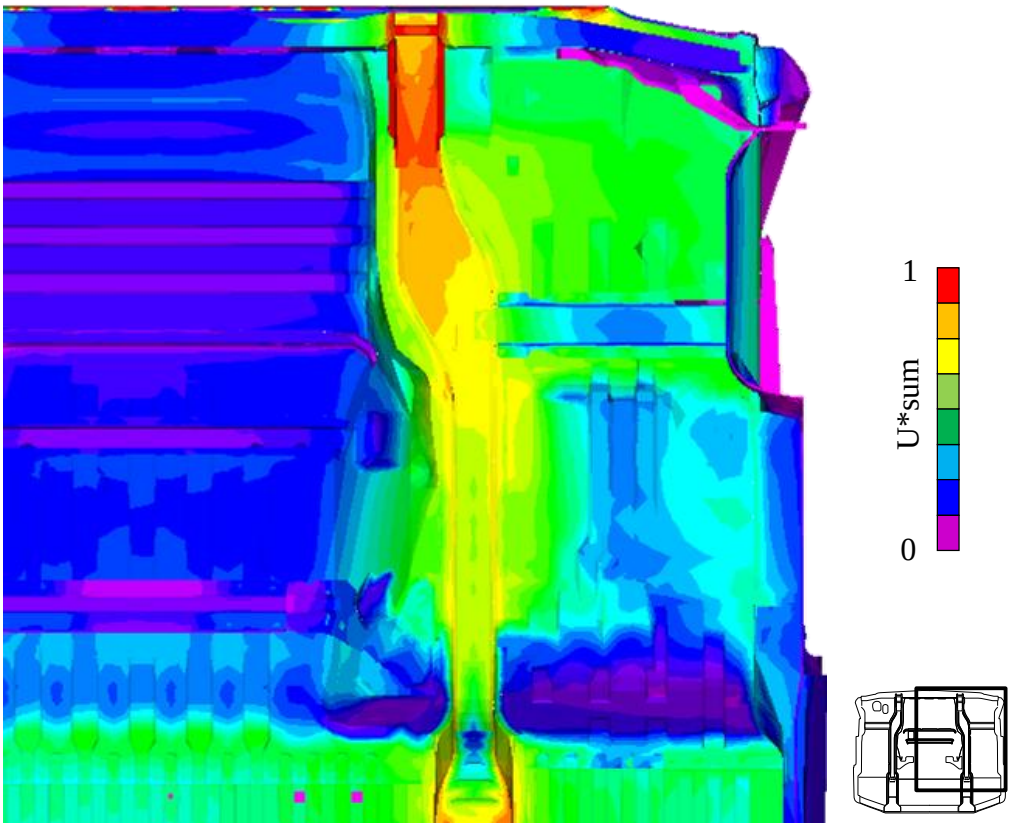

(a) Distribution of U*sum in floor structure

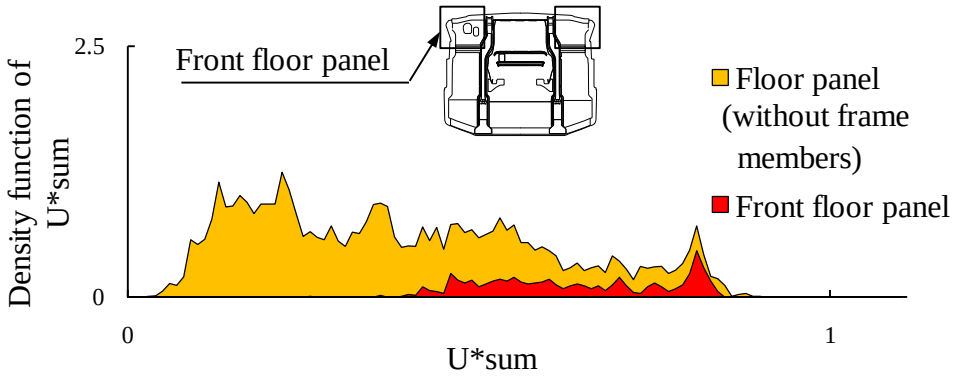

(b) Histograms of floor panel and front floor panel

Fig. 8. 7 Distribution of U*sum and Histograms in Floor Panels (m2-4msU*sum)

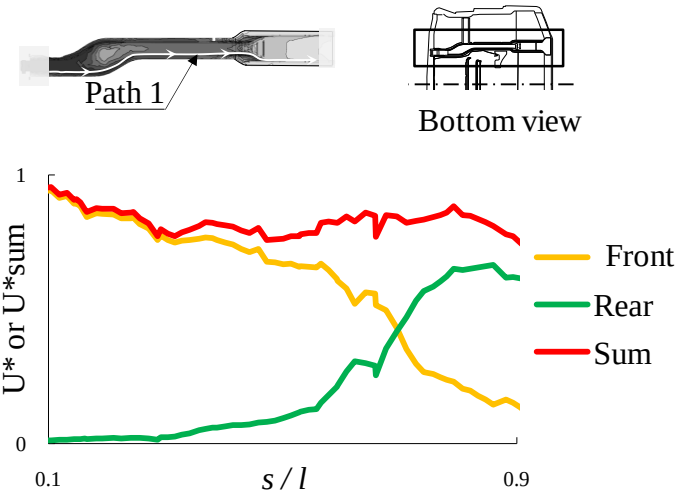

(a) U* and U*sum along load path 1
(m = 2, t = 4ms)

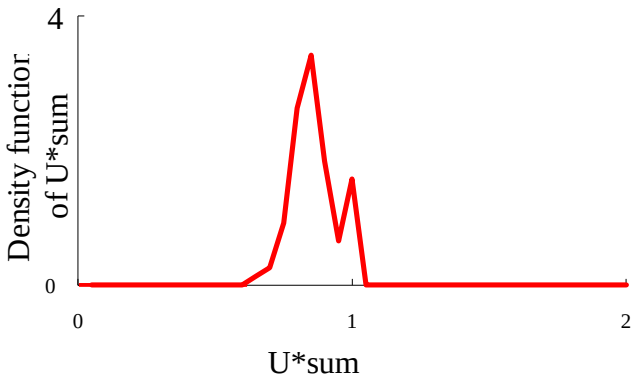

(b) Histogram of U*sum along load path 1

Fig. 8. 8 Distribution of U*sum along A Load Path

8.6 Summary

Concepts of U*sum and its histogram were used to express the effectiveness of the load transfer. Using these expressions, we were able to see in the present floor structure that the loading is transferred non-uniformly between each member.

The distribution of U*sum of the main floor member shows a desirable curve, and the histogram of the load path shows a sharp peak. These results indicate that the main member of this cab transfers loading quite effectively.

9. Load Path Analysis for Passenger Car Structures Using Separation Structure Method

9.1 Distribution of U**

*9.1.1 Distribution of U** in Floor Panels from Dash Panels*

According to the method mentioned in Chapter 3, the load transfer analysis in the compartment structure of a passenger car is analyzed. The index U** is used to reveal the variation of variable distributed loadings due to three reasons. Firstly, the contact regions between the frontal parts and middle elastic parts are varying in the dynamic impact. Secondly, inertial forces are considered in this study. Thirdly, the frontal parts work as a crushable barrier which is summarized to be suitable for U** calculations.

After applying the distributed loadings to the elastic compartment, the U** calculation is performed to analyze the load transfer and load paths in the elastic compartment. The U** distribution of floor panels at 15ms is depicted in Fig. 9.1. Based on the observation of Fig. 9.1, it is found out that the predominant load paths are along the floor main members.

It is necessary to notice that the range of U** value is extremely small, compared with the results shown in the previous chapters. This is inevitable in the multiple loading conditions due to the increasing of the complementary strain energy W in Eq. 2.15. By increasing the loading points, the variation of the ratio value of term W'/W becomes

insensitive to the free and fix conditions which are applied to the arbitrary point C in a structure, which means the variation of complementary strain energy *W'* is rather small in the present condition. It is summarized that the value of U** in a structure is very small due to the insensitivity of complementary strain energy *W'* in the case of multiple loading conditions. However, based on the observation of the ratio value of strain or

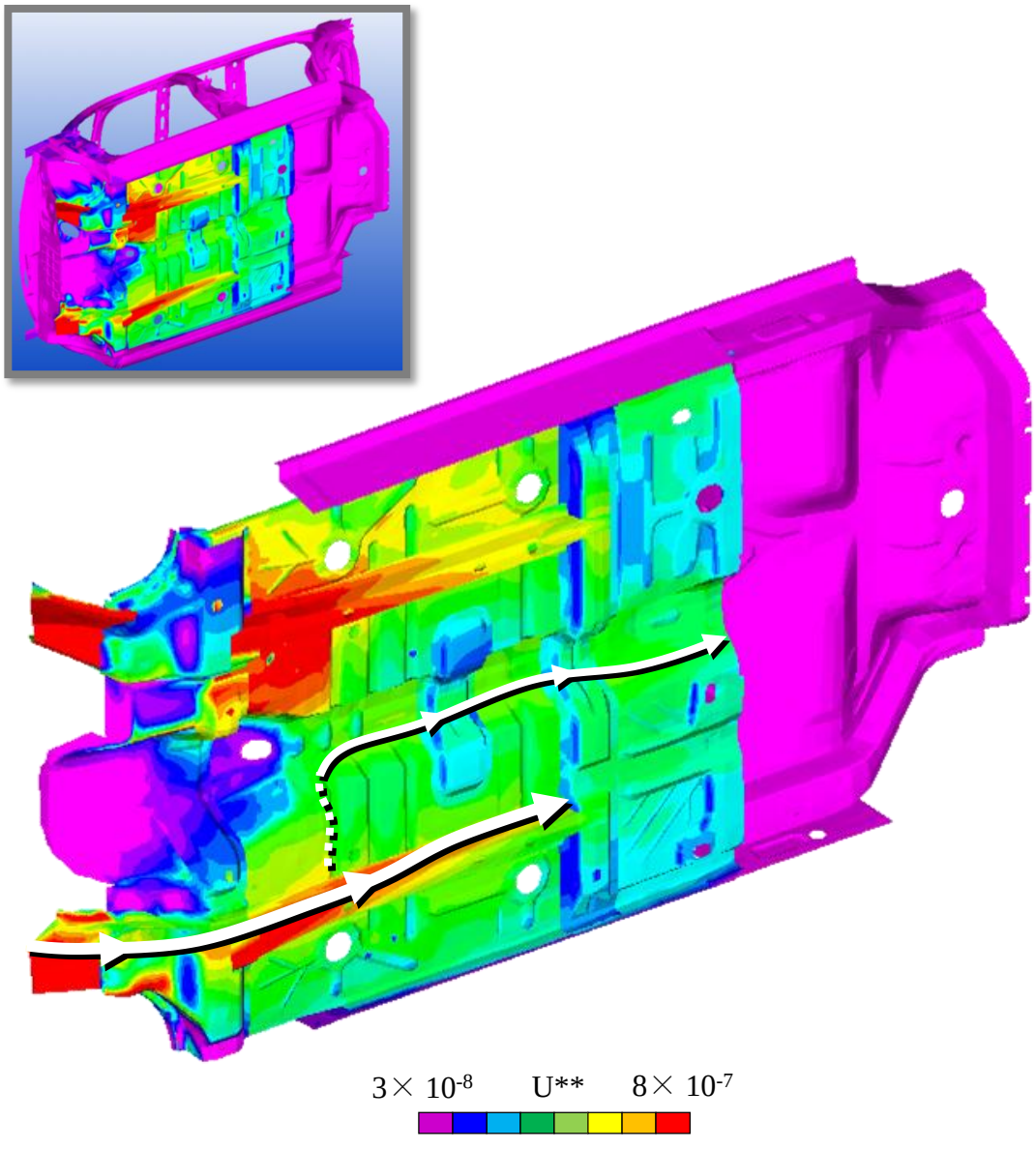

Fig. 9. 1 Distribution of U in Floor Panels (Frontal)**

complementary strain energies, the load transfer and load paths in a structure can be investigated properly.

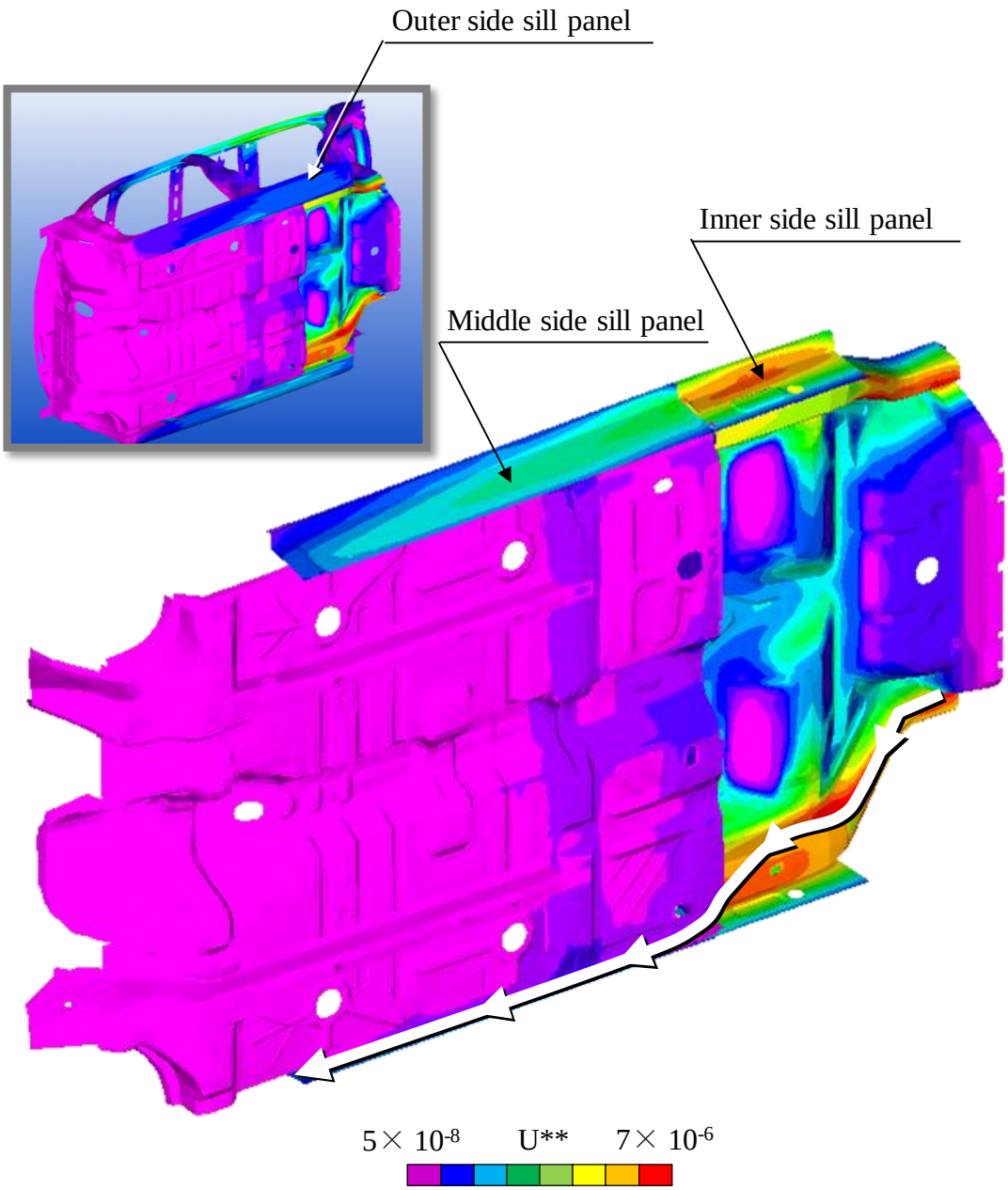

Fig. 9. 2 Distribution of U in Floor Panels (Rear)**

*9.1.2 Distribution of U** in Floor Panels from Rear Structure*

As mentioned in Chapter 2, aiming to obtain the U**sum distribution, the loading and constraint conditions in the static analysis are reversed, and the forced displacement loadings are changed to force loadings. The loadings apply to the edge between elastic and rigid structures are the same in the quantity of the frontal loadings. In the case of applying loadings from rear structures, the dash boards are constraint approximately, although their shapes are varying with the progress of crashing. By introducing this approach of boundary conditions mentioned in Chapter 5, the U** distribution in the floor panels at 15ms is represented in Fig. 9.2.

*9.1.3 Distribution of U**sum in Floor Panels and Its Histogram*

The distribution of U**sum in the floor structure at 15ms shown in Fig. 9.3 are based on the summation of U** distribution from the frontal loadings (Fig. 9.1) and from the rear loadings (Fig. 9.2). The histogram of U**sum at 15ms in the floor panel is shown in Fig. 9.4. The enlarged histogram distribution when U** values ranging from 0 to 1.5×10^{-6} is demonstrated in Fig. 9.5.

From the observation of U**sum distributions in the floor panels shown in Figs. 9.3, the rear main members, side sills and pillars also demonstrate some effects in the load transfers except the floor main members. Meanwhile, also due to the shear effect, the loadings are conveyed from floor main members to the side sills and tunnel structures, which also has been found in the study of trucks mentioned in Chapters 6 and 7. The

detail investigation of the load tranfer in side sills, pillars and other sub-structures will be shown in the next section.

9.2 Load Transfer and Load Paths in Floor Structures

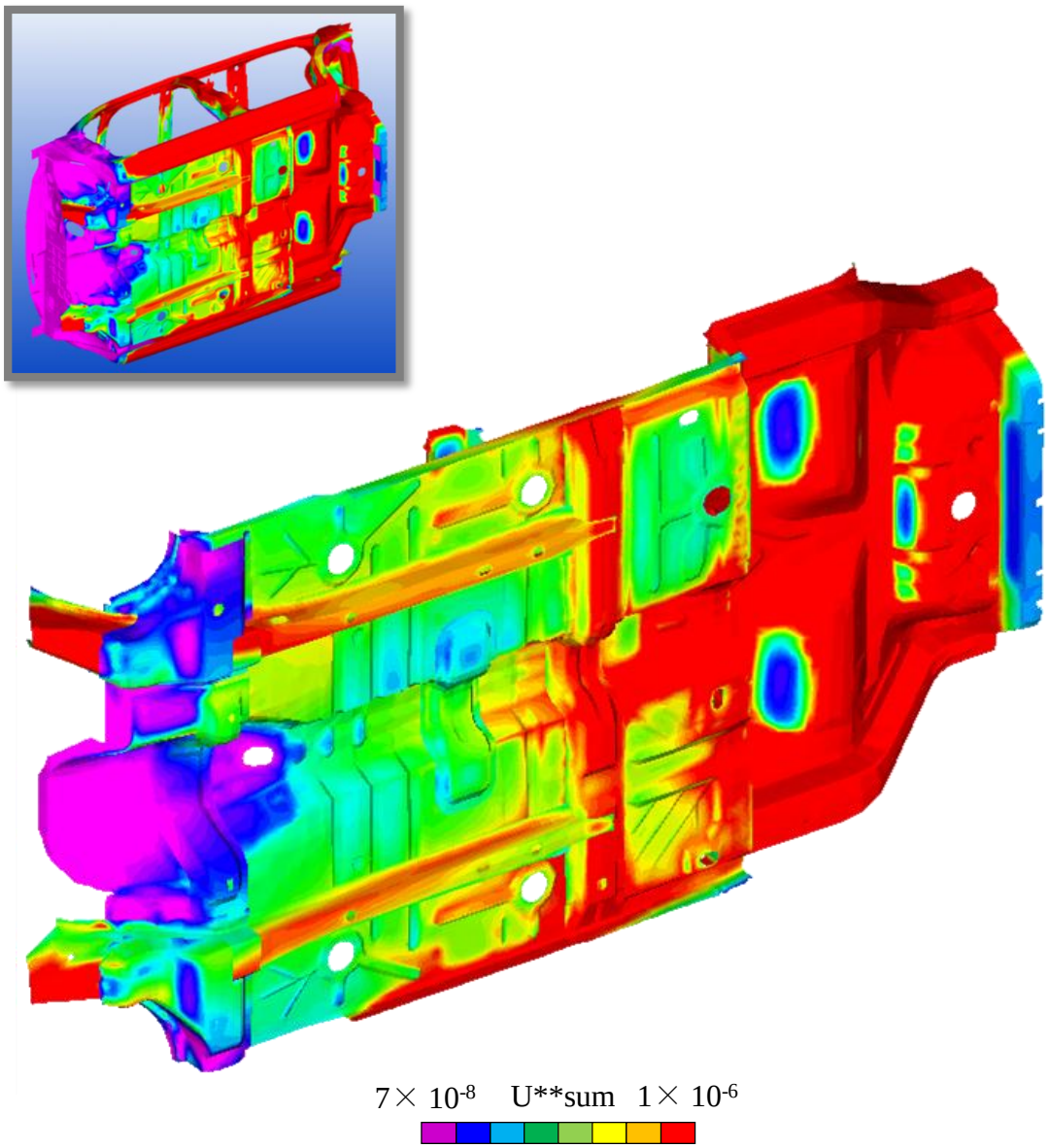

Fig. 9. 3 Distribution of Usum in Floor Panels**

9.2.1 Load Paths along Main Members

For the floor main members, the load paths from the loading point and the constraint point are shown in Figs. 9.1 and 9.2, respectively. From the high U** values observed at

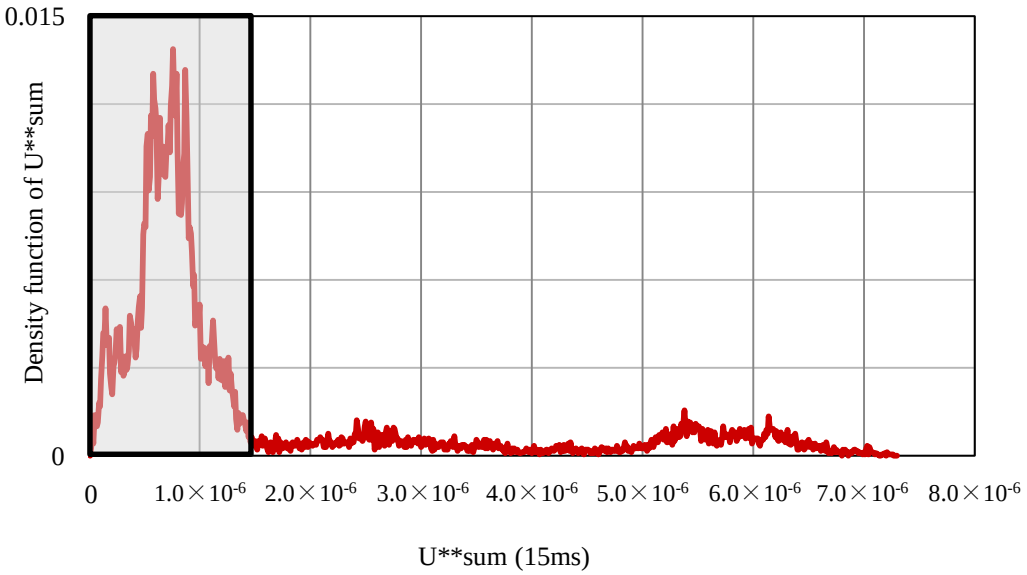

Fig. 9. 5 Histogram of Floor Panels

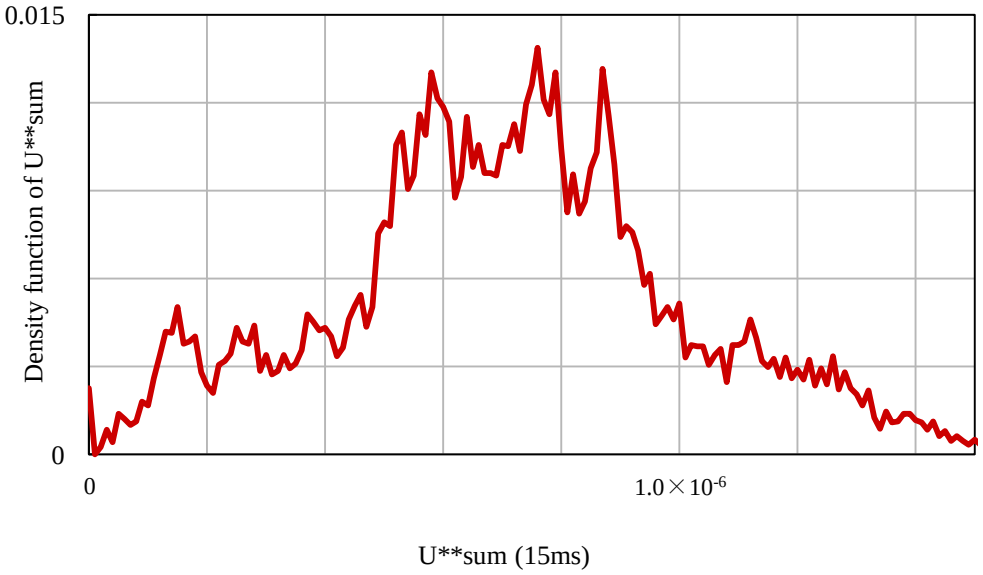

Fig. 9. 4 Enlarged Histogram of Floor Panels (0-1.5×10^{-6})

the corners of the floor main members, it reveals that the corner of a member plays an important role in the load transfer. Also the cross-sectional design with multi corners shown in Fig. 6.5 is preferable and effective for the load transfer. In the present Neon model, the structural design of cross sections of floor main members has introduced multi-corners to increase load paths and its ability in the load transfer.

From Fig. 9.6, the load paths from rear floor panels to the frontal floor panels are plotted. It can be seen that the predominant load paths are along the rear main members to the side sills. Meanwhile, the rear floor panels also transfers loadings through their corners to the side sills. The inner side sill panels are effective in the load transfer compared with the middle and outer side sill panels. The shear effect on the middle floor panels is significant in conveying loading to the side sills.

9.2.2 Load Transfer in Middle Floor Panels

Based on the comparison of Figs. 9.1 and 9.7, we find out that the side sills are the most crucial and effective structures to connect the frontal and rear floor panels. Due to the effect of middle floor panels, the connectivity between the frontal and rear floor panels is disturbed. The U** distribution in the middle floor panels is shown in Fig. 9.7. From Fig. 9.7, the drastic variation of U** distributions at 15ms in the middle floor panels are highlighted. It can be concluded that the present design of middle floor panels are ineffective for the load transfer, which is inevitable due to the existence of the gas tank. This observation is suggesting that the necessary stiffener members which can effectively convey the loadings between the frontal floor panels and the rear floor panels.

9.2.3 Load Transfer in Side Sills

In Fig. 9.7, the U** distribution of side sills are shown. The load paths from frontal and rear loadings are plotted. From the illustration of load paths along the side sills, we find out that the side sills play important role in the load transfer under both frontal and rear loadings conditions due to the inefficient design of middle floor panels as mentioned in

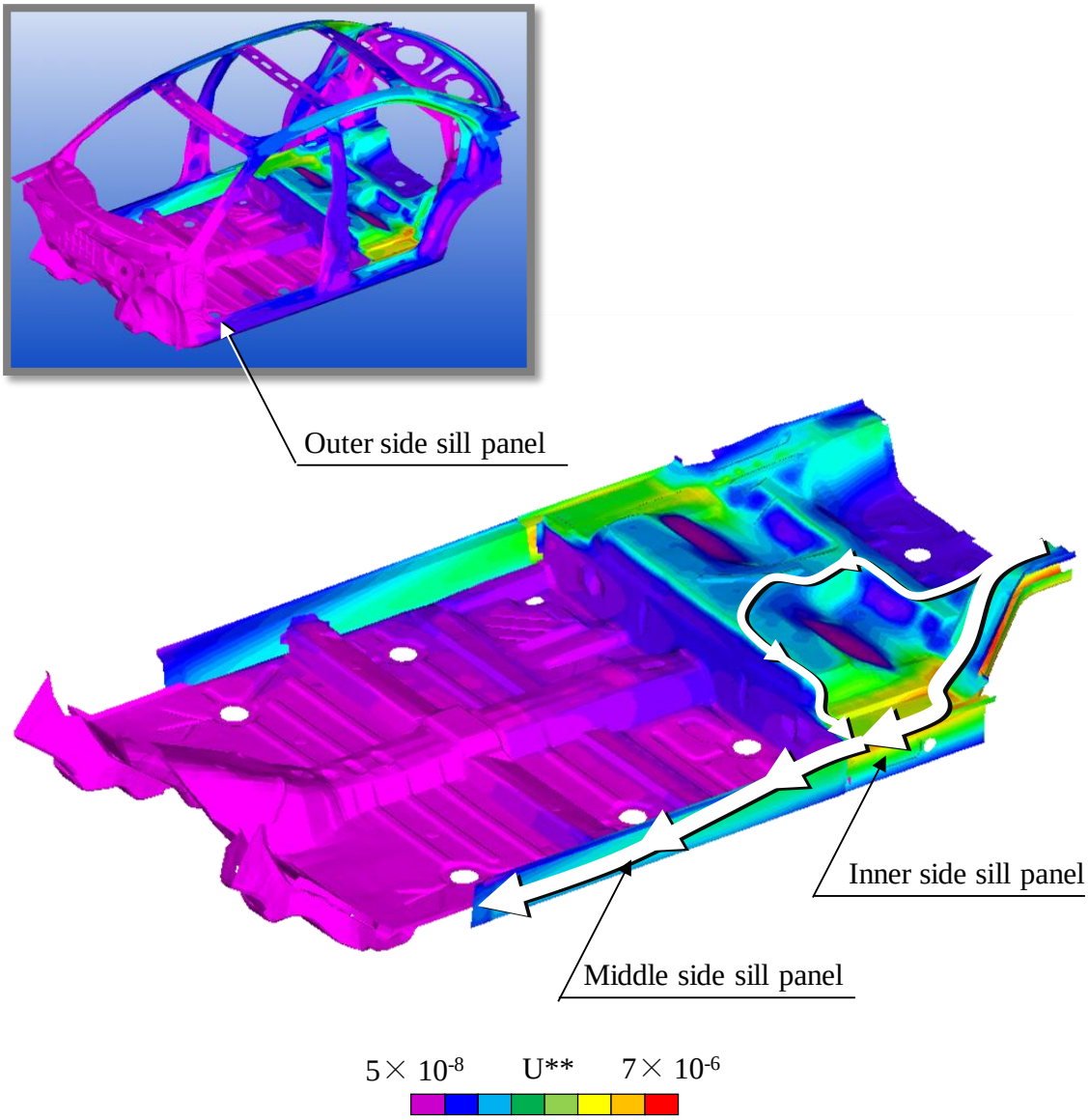

Fig. 9. 6 Distribution of U in Floor Panels**

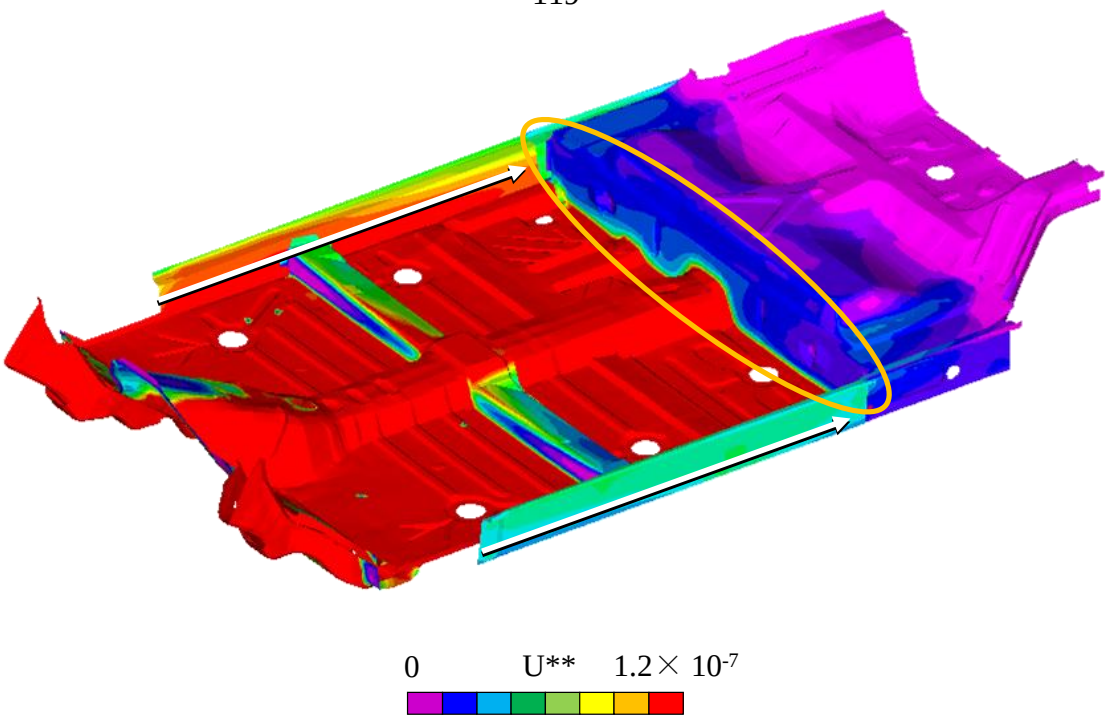

(a) Distribution of U** (Frontal)

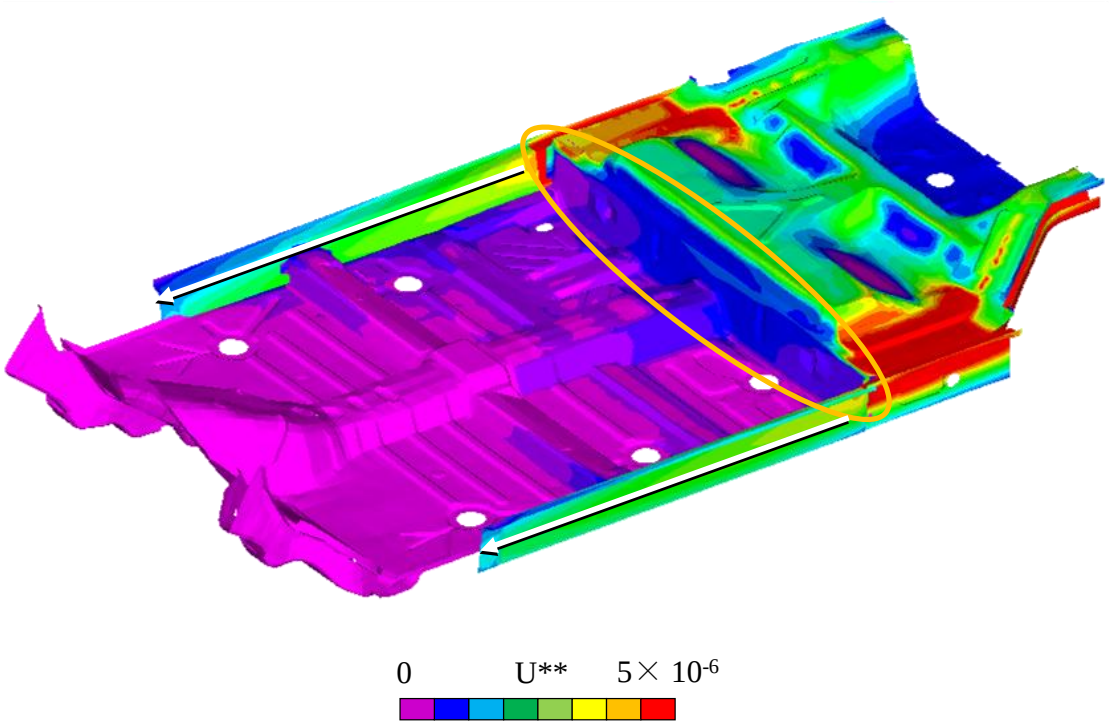

(a) Distribution of U** (Rear)

Fig. 9. 7 Distribution of U in Side Sills**

Section 9.2.2.

9.2.4 Load Transfer in Tunnel Structure

Based on the observation of U** distribution and the U**sum distribution in tunnel structure shown in Figs 9.1 and 9.3, it can be observed that tunnel structures also play an important role for the load transfer.

9.2.5 Load Transfer in Pillars

The U** distribution in compartment structure under frontal loading conditions is shown

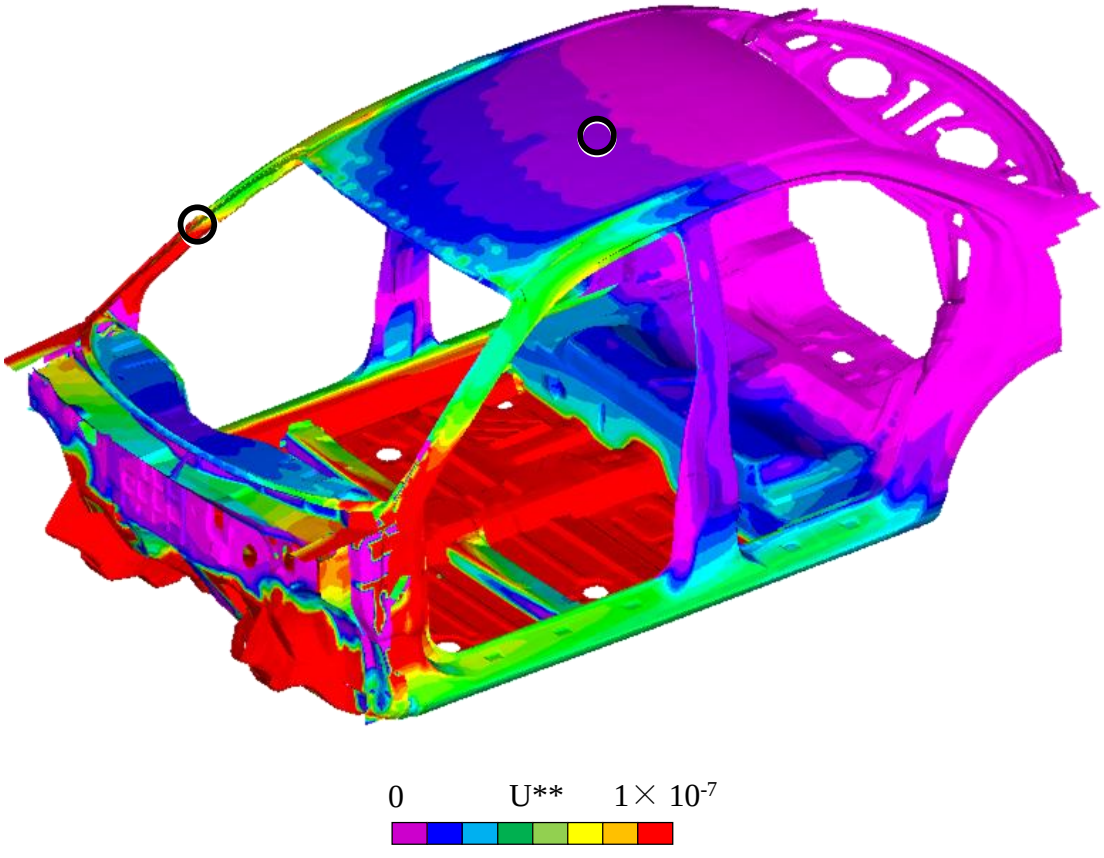

Fig. 9. 8 Distribution of U in Pillars and Roof Panels**

in Fig. 9.8 in which contour scales are adjusted to represent the load transfer in pillars. A-pillars show effects in conveying frontal impact loadings to the rear structures. The relatively lower U** values shown in B-pillars reveal that the B-pillars have no effect in transferring frontal impact loadings. Meanwhile, the U** values in the roof panels are also very small. In contrast, the floor panels are very effective in the load transfer as shown in Fig. 9.8.

In Fig. 9.9, the roof panel is removed to show the effect of roof cross members and the load paths. As shown in Fig. 9.9, the load paths are along the corners of pillars and roof members. The middle roof cross member is low in U** values. It is necessary to mention that although both middle roof cross member and B-pillars are not effect in the load transfer under frontal and rear loading conditions, in the case of side impacts they are the most important structures to protect occupants. Also B-pillars are effective in resisting the buckling of the roof members.

9.3 Summary

(1) The index U** is applied to the compartment of a passenger car to analyze the load transfer and load paths. The distributions of U**, U**sum and histograms are presented. The similar shear effect of floor panels in conveying loadings is also observed in the present study of passenger cars.

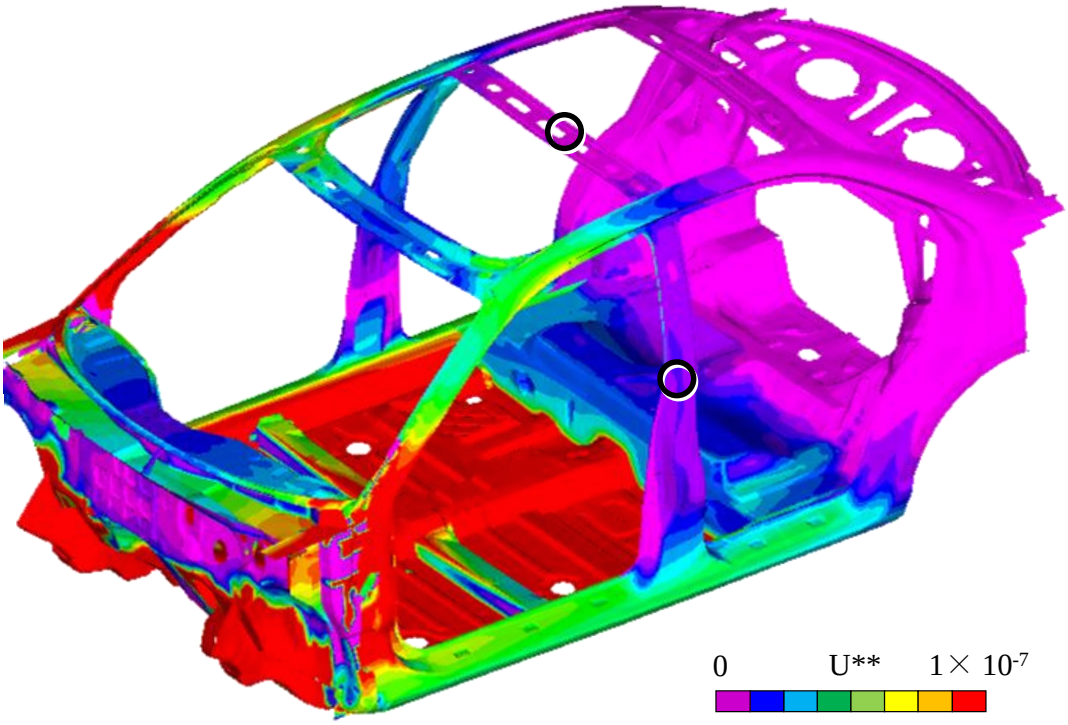

(a) Distribution of U** (Frontal)

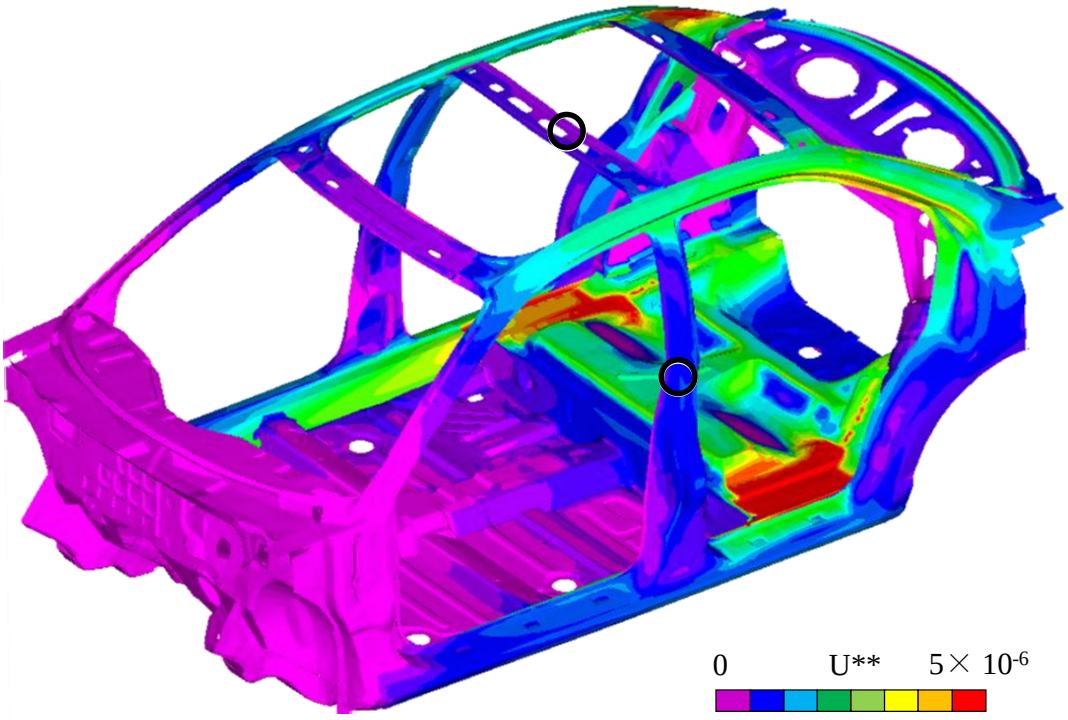

(a) Distribution of U** (Rear)

Fig. 9. 9 Distribution of U in Pillars and Roof Cross Members**

(2) In the present floor panels the loadings are not transferred uniformly. The predominant load paths are along the floor main members. The outer side sill panels are not effectively for load transfer. Rear floor panels and side sills are effective in the load transfer compared with frontal floor panels. Tunnel walls also play an important role for the load transfer. The necessary stiffener members should be introduced to increase the connectives of the load transfer.

10. Conclusions

10.1 Novel Aspects of This Research

The primary aim of this research was to introduce indexes U* and U** to make an investigation of the load transfer and load paths in vehicle structures under collision. These results enable structural designers to make an assessment of how loadings transfer in a structure and help them improve the structural stiffness and crashworthiness.

The research has focused on developing the way to make the load transfer and load paths analyses in motor vehicle compartments at the initial stage of a collision. After obtaining the deformed body by a dynamic crash simulation, the extracted deformed body are calculated statically using indexes U* and U**. Since the main part of the compartment retains its linear elasticity to ensure the safety of the occupants, the author points out that the linear U* and U** analyses can be applied during the initial crash stage, and develops a dynamic-static method.

For the study of a truck compartment, the author originally introduces a substitution modulus method to reproduce the material and geometrical nonlinearities. The index "m2-4msU**" is proposed as a standard condition for the truck cab. The distribution of U* is compared with that of U** and the characteristic difference between these indexes is revealed. It is shown that the main member of this cab transfers the loading effectively, and the corners of a member play an important role in the load transfer.

In the study of a passenger car compartment, a separation structure method is newly developed. The front end and suspension parts are not altered from the actual body, but the material of the compartment is assumed to have simple elastic property. The calculated U** distribution shows that the floor member plays a paramount role in the transfer of the impact loading and the shearing force in the floor panel distributes the loading to body sides. These results show the effectiveness of the new methods that use U* and U** in vehicle crash analysis.

10.2 Research Achievements

This research has applied the index U** to express the load transfer in heavy-duty truck cabs during the initial crash phase. Several results are obtained. Firstly, since the main part of a compartment should be maintained in the linear elastic condition for the safety of occupants, a linear static analysis of U** is applicable to the main part of a truck cab. Secondly, a deformed cab body at the initial crash stage is obtained by a dynamic simulation. The deformed body is extracted and the U** distribution for this body can be statically calculated, called the dynamics-static method. In this process, a method of the substitution modulus is applied to reproduce the material and geometrical non-linearities for the load path U** analysis. Thirdly, the most appropriate index "m2-4msU**" is proposed as the standard condition for the load path U** analysis for the estimation of the effect of newly designed stiffeners in the cab. Fourthly, the predominant load paths are observed along the main floor member, and the load transfer based on the shear effect of the floor panel is demonstrated. The tunnel wall is playing an important role together

with the main member for the load transfer. The side sill also plays some roles in transferring loads to the rear structures in each time step. The load path in the cross-member is regarded as a secondary load path. The roof rail structure does not show its proper ability in the load transfer. Fifthly, the frontal panel and the roof panel do not show proper abilities in the load transfer. It is found that at 4ms frontal loadings become stabilized. The load transfer and load paths analysis of the cab structure should take 4ms for U** calculations.

Moreover, the index U* was applied to a truck cab structure under a frontal collision during the initial crash stage to investigate the load transfer and load paths. For the comparison with our previous results involving U**, a dynamic-static method and a substitution-modulus method which had previously been introduced by the authors were used. The following results are obtained. At first, the difference in load transfer with respect to the parameter *m* and the time *t* is small. We chose the most suitable set of *m* = 2 and *t* = 4 ms, and we referred to the U* value with this combination as the index "m2-4msU*". At second, the shape of the U* and U** distributions is almost the same. However, the absolute value of U* is greater than U** by about 1.6 times. The difference is inevitable because of the difference in their definitions. At last, for a flat barrier collision, U* is adequate, while for the case of a honeycomb barrier collision, U** is suitable. However, both indexes show almost the same distribution.

Concepts of U*sum and its histogram were used to express the effectiveness of the load transfer. Using these expressions, we were able to see in the present floor structure that

the loading is transferred non-uniformly between each member. The distribution of U*sum of the main floor member shows a desirable curve, and the histogram of the load path shows a sharp peak. These results indicate that the main member of this cab transfers loading quite effectively.

The index U** is applied to the compartment of a passenger car to analyze the load transfer and load paths. The distributions of U**, U**sum and histograms are presented. The similar shear effect of floor panels in conveying loadings is also observed in the present study of passenger cars. In the present floor panels the loadings are not transferred uniformly. The predominant load paths are along the floor main members. The outer side sill panels are not so efficient in the load transfer compared with the inner side sill panels. Rear floor panels and side sills are effectively for load transfer compared with frontal floor panels. Tunnel walls also play an important role for the load transfer. The necessary stiffener members should be introduced to increase the connectives of the load transfer.

10.3 Future Research

There are many potential areas of further study which can build upon different aspects of this research. There are obviously more works to be done related to commercialize present methods, particularly in the application of trucks and passenger cars for the automotive industry. A significant problem related to the present study is the procedure of the dynamic-static method. Regarding to the non-standardized interface between LS-

DYNA and MSC.Nastran, it is difficult to make the operation of model conventions, especially the translation of connectors. With the development of CAE software or API extension, the efficiency of the model translation will be improved significantly in the future.

In the present study of both trucks and cars, although the condition of the distributed loadings has been represented and analyzed using index U**, the effect of inertial forces for the load transfer is not reflected properly. For example, the inertial forces of occupants, seats, tires, suspensions, fans, clutch, brakes, window shields, and so on are excluded. In the future, the internal distributed loadings of these substructures obtained by dynamic calculations will be added as external loadings in the static calculation to regenerate the effect of inertial forces.

As mentioned in Chapter 1, except the present full width frontal impact test there are many kinds of other impact tests, such as offset frontal impact, side impact, rear impact and rollover. Although the present methods of investigating the load transfer and load paths in motor vehicles is developed from the numerical results of full width frontal impact test, they are still valid to testify other tests after introducing a few improvements. In the future, there will be dozens of the valuable findings obtained by examining different impact tests.

Several research achievements have mentioned that stiffeners are needed to improve the connectivity among structures. But from the viewpoint of structural designs, engineers

may be wandering where the stiffeners should be added, which kind of material the stiffeners should be made of, how much the stiffeners are in length, and so on so forth. Therefore, a detail investigation of the local structural design by using indexes U* and U** should be considered in the future.

In the present body design of vehicle structures, reinforced materials and non-metal materials are being widely used to increase the structure crashworthiness and decrease the energy consumption. For example, in the structure of front ends polymeric foams are injected into metal tubes to increase the energy absorption, and the structure with a sandwich configuration also can be found in the design of vehicle floor panels to decrease weights. By introducing new materials in the structural design of vehicle bodies, the characteristics of the load transfer and load paths are definitely changed compared with the conventional one. Thus, the effects of these new materials for the load transfer and load paths should be investigated in the future.

Finally, undertaking this research was an encompassing task, as it pulled together both dynamic and static analysis technologies. The final results of this research are pleasing as all the aims of the research were fulfilled, and the work will be provided to the engineers of structural designs which can help them insight into revealing the load transfer and load paths in a structure under collision. This study can be applied to a wide variety of structures under collision, and the work undertaken can be widespread to automotive industries.

Acknowledgements

This dissertation would not have been possible without the guidance and encouragement from my supervisor Prof. Kunihiro Takahashi and Prof. Masaki Omiya. I appreciate their honesty, motivating words and willingness to put their personal time aside to help me achieve my research goals. In addition to this, I thank them for helping secure financial support for this project and generously donating some of their funding to help me attending conferences.

Prof. Kazuyuki Shizawa, Prof. Jun Komotori, and Prof. Masayuki Kohiyama, without you I don't think this dissertation would have ever been pulled into shape. Thank you for stepping on board and presenting your precious comments about this dissertation.

I would like to thank Mr. Yuki Yoshikuni, Mr. Qiushi Guo, and Mr. Kentaro Nagai for their support throughout this project. I especially appreciate Dr. Hiroaki Hoshino for their firsthand industry expertise.

Moreover, I would like to appreciate Dr. Tetsuo Nohara and Dr. Hideaki Ishii from Nissan Diesel Co. Ltd. (UD Trucks Co. Ltd.) for their support for providing firsthand industry expertise and numerical models.

Financial support for this project was generously provided by Keio Advanced Research Center and Niki Saneyoshi Co. Ltd. Their scholarship removed the financial burden of

everyday life, making it possible for me to absorb myself in the academic lifestyle, and concentrate solely on the research.

To my dearest family: I thank you for jumping, unquestioning into my sidecar and coming along for the ride, on this journey that has been a series of bumpy roads, steep tough climbs and exhilarating descents. Your love, support, laughs and smiles have all been very much appreciated.

Thank you to everyone that has helped me to research the wonderful fanciful world that is “post PhD”.

References

[1] J. Fenton and R. Hodkinson: Lightweight electric/hybrid vehicle design: Butterworth-Heinemann, (2001).

[2] A. E. Fuhs: Hybrid vehicles and the future of personal transportation: CRC Press, (2009).

[3] J. Weber: Automotive Development Processes: Processes for Successful Customer Oriented Vehicle Development: Springer, (2009).

[4] H. Heisler: Advanced vehicle technology: Butterworth-Heinemann, (2002).

[5] J. C. Brown, A. J. Robertson, and S. T. Serpento: Motor vehicle structures: concepts and fundamentals: Butterworth-Heinemann, (2002).

[6] E. B. Blanchard and E. J. Hickling: After the crash: assessment and treatment of motor vehicle accident survivors: American Psychological Association, (1997).

[7] T. K. Garrett, K. Newton, and W. Steeds: The motor vehicle: Butterworth-Heinemann, (2001).

[8] G. A. Peters and B. J. Peters: Automotive vehicle safety: Taylor & Francis, (2002).

[9] B. Cantor: Automotive engineering: lightweight, functional, and novel materials: Taylor & Francis, (2008).

[10] D. Crolla: Automotive Engineering: Powertrain, Chassis System and Vehicle Body: Butterworth-Heinemann, (2009).

[11] A. Robinson, W. A. Livesey, and A. Livesey: Repair of vehicle bodies: Butterworth-Heinemann, (2006).

[12] D. Karnopp: Vehicle stability: Marcel Dekker, (2004).

[13] J. Happian-Smith: An introduction to modern vehicle design: Elsevier, (2001).

[14] J. P. D. Hartog: Strength of materials: Courier Dover Publications, (1961).

[15] G. Lu and T. Yu: Energy absorption of structures and materials: Woodhead Publishing, (2003).

[16] M. A. Meyers: Dynamic behavior of materials: Wiley-IEEE, (1994).

[17] M. Ohring: Engineering materials science: Academic Press, (1995).

[18] S. Abrate: Impact on composite structures: Cambridge University Press, (1998).

[19] N. Tucker and K. Lindsey: An introduction to automotive composites: iSmithers Rapra Publishing, (2002).

[20] A. K. Kaw: Mechanics of composite materials: Taylor & Francis, (2006).

[21] S. W. Tsai: Strength & life of composites: Stanford University, (2009).

[22] C. Bisagni and D. Terletti: Structural optimisation of composite elements of a Formula One racing car: International Journal of Vehicle Design, 48(1-2)(2008), pp. 149-170.

[23] M. F. Ashby and D. R. H. Jones: Engineering materials 2: an introduction to microstructures, processing and design: Butterworth-Heinemann, (2006).

[24] W. Fung and M. Hardcastle: Textiles in automotive engineering: Woodhead Publishing, (2001).

[25] J. Fenton: Advances in vehicle design: Professional Engineering Pub., (1999).

[26] G. Genta and L. Morello: The Automotive Chassis: Components design: Springer, (2009).

[27] G. Genta and L. Morello: The Automotive Chassis: System design: Springer, (2009).
[28] T. D. Gillespie: Fundamentals of vehicle dynamics: Society of Automotive Engineers, (1992).
[29] D. Newbold and A. W. M. Bonnick: A practical approach to motor vehicle engineering and maintenance: Butterworth-Heinemann, (2005).
[30] J. E. Akin: Finite element analysis with error estimators: an introduction to the FEM and adaptive error analysis for engineering students: Butterworth-Heinemann, (2005).
[31] M. Y. H. Bangash: Shock, Impact and Explosion: Structural Analysis and Design: Springer, (2008).
[32] K.-J. Bathe: Finite element procedures: Prentice Hall, (1996).
[33] J. Bonet and R. D. Wood: Nonlinear continuum mechanics for finite element analysis: Cambridge University Press, (1997).
[34] R. G. Budynas: Advanced strength and applied stress analysis: WCB/McGraw-Hill, (1999).
[35] W.-F. Chen and T. Atsuta: Theory of Beam-Columns, Volume 1: In-Plane Behavior and Design: J. Ross Publishing, (2007).
[36] P. W. Christensen and A. Klarbring: An Introduction to Structural Optimization: Springer, (2008).
[37] M. A. Crisfield: Non-linear finite element analysis of solids and structures: Wiley, (1997).
[38] N. Cristescu: Dynamic plasticity: World Scientific, (2007).
[39] F. Dunne and N. Petrinic: Introduction to computational plasticity: Oxford University Press, (2005).
[40] J. Fenton: Handbook of vehicle design analysis: Society of Automotive Engineers, (1996).
[41] A. J. M. Ferreira: MATLAB codes for finite element analysis: solids and structures: Springer, (2008).
[42] P. I. Kattan: MATLAB guide to finite elements: an interactive approach: Springer, (2003).
[43] J. Fish and T. Belytschko: A first course in finite elements: John Wiley and Sons, (2007).
[44] W. Goldsmith: Impact: the theory and physical behaviour of colliding solids: Courier Dover Publications, (2001).
[45] X. Huang and M. Xie: Evolutionary Topology Optimization of Continuum Structures: Methods and Applications: John Wiley and Sons, (2010).
[46] N. Jones: Structural impact: Cambridge University Press, (1997).
[47] N. Jones and T. Wierzbicki: Structural crashworthiness and failure: Taylor & Francis, (1993).
[48] I. A. Karnovsky and O. Lebed: Advanced Methods of Structural Analysis: Springer, (2009).
[49] P. M. Kurowski: Finite Element Analysis For Design Engineers: SAE International, (2004).

[50] H. Kurtaran: Optimization of Structures Under Crash and Impact: VDM Verlag, (2008).
[51] P. Ladevèze and J. P. Pelle: Mastering calculations in linear and nonlinear mechanics: Springer, (2005).
[52] T. A. Laursen: Computational contact and impact mechanics: fundamentals of modeling interfacial phenomena in nonlinear finite element analysis: Springer, (2002).
[53] E. d. S. Neto, D. Perić, D. Owens, and D. R. J. Owen: Computational Methods for Plasticity: Theory and Applications: Wiley, (2008).
[54] E. Oñate and R. Owen: Computational Plasticity: Springer, (2007).
[55] N. S. Ottosen and H. Petersson: Introduction to the finite element method: Prentice Hall, (1992).
[56] J. N. Reddy: An introduction to nonlinear finite element analysis: Oxford University Press, (2004).
[57] D. W. A. Rees: Basic engineering plasticity: an introduction with engineering and manufacturing applications: Butterworth-Heinemann, (2006).
[58] J. C. Simó and T. J. R. Hughes: Computational inelasticity: Springer, (1998).
[59] W. J. Stronge: Impact Mechanics: Cambridge University Press, (2004).
[60] B. Y. Tonge: The indeterminate beam: theory and examples: Butterworths, (1972).
[61] P. Wriggers: Computational contact mechanics, 2nd ed.: John Wiley and Sons, (2007).
[62] P. Wriggers: Computational contact mechanics: John Wiley and Sons, (2002).
[63] P. Wriggers: Nonlinear finite element methods: Springer, (2008).
[64] O. C. Zienkiewicz, R. L. Taylor, and R. L. Taylor: The finite element method for solid and structural mechanics: Butterworth-Heinemann, (2005).
[65] J. A. Zukas: Introduction to hydrocodes: Elsevier, (2004).
[66] K. Takahashi: Foundations for the Theory of Elasticity, 1st ed.: Corona Publishing Co., Ltd., (1998).
[67] S. Hiermaier: Structures under crash and impact: continuum mechanics, discretization and experimental characterization: Springer, (2008).
[68] M. Huang: Vehicle crash mechanics: CRC Press, (2002).
[69] J. Chang, J. Zhang, and R. Zia: Modelling deformations in car crash animation: The Visual Computer, 25(12)(2009), pp. 1063-1072.
[70] D. Kelly, C. Reidsema, and M. Lee: On load paths and load bearing topology from finite element analysis: IOP Conference Series: Materials Science and Engineering, 10(2010), p. 12192.
[71] D. W. Kelly and M. Elsley: A Procedure for Determining Load Paths in Elastic Continua: Engineering Computations, 12(5)(1995), pp. 415-424.
[72] D. W. Kelly, P. Hsu, and M. Asudullah: Load paths and load flow in finite element analysis: Engineering Computations, 18(1-2)(2001), pp. 304-313.
[73] D. W. Kelly and M. W. Tosh: Interpreting load paths and stress trajectories in elasticity: Engineering Computations, 17(2-3)(2000), pp. 117-135.
[74] G. Kelly: Load transfer in hybrid (bonded/bolted) composite single-lap joints: Composite Structures, 69(1)(2005), pp. 35-43.

[75] R. Li, D. Kelly, A. Crosky, H. Schoen, and L. Smollich: Improving the efficiency of fiber steered composite joints using load path trajectories: Journal of Composite Materials, 40(18)(2006), pp. 1645-1658.

[76] W. Waldman, M. Heller, R. Kaye, and F. Rose: Advances in two-dimensional structural loadflow visualisation: Engineering Computations, 19(3)(2002), pp. 305 - 326.

[77] J. S. Arora: Optimization of structural and mechanical systems: World Scientific, (2007).

[78] H. Harasaki and J. S. Arora: A new class of evolutionary methods based on the concept of transferred force for structural design: Structural and Multidisciplinary Optimization, 22(1)(2001), pp. 35-56.

[79] H. Harasaki and J. S. Arora: New concepts of transferred and potential transferred forces in structures: Computer Methods in Applied Mechanics and Engineering, 191(3-5)(2001), pp. 385-406.

[80] H. Harasaki and J. S. Arora: Optimal structural design with indirect use of Transferred Forces: Structural and Multidisciplinary Optimization, 22(5)(2001), pp. 384-393.

[81] H. Harasaki and J. S. Arora: Topology design based on transferred and potential transferred forces: Structural and Multidisciplinary Optimization, 23(5)(2002), pp. 372-381.

[82] K. Takahashi: Relative Rigidity of Structures and Saint Venant's Principle: Transactions of the Japan Society of Mechanical Engineers - Part A, 52(484)(1986), pp. 2615-2621, (in Japanese).

[83] K. Takahashi: Mesomechanics of continua and revised field equations: JSME International Journal Series A - Solid Mechanics and Material Engineering, 40(2)(1997), pp. 99-107.

[84] H. Hoshino, T. Sakurai, and K. Takahashi: Vibration reduction in the cabins of heavy-duty trucks using the theory of load transfer paths: JSAE Review, 24(2)(2003), pp. 165-171.

[85] M. Shinobu, D. Okamoto, S. Ito, H. Kawakami, and K. Takahashi: Transferred load and its course in passenger car bodies: JSAE Review, 16(2)(2004), pp. 145-150

[86] K. Takahashi: 2003 IBC load path and continuity in engineered wood-framed buildings : based on the 2003 International building code (IBC). Falls Church, VA: International Code Council, (2005).

[87] T. Sakurai, M. Tada, H. Ishii, T. Nohara, H. Hoshino, and K. Takahashi: Load Path Analysis of Structures and Generalized Support Conditions: Transactions of the Japan Society of Mechanical Engineers - Part A, 71(712)(2005), pp. 1605-1611.

[88] K. Takahashi and T. Sakurai: A concept of a parameter U*: Transactions of the Japan Society of Mechanical Engineers - Part A, 17(8)(2005), pp. 1097-1102, (in Japanese).

[89] K. Takahashi and T. Sakurai: Expression of Load Transfer Paths in Structures: Transactions of the Japan Society of Mechanical Engineers - Part A, 71(708)(2005), pp. 1097-1102, (in Japanese).

[90] T. Sakurai, M. Abe, H. Ishii, T. Nohara, H. Hoshino, and K. Takahashi: Load Path Analysis of Truck Cab Structure: Transactions of the Society of Automotive Engineers of Japan, 37(5)(2006), pp. 7-12, (in Japanese).

[91] T. Sakurai, H. Kawakami, M. Abe, and K. Takahashi: Reduction of Calculation Time for Load Path U* Analysis of Structures: Transactions of the Japan Society of Mechanical Engineers - Part A, 19(9)(2007), pp. 975-980, (in Japanese).

[92] T. Sakurai, M. Tada, H. Ishii, T. Nohara, H. Hoshino, and K. Takahashi: Load Path U* Analysis of Structures under Multiple Loading Conditions: Transactions of the Japan Society of Mechanical Engineers - Part A, 73(726)(2007), pp. 195-200.

[93] T. Sakurai, M. Tada, H. Ishii, T. Nohara, H. Hoshino, and K. Takahashi: Load Path U* Analysis of Structures under Multiple Loading Conditions: Transactions of the Japan Society of Mechanical Engineers - Part A, 19(2)(2007), pp. 195-200, (in Japanese).

[94] T. Sakurai, K. Takahashi, H. Kawakami, and M. Abe: Reduction of Calculation Time for Load Path U* Analysis of Structures: Journal of Solid Mechanics and Materials Engineering, 1(11)(2007), pp. 1322-1330.

[95] M. Kamimura, Y. Hatta, S. Ito, Y. Koga, T. Sakurai, and K. Takahashi: Structural Optimization and Load Paths: Nippon Kikai Gakkai Ronbunshu A Hen, 74(737)(2008), pp. 6-12, (Japanese).

[96] Y. Sekine, K. Takahashi, H. Hayamizu, D. Kawamoto, and D. Nakagawa: Compatibility between sports-utility vehicles and sedan-type vehicles: International Journal of Crashworthiness, 13(5)(2008), pp. 551-558.

[97] M. Kamimura, Y. Hatta, S. Ito, Y. Koga, T. Sakurai, and K. Takahashi: Structural Optimization and Load Paths: Transactions of the Japan Society of Mechanical Engineers - Part A, 74(737)(2008), pp. 6-12, (in Japanese).

[98] T. Matsunaga, T. Nakada, M. Hanazato, K. Inoue, and K. Takahashi: Load Path Analysis of Structures under Distributed Loading: Transactions of the Japan Society of Mechanical Engineers - Part A, 75(753)(2009), pp. 559-565, (in Japanese).

[99] Y. Okano, S. Maruyama, T. Matsunaga, K. Takahashi, and M. Hanazato, Load Path Analysis of Vehicle Body Structures under Eigenmode Deformation of Bending Vibration, in *SAE World Congress*, Detroit, 2009, pp. 1-6.

[100] S. Miyagawa, M. Omiya, and K. Takahashi: Extension of U* to Electro-Static Problem and Its Application to Structural Design for Porous Low-k Dielectric Film: Transactions of the Japan Society of Mechanical Engineers - Part A, 75(756)(2009), pp. 999-1006.

[101] Y. Takahashi, D. Okumura, and N. Ohno: Yield and buckling behavior of Kelvin open-cell foams subjected to uniaxial compression: International Journal of Mechanical Sciences, 52(2)(2010), pp. 377-385.

[102] K. Marhadi and S. Venkataraman: Comparison of Quantitative and Qualitative Information Provided by Different Structural Load Path Definitions: Int. J. Simul. Multidisci. Des. Optim., 3(3)(2009), pp. 384-400.

[103] M. J. Nunney: Light and heavy vehicle technology: Butterworth-Heinemann, (2006).

[104] S. Timoshenko and J. N. Goodier: Theory of elasticity: McGraw-Hill, (1951).
[105] R. W. Hertzberg: Deformation and fracture mechanics of engineering materials: J. Wiley & Sons, (1996).
[106] Z. P. Bažant, Z. P. Bazant, and L. Cedolin: Stability of structures: elastic, inelastic, fracture, and damage theories: Courier Dover Publications, (2003).
[107] R. S. Salzar, D. Genovese, C. R. Bass, J. R. Bolton, H. Guillemot, A. M. Damon, and J. R. Crandall: Load path distribution within the pelvic structure under lateral loading: International Journal of Crashworthiness, 14(1)(2009), pp. 99-110.
[108] J. R. Barber: Elasticity: Springer, (2010).
[109] J. R. Barber: Intermediate Mechanics of Materials: Springer, (2010).
[110] G. Simitses and D. H. Hodges: Fundamentals of Structural Stability: Butterworth-Heinemann, (2006).
[111] T. V. Galambos: Guide to Stability Design Criteria for Metal Structures, 5th Edition: Wiley, (1998).
[112] A. Chajes: Principles of structural stability theory: Prentice-Hall, (1974).
[113] T. V. Galambos and A. E. Surovek: Structural stability of steel: concepts and applications for structural engineers: John Wiley and Sons, (2008).
[114] J. P. D. Hartog: Advanced strength of materials: Courier Dover Publications, (1987).
[115] R. M. Jones: Buckling of Bars, Plates, and Shells: Bull Ridge Corporation, (2006).
[116] M. Kojić and K.-J. Bathe: Inelastic analysis of solids and structures: Springer, (2005).
[117] A. Love and H. Edward: A treatise on the mathematical theory of elasticity: Courier Dover Publications, (1944).
[118] J. Singer, J. Arbocz, and T. Weller: Buckling Experiments: Basic concepts, columns, beams, and plates: John Wiley and Sons, (1998).
[119] H. Tada, P. C. Paris, and G. R. Irwin: The stress analysis of cracks handbook: by Hiroshi Tada, with the cooperation of Paul C. Paris and George R. Irwin: Paris Productions & (Del Research Corp.), (1985).
[120] O. C. Zienkiewicz, R. L. Taylor, R. L. Taylor, and J. Z. Zhu: The finite element method: its basis and fundamentals: Butterworth-Heinemann, (2005).
[121] LS-DYNA Keyword User's Manual, Version 971 ed.: Livermore Software Technology Coporation Inc., (2007).
[122] Y. Okano: Load path analysis of vehicle body structures under eigenvalue deformation of bending viberation: International journal of Automotive Engineers of Japan, 63(7)(2009), pp. 98-101, (in Japanese).
[123] NASTRAN Reference Manual, Version 2004 ed.: MSC Software Inc., (2004).
[124] S. Torikai, Q. Guo, Y. Urusiyama, H. Kobayashi, and K. Takahashi: Load Transfer in Vehicle Bodies under Torsion and Contribution of Windshield Glass Adhesion: Transactions of Society of Automotive Engineering of Japan, 41(5)(2010), pp. 963-968, (in Japanese).
[125] J. O. Hallquist: LS-DYNA Theory Manual: Livermore Software Technology Corporation Inc., (2006).

Appendix A. Summary of LS-DYNA Calculation

The parameters for LS-DYNA nonlinear simulation in the truck compartment and the passenger car are presented in Table A.1 and Table A.2, respectively. The abbreviated LS-DYNA cards are shown in A.3

Table A. 1 Truck Compartment Model

Truck			
Simulation time		15.0 ms	
Kinetic energy		1.86658 × 105 N·mm	
Time period for complete output states		0.1 ms	
Material Definition	Rigid bar	*MAT_20 (*MAT_RIGID)	
	Plate element	*MAT_24 (1) (*MAT_PIECEWISE_LINEAR_PLASTICITY)	
	Spot-weld	*MAT_100 (*MAT_SPOTWELD)	
Contact type	Body structure	*CONTACT_AUTOMATIC_GENERAL	
	Rigid wall	Frictionless sliding after contact (Flexible body vs. Rigid Wall)	
Constitutive law (MAT_24)	$\sigma_Y = \left[1+\left(\frac{\dot{\varepsilon}}{C}\right)^{1/P}\right]\left[\sigma_0 + E_p\left(\varepsilon_{eff}^p\right)\right]$		
	σ_Y	Instantaneous yield stress	
	σ_0	Initial yield stress	$\sigma_0 = 300\,\text{MPa}$
	E_p	Plastic hardening modulus	$E_p = \frac{E_t E_i}{E_i - E_t}$
	E_t	Tangent modulus (2)	
	E_i	Initial elastic modulus	200 GPa

	ε_{eff}^{p}	Effective plastic strain	
	$\dot{\varepsilon}$	Strain rate	$\dot{\varepsilon}=\sqrt{\dot{\varepsilon}_{ij}\dot{\varepsilon}_{ij}}$ (summation convention used)
	C, P	Strain rate parameters (Cowper-Symonds) [3]	$\left(\frac{\dot{\varepsilon}}{C}\right)^{1/P}=0$
Hardening		Isotropic hardening [4]	
Stress - strain curve		Piecewise true stress versus effective plastic strain curve[5]	
Time integration method		Explicit method : Modified central difference method (LS-DYNA) [6]	
Time step	$\Delta t=\frac{L_s}{c}$		
	Δt	Critical time step for integration	3.6 × 10-3 ms
	L_s	Characteristic length (*CONTROL_TIMESTEP, ISDO=0)	$L_s=\frac{(1+\beta)A_s}{\max(L_1,L_2,L_3,(1-\beta)L_4)}$
	c	Sound speed	$c=\sqrt{\frac{E}{\rho(1-\nu^2)}}$
	A_s	Area of shell elements	
	L_i (i = 1,2,3,4)	Length of sides defining in the shell elements	
	β	Quadrilateral shell (β=0) ; Triangular shell (β=1)	
Shell element		Belytschko-Tsay shell (4 nodes)	
		Integration points (Gauss)	2 points (±0.5773503)
Solid element		Constant stress solid (8 nodes)	

Beam element		Spot-weld beam (2 nodes)
Impact speed		15.6 m/s
Rear cargo mass		5,000 kg
Element number		73,346
Poisson's ratio	v	0.3
Density of steel	ρ	7,830 kg/m3

(1) Material type 24 is an elasto-plastic material with an arbitrary true stress and effective plastic strain curve, and arbitrary strain rate dependency can be defined.
(2) Tangent modulus is obtained from true stress effective plastic strain curve.
(3) The effect of strain rates is not consider at present stage for the sake of simplicity to introduce conventional U* and U** indexes to represent the load transfer and load paths in at truck structure. For the study of passenger cars, the strain rate effect has been included.
(4) The definition of Material type 24 only contains isotropic hardening [125].
(5) The true stress and effective plastic strain curve was obtained based on the experimental data of National Crash Analysis Center.
(6) The definition of modified central difference method in LS-DYNA can be from LS-DYNA Theory Manual.

Table A. 2 Passenger Car Model

Passenger car		
Simulation time		150 ms
Kinetic energy		1. 71642 × 108 N·mm
Time period for complete output states		5 ms
Material Definition	Rigid bar	*MAT_20 (*MAT_RIGID)
	Elastic element	*MAT_1 (*MAT_ELASTIC)
	Plate element	*MAT_24 (1) (*MAT_PIECEWISE_ LINEAR_PLASTICITY)
	Spot-weld	*MAT_100 (*MAT_SPOTWELD)
Contact type	Body structure	*CONTACT_AUTOMATIC_SINGLE_SURFACE

	Rigid wall	Frictionless sliding after contact (Flexible body vs. Rigid Wall)	
Constitutive law (MAT_24)	$\sigma_Y = \left[1+\left(\frac{\dot{\varepsilon}}{C}\right)^{1/P}\right]\left[\sigma_0 + E_p\left(\varepsilon_{eff}^p\right)\right]$		
	σ_Y	Instantaneous yield stress	
	σ_0	Initial yield stress	$\sigma_0 = 250\,\text{MPa}$
	E_p	Plastic hardening modulus	$E_p = \frac{E_t E_i}{E_i - E_t}$
	E_t	Tangent modulus [2]	
	E_i	Initial elastic modulus	210 GPa
	ε_{eff}^p	Effective plastic strain	
	$\dot{\varepsilon}$	Strain rate	$\dot{\varepsilon} = \sqrt{\dot{\varepsilon}_{ij}\dot{\varepsilon}_{ij}}$ (summation convention used)
	C, P	Strain rate parameters (Cowper-Symonds)	C = 80, P = 4.5
Hardening		Isotropic hardening [3]	
Stress - strain curve		Piecewise true stress versus effective plastic strain curve[4]	
Time integration method		Explicit method : Modified central difference method (LS-DYNA) [5]	
Time step	$\Delta t = \frac{L_s}{c}$		
	Δt	Critical time step for integration	1.08 × 10-3 ms
	L_s	Characteristic length (*CONTROL_TIMESTE	$L_s = \frac{(1+\beta)A_s}{\max(L_1, L_2, L_3, (1-\beta)L_4)}$

		P, ISDO=0)	
	c	Sound speed	$c=\sqrt{\frac{E}{\rho(1-\nu^2)}}$
	A_s	Area of shell elements	
	L_i (i = 1,2,3,4)	Length of sides defining in the shell elements	
	β	Quadrilateral shell (β=0) ; Triangular shell (β=1)	
Shell element		Belytschko-Tsay shell (4 nodes)	
		Integration points (Gauss)	3 points 0, (±0.7745967)
Solid element		Constant stress solid (8 nodes)	
Beam element		Spot-weld beam and Hughes-Liu beam (2 nodes)	
Impact speed		15.6 m/s	
Poisson's ratio	ν	0.3	
Density of steel	ρ	7,830 kg/m3	

(1) Material type 24 is an elasto-plastic material with an arbitrary true stress and effective plastic strain curve, and arbitrary strain rate dependency can be defined.
(2) Tangent modulus is obtained from true stress effective plastic strain curve.
(3) The definition of Material type 24 only contains isotropic hardening [125].
(4) The true stress and effective plastic strain curve was obtained based on the experimental data of National Crash Analysis Center.
(5) The definition of modified central difference method in LS-DYNA can be from LS-DYNA Theory Manual.

A.3. Abbreviated LS-DYNA Card

A.3.1 Truck Compartment

The abbreviated version of LS-DYNA Cards of the truck compartment model is shown in this section.

```
$$$$$$$$$$$$$$$$$$$$$$$$$$$$$$$$$$$$$$$$$$$$$$$$$$$$$$$$$$$$$$$$$$$$$$$$$$$$$$$$$$$$$$$$$$$$
$# LS-DYNA Keyword file created by LS-PREPOST 2.1 - 25Apr2007(12:56)           $$
$# Created on Nov-08-2007 (15:34:25)                                           $$
$$ HM_OUTPUT_DECK created 16:50:50 04-24-2008 by HyperMesh Version 8.0   $$
$$ Ls-dyna Input Deck Generated by HyperMesh Version  : 8.0                    $$
$$ Generated using HyperMesh-Ls-dyna 970 Template Version : 8.0                $$
$$$$$$$$$$$$$$$$$$$$$$$$$$$$$$$$$$$$$$$$$$$$$$$$$$$$$$$$$$$$$$$$$$$$$$$$$$$$$$$$$$$$$$$$$$$$

*KEYWORD
*CONTROL_TERMINATION
$$  ENDTIM    ENDCYC    DTMIN    ENDENG    ENDMAS
    15.0         0       0.0       0.0       0.0
*CONTROL_TIMESTEP
$$  DTINIT    TSSFAC     ISDO    TSLIMT     DT2MS     LCTM     ERODE     MSIST
                          0                -0.004
$$DATABASE_OPTION -- Control Cards for ASCII output
*DATABASE_ELOUT
     0.1         1
*DATABASE_GLSTAT
     0.1         1
*DATABASE_MATSUM
     0.1         1
*DATABASE_NODOUT
     0.1         1
*DATABASE_RWFORC
     0.1         1
*DATABASE_SECFORC
     0.1         1
*DATABASE_BINARY_D3PLOT
$$ DT/CYCL      LCDT      BEAM     NPLTC
     0.1         0         0         0
       0
*NODE
     1       -1078.4        1430.71          350.8
...
 1220533         443.5       -189.615        -235.532
 2100001         480.0         -265.0          -235.0
 2100003           0.0         -350.0             0.0
 2100004           0.0         3000.0             0.0
*MAT_RIGID
    10027.9000E-06     210.0       0.3
     0.0
       0
*MAT_PIECEWISE_LINEAR_PLASTICITY
```

```
$HMNAME MATS       3Steel
       37.8300E-06     200.0       0.3       0.3               1.0
                       1


*MAT_SPOTWELD
$      MID        RO         E        PR      SIGY        ET        DT
       10  7.85e-06     210.0       0.3       0.5       500
$    EFAIL       NRR       NRS       NRT       MRR       MSS       MTT
     10.0      10.0      50.0      50.0      99.0      99.0      99.0
*PART
       3         3         3         0         0         0         0
      ...
      122       122        10         0         0         0         0
*PART_INERTIA
      123       119      1002
           -15.0

*SECTION_BEAM
      120         9       0.0       0.0       1.0
     10.0      10.0       0.0       0.0       0.0       0.0
       ...
*SECTION_SHELL
       3                        0               0.0
      1.0       1.0       1.0       1.0
           …
*SECTION_SOLID
      119         1
*INITIAL_VELOCITY
              0         1
           -15.0
*DEFINE_BOX
       1   -1200.0    1650.0    -400.0    3100.0    -400.0    1600.0
*CONTACT_AUTOMATIC_GENERAL_ID
       3
       2                 6
     0.15

*CONSTRAINED_EXTRA_NODES_SET
      123         1
*SET_NODE_LIST
       1       0.0       0.0       0.0       0.0
  1110000   1110001   1110002   1110003   1110004   1110005   1110006   1110007
       ...
  1114224   1114225   1114226   1114227
*RIGIDWALL_PLANAR_ID
       4
       0                 1
      0.0    -350.0       0.0       0.0    -349.0       0.0       1.0
*ELEMENT_BEAM
 1568610     120  800003      58
       ...
1573717     122    2411  870044
*ELEMENT_SHELL
```

```
  30000       3   30010   30011   30020   30020
        ...
1220584     118 1220122 1220129 1220061 1220053
*ELEMENT_SOLID
1160585     119 1160117 1160116     149     150     144     144     146     146
          ...
1220630     119 1220113    2575    2579    2596 1220114 1220114    2597    2597
*ELEMENT_SOLID
 1160609     119 1160509 1160508 1160507 1160506  410859  410846  410860  410867
     ...
 1220606     119  480581  480580  480579  480578 1220426 1220427 1220428 1220425
*SET_PART_LIST
       2
     123
*DEFINE_CURVE
       1         0 0.0000000 0.0000000 0.0000000 0.0000000
     0.00000000E+00      3.00000000E-01
     1.50000000E-02      3.50000000E-01
     1.00000000E-01      3.50000000E-01
     1.00000000E+00      3.50000000E-01
*END

$$$$$$$$$$$$$$$$$$$$$$$$$$$$$$$$$$$$$$$$$$$$$$$$$$$$$$$$$$$$$$$$$$$$$$$$$$$$$$$$$$$$$$$$$$$$$$
$$                                                                                          $$
$$                                        END                                               $$
$$                                                                                          $$
$$$$$$$$$$$$$$$$$$$$$$$$$$$$$$$$$$$$$$$$$$$$$$$$$$$$$$$$$$$$$$$$$$$$$$$$$$$$$$$$$$$$$$$$$$$$$$
```

A.3.2 Passenger Car

The abbreviated version of LS-DYNA Cards of the passenger car model is shown in this section.

```
$$$$$$$$$$$$$$$$$$$$$$$$$$$$$$$$$$$$$$$$$$$$$$$$$$$$$$$$$$$$$$$$$$$$$$$$$$$$$$$$$$$$$$$$$$$$$$$$$$$$$$$$$$
$$ HM_OUTPUT_DECK created 22:16:17 11-21-2010 by HyperMesh Version 10.0build6        $$
$$ Ls-dyna Input Deck Generated by HyperMesh Version  : 10.0build60                  $$
$$ Generated using HyperMesh-Ls-dyna 971 Template Version : 10.0build60              $$
$$$$$$$$$$$$$$$$$$$$$$$$$$$$$$$$$$$$$$$$$$$$$$$$$$$$$$$$$$$$$$$$$$$$$$$$$$$$$$$$$$$$$$$$$$$$$$$$$$$$$$$$$$

*KEYWORD
*CONTROL_TERMINATION
$$  ENDTIM    ENDCYC     DTMIN    ENDENG    ENDMAS
     0.15         0       0.0       0.0       0.0
*CONTROL_TIMESTEP
$$  DTINIT    TSSFAC      ISDO    TSLIMT     DT2MS      LCTM     ERODE     MSIST
       0.0       0.0         01.1120E-06-1.112E-06         0         0         0
       0.0         0         0
*CONTROL_SHELL
```

```
$$ WRPANG    ESORT    IRNXX    ISTUPD    THEORY      BWC     MITER     PROJ
     0.0        1        0        0        0        0        0        0
     1.0        0        0        1        0        0        0        0
*CONTROL_SOLID
$$   ESORT    FMATRX   NIPTETS    SWLOCL
       1        0        0        0
$$   PM1    PM2    PM3    PM4    PM5    PM6    PM7    PM8    PM9    PM10
     0      0      0      0      0      0      0      0      0      0
*CONTROL_CONTACT
$$ SLSFAC   RWPNAL   ISLCHK   SHLTHK   PENOPT   THKCHG    ORIEN   ENMASS
     0.0      0.0        1        2        0        0        1        0
$$ USRSTR    USRFRC     NSBCS    INTERM    XPENE    SSTHK     ECDT   TIEDPRJ
       0        0        0        0      0.0        0        0        0
$$   SFRIC     DFRIC      EDC    INTVFC       TH    TH_SF    PEN_SF
     0.0       0.0       0.0       0.0       0.0       0.0       0.0
$$ IGNORE    FRCENG   SKIPRWG    OUTSEG   SPOTSTP   SPOTDEL   SPOTHIN
       1        0        0        0        0        0
*CONTROL_OUTPUT
$$   NPOPT    NEECHO    NREFUP    IACCOP     OPIFS    IPNINT    IKEDIT
       1        3        0        0      0.0        0        0        0
       2        0        0        0        0
*CONTROL_ENERGY
$$    HGEN      RWEN    SLNTEN     RYLEN
       2        2        2        2
$$DATABASE_OPTION -- Control Cards for ASCII output
*DATABASE_ABSTAT
1.0000E-03        1
*DATABASE_DEFORC
1.0000E-03        1
*DATABASE_GLSTAT
1.0000E-03        1
*DATABASE_JNTFORC
1.0000E-03        1
*DATABASE_MATSUM
1.0000E-03        1
*DATABASE_NODOUT
1.0000E-04        1
*DATABASE_RCFORC
2.0000E-04        1
*DATABASE_RWFORC
1.0000E-04        1
*DATABASE_SLEOUT
1.0000E-03        1
*DATABASE_BINARY_D3PLOT
$$ DT/CYCL      LCDT      BEAM      NPLTC
    0.005         0         0         0         0
        0
*DATABASE_BINARY_D3THDT
$$ DT/CYCL      LCID
     5.0         0
*DATABASE_BINARY_INTFOR
$$ DT/CYCL      LCID
     5.0         0
*DATABASE_EXTENT_BINARY
```

```
$$  NEIPH    NEIPS    MAXINT   STRFLG   SIGFLG   EPSFLG   RLTFLG   ENGFLG
       0        0        0        0        2        0        2        0
$$  CMPFLG   IEVERP   BEAMIP   DCOMP    SHGE     STSSZ    N3THDT   IALEMAT
       0        1        0        0        0        3        0        0
$$ NINTSLD   PKP_SEN     SCLP           MSSCL    THERM
       1        0                       0        0
*NODE
 2000001    3003.1186523    813.46862793    225.53955078
   ...
 2810445    3239.7597656    810.96563721    233.57048035
*MAT_ELASTIC
  20001601.9640E-09  210000.0       0.3       0.0       0.0
      ...
*MAT_RIGID
  20001567.8900E-10  200000.0       0.3       0.0       0.0       0.0       0.
     0.0
     0.0       0.0       0.0       0.0       0.0       0.0
      ...
*MAT_PIECEWISE_LINEAR_PLASTICITY
  20001617.8900E-09  210000.0       0.3     250.0       0.0       0.0       0.0
    80.0       4.5   2000005         0       0.0
     0.0       0.0       0.0       0.0       0.0       0.0       0.0       0.0
     0.0       0.0       0.0       0.0       0.0       0.0       0.0       0.0
      ...
*MAT_SPOTWELD
  20008137.8000E-09  210000.0      0.28     370.0       0.51.2000E-06       0.0
     0.0       0.0       0.0       0.0       0.0       0.0       0.0       0.0
*PART
  2000152   2000152   2000152         0         0         0         0         0
    ...
  2000830   2000830   2000830         0         0         0         0         0
*SECTION_BEAM
  2000174         1       0.0       2.0       1.0       0.0       0.0
    12.0      12.0       0.0       0.0
    ...
  2000821         2       0.0       0.0       0.0       0.0       0.0
314.2     7854.0    7854.0    15708.0   282.70001
*SECTION_DISCRETE
  2000808         0       0.0       0.0       0.0       0.0
    ...
*SECTION_SHELL
  2000156         2       0.0         3       0.0       0.0         0
     1.0       1.0       1.0       1.0       0.0       0.0       0.0         0
    ...
*SECTION_SOLID
  2000152         1         0
    ...
  2000807         0         0
*INITIAL_VELOCITY_GENERATION       3
  2000011         3       0.0   15650.0       0.0       0.0         0
     0.0       0.0       0.0       0.0       1.0       0.0         0
    ...
*LOAD_BODY_Z
  2000014       1.0         0                           0
```

```
*CONTACT_TIED_SHELL_EDGE_TO_SURFACE_ID
       2DYNA_BEAM_WELD
  2000929   2000928        2        2        0        0        0        0
      0.1      0.1      0.0      0.0      0.0        0      0.0      0.0
      1.0      1.0      0.0      0.0      1.0      1.0      1.0      1.0
        0      0.1        0      0.0      0.0        2        0        1
      0.0        0        0        0        0        0      0.0      0.0
        0        0
*CONTACT_AUTOMATIC_SINGLE_SURFACE_ID
       1
  2000001                2                0        0        0        0
     0.01    0.005      0.0      0.0      0.0        0      0.0      0.0
      0.0      0.0      0.0      0.0      0.0      0.0      0.0      0.0
        1      0.0        0      0.0      0.0        0        0        0
      0.0        0        0        0        0        0      0.0      0.0
        0        0
*CONSTRAINED_EXTRA_NODES_SET
  2000156   2000952
*SET_NODE_LIST
  2000952      0.0      0.0      0.0      0.0
  2800001   2800003
     ...
*RIGIDWALL_PLANAR_ID
       5
  2000712        0        0      0.0
     0.0      0.0     -1.0      0.0      0.0      0.0      0.9
     ...
*ELEMENT_MASS
 2732233 27990004.9999999000E-06 2000831
   ...
 2796387 2021651        0.00125 2000831
*CONSTRAINED_SPOTWELD_ID
  2792914
  2460009   2247654      0.0      0.0      0.0      0.0      0.0      0.0
     ...
  2799784
  2114027   2034802      0.0      0.0      0.0      0.0      0.0      0.0
*ELEMENT_BEAM
 2572838 2000289 2300419 2157516 2300413       0       0       0       0       0
   ...
 2792240 2000174 2303801 2304062 2303824       0       0       0       0       0
*ELEMENT_SHELL
 2003163 2000308 2000463 2000449 2000443 2000443
   ...
 2792940 2000353 2810438 2810445 2076467 2076466
*ELEMENT_SOLID
 2785829 2000154 2808959 2808956 2297203 2297202 2808958 2808958 2297201 2297201
   ...
 2787002 2000182 2809455 2306263 2306258 2809456 2809458 2306265 2306255 2809459
*SET_NODE_LIST
  2000011      0.0      0.0      0.0      0.0
     ...
  2800421   2800422   2800423   2800424   2800431   2800432   2800433   2800434
    ...
```

```
  2303843  2303844  2306215  2306218  2306221  2306262  2306264  2306274
*SET_PART_LIST
  2000001      0.0      0.0      0.0      0.0
    ...
  2000929      0.0      0.0      0.0      0.0
  2000813
*BOUNDARY_SPC_NODE
  2029071                1        1        1        1        1
    ...
  2810425                1        1        1        1        1
*DATABASE_HISTORY_NODE_SET
  2000720
*DEFINE_CURVE
$HMNAME CURVES 2000001LoadCurve_2000001
$HWCOLOR CURVES 2000001       3
$HMCURVE     1    1 LoadCurve2000001
  2000001        0      1.0      1.0      0.0      0.0        0
            0.0            600.0
           0.02            816.0
          0.063           1118.25
          0.091       1281.1500244
          0.122       1344.6999512
      0.16599999           1500.0
          0.186           1700.0
          0.219           2154.0
            1.0           2164.0
*DEFINE_CURVE
$HMNAME CURVES 2000003LoadCurve_2000003
$HWCOLOR CURVES 2000003       4
$HMCURVE     3    3 LoadCurve2000003
  2000003        0      1.0      1.0      0.0      0.0        0
            0.0            370.0
          0.034            414.0
          0.082       455.70001221
          0.127        499.3999939
           0.17       527.32501221
       0.25099999           578.25
       0.32600001            700.0
       0.39500001            900.0
            1.0            910.0
*DEFINE_CURVE
$HMNAME CURVES 2000004LoadCurve_2000004
$HWCOLOR CURVES 2000004       5
$HMCURVE     1    1 LoadCurve2000004
  2000004        0      1.0      1.0      0.0      0.0        0
            0.0            570.0
          0.034            621.0
          0.082       661.84997559
          0.127       703.70001221
           0.17       746.54998779
          0.211            850.0
          0.243            980.0
          0.289           1200.0
            1.0           1210.0
```

```
*DEFINE_CURVE
$HMNAME CURVES 2000005LoadCurve_2000005
$HWCOLOR CURVES 2000005       6
$HMCURVE     2    2 LoadCurve2000005
  2000005         0       1.0       1.0       0.0       0.0         0
              0.0             250.0
            0.039               302.0
            0.086               338.0
        0.17399999              381.0
            0.255               426.0
            0.329               473.0
        0.36500001              520.0
        0.39899999              600.0
*DEFINE_CURVE
$HMNAME CURVES 2000006LoadCurve_2000006
$HWCOLOR CURVES 2000006       7
$HMCURVE     3    3 LoadCurve2000006
  2000006         0       1.0       1.0       0.0       0.0         0
              0.0             300.0
            0.039               333.0
            0.077               367.0
            0.122               395.0
        0.16599999              425.0
        0.24699999              474.0
            0.322               550.0
        0.39199999              700.0
              1.0             710.0
*DEFINE_CURVE
$HMNAME CURVES 2000007LoadCurve_2000007
$HWCOLOR CURVES 2000007       8
$HMCURVE     1    1 LoadCurve2000007
  2000007         0       1.0       1.0       0.0       0.0         0
              0.0             330.0
             0.02               367.0
            0.049               372.0
            0.082               379.0
            0.127               380.0
             0.17               381.0
        0.23100001              430.0
            0.278               500.0
              1.0             510.0
*DEFINE_CURVE
$HMNAME CURVES 2000008LoadCurve_2000008
$HWCOLOR CURVES 2000008       9
$HMCURVE     2    2 LoadCurve2000008
  2000008         0       1.0       1.0       0.0       0.0         0
              0.0             400.0
            0.039               426.0
            0.077               453.0
            0.122               480.0
        0.16599999              507.0
            0.199               550.0
        0.23100001              600.0
        0.24699999              670.0
```

```
            1.0             680.0
*DEFINE_CURVE
$HMNAME CURVES 2000009LoadCurve_2000009
$HWCOLOR CURVES 2000009      13
$HMCURVE     3    3 LoadCurve2000009
  2000009         0       1.0       1.0       0.0       0.0         0
              0.0             400.0
             0.03             489.25
            0.077         523.79998779
            0.122         553.70001221
            0.182             630.0
       0.23100001             700.0
              1.0             710.0
*DEFINE_CURVE
$HMNAME CURVES 2000010LoadCurve_2000010
$HWCOLOR CURVES 2000010      17
$HMCURVE     1    1 LoadCurve2000010
  2000010         0       1.0       1.0       0.0       0.0         0
              0.0             400.0
            0.015             450.0
            0.054             460.0
            0.082             470.0
            0.122             505.0
       0.14399999             550.0
              1.0             560.0
*DEFINE_CURVE
$HMNAME CURVES 2000011LoadCurve_2000011
$HWCOLOR CURVES 2000011      20
$HMCURVE     2    2 LoadCurve2000011
  2000011         0       1.0       1.0       0.0       0.0         0
              0.0             800.0
            0.039            1040.0
            0.072            1247.0
            0.118            1552.5
            0.161           1797.75
            0.186            1928.0
            0.223            2200.0
            0.243         2484.9199219
              1.0            2494.0
*DEFINE_CURVE
$HMNAME CURVES 2000012LoadCurve_2000012
$HWCOLOR CURVES 2000012      21
$HMCURVE     3    3 LoadCurve2000012
  2000012         0       1.0       1.0       0.0       0.0         0
             0.16              2.0
              0.2         0.89700001
       0.80000001         0.89600003
              1.0              0.0
*DEFINE_CURVE
$HMNAME CURVES 2000013LoadCurve_2000013
$HWCOLOR CURVES 2000013      24
$HMCURVE     1    1 LoadCurve2000013
  2000013         0       1.0       1.0       0.0       0.0         0
              0.0             138.0
```

```
            0.0025              175.0
             0.005             207.0
        0.15000001              210.0
              10.0             211.0
*DEFINE_CURVE
$HMNAME CURVES 2000014LoadCurve_2000014
$HWCOLOR CURVES 2000014      25
$HMCURVE     2     2 LoadCurve2000014
   2000014         0       1.0       1.0       0.0       0.0         0
               0.0               0.0
1.00000000000000E-03            9810.0
               1.0            9810.0
*DEFINE_CURVE
$HMNAME CURVES 2000015LoadCurve_2000015
$HWCOLOR CURVES 2000015      28
$HMCURVE     3     3 LoadCurve2000015
   2000015         0       1.0       1.0       0.0       0.0         0
               0.0              0.05
1.00000000000000E-03              0.05
1.10000000000000E-03               0.0
               1.0               0.0
*DEFINE_CURVE
$HMNAME CURVES 2000301LoadCurve_2000301
$HWCOLOR CURVES 2000301      29
$HMCURVE     1     1 LoadCurve2000301
   2000301         0       1.0       1.0       0.0       0.0         0
               0.0               0.0
              0.05        0.50999999
               0.1        0.75999999
        0.15000001        0.89999998
               0.2        0.97000003
              0.25        1.03999996
        0.30000001              1.12
        0.34999999        1.20000005
        0.40000001        1.30999994
        0.44999999        1.48000002
               0.5        1.72000003
        0.55000001        2.01999998
        0.60000002        2.38000011
        0.64999998         2.9000001
        0.89999998               5.5
        0.99000001             185.5
*END

$$$$$$$$$$$$$$$$$$$$$$$$$$$$$$$$$$$$$$$$$$$$$$$$$$$$$$$$$$$$$$$$$$$$$$$$$$$
$$                                                                       $$
$$                               END                                     $$
$$                                                                       $$
$$$$$$$$$$$$$$$$$$$$$$$$$$$$$$$$$$$$$$$$$$$$$$$$$$$$$$$$$$$$$$$$$$$$$$$$$$$
```